RADIOPHARMACEUTICALS FOR SENTINEL LYMPH NODE DETECTION: STATUS AND TRENDS

IAEA
International Atomic Energy Agency

IAEA RADIOISOTOPES AND
RADIOPHARMACEUTICALS SERIES PUBLICATIONS

One of the main objectives of the IAEA Radioisotope Production and Radiation Technology programme is to enhance the expertise and capability of IAEA Member States in deploying emerging radioisotope products and generators for medical and industrial applications in order to meet national needs as well as to assimilate new developments in radiopharmaceuticals for diagnostic and therapeutic applications. This will ensure local availability of these applications within a framework of quality assurance.

Publications in the IAEA Radioisotopes and Radiopharmaceuticals Series provide information in the areas of: reactor and accelerator produced radioisotopes, generators and sealed sources development/production for medical and industrial uses; radiopharmaceutical sciences, including radiochemistry, radiotracer development, production methods and quality assurance/quality control (QA/QC). The publications have a broad readership and are aimed at meeting the needs of scientists, engineers, researchers, teachers and students, laboratory professionals, and instructors. International experts assist the IAEA Secretariat in drafting and reviewing these publications. Some of the publications in this series may also be endorsed or co-sponsored by international organizations and professional societies active in the relevant fields.

There are two categories of publications: the **IAEA Radioisotopes and Radiopharmaceuticals Series** and **IAEA Radioisotopes and Radiopharmaceuticals Reports**.

IAEA RADIOISOTOPES AND RADIOPHARMACEUTICALS SERIES

Publications in this category present guidance information or methodologies and analyses of long term validity, for example protocols, guidelines, codes, standards, quality assurance manuals, best practices and high level technological and educational material.

IAEA RADIOISOTOPES AND RADIOPHARMACEUTICALS REPORTS

In this category, publications complement information published in the IAEA Radioisotopes and Radiopharmaceuticals Series in areas of the: development and production of radioisotopes and generators for medical and industrial applications; and development, production and QA/QC of diagnostic and therapeutic radiopharmaceuticals. These publications include reports on current issues and activities such as technical meetings, the results of IAEA coordinated research projects, interim reports on IAEA projects, and educational material compiled for IAEA training courses dealing with radioisotope and radiopharmaceutical related subjects. In some cases, these reports may provide supporting material relating to publications issued in the IAEA Radioisotopes and Radiopharmaceuticals Series.

All of these publications can be downloaded cost free from the IAEA web site:

http://www.iaea.org/Publications/index.html

Further information is available from:

Marketing and Sales Unit
International Atomic Energy Agency
Vienna International Centre
PO Box 100
1400 Vienna, Austria

Readers are invited to provide feedback to the IAEA on these publications. Information may be provided through the IAEA web site, by mail at the address given above, or by email to:

Official.Mail@iaea.org

RADIOPHARMACEUTICALS FOR SENTINEL LYMPH NODE DETECTION: STATUS AND TRENDS

The following States are Members of the International Atomic Energy Agency:

AFGHANISTAN
ALBANIA
ALGERIA
ANGOLA
ARGENTINA
ARMENIA
AUSTRALIA
AUSTRIA
AZERBAIJAN
BAHAMAS
BAHRAIN
BANGLADESH
BELARUS
BELGIUM
BELIZE
BENIN
BOLIVIA
BOSNIA AND HERZEGOVINA
BOTSWANA
BRAZIL
BRUNEI DARUSSALAM
BULGARIA
BURKINA FASO
BURUNDI
CAMBODIA
CAMEROON
CANADA
CENTRAL AFRICAN
   REPUBLIC
CHAD
CHILE
CHINA
COLOMBIA
CONGO
COSTA RICA
CÔTE D'IVOIRE
CROATIA
CUBA
CYPRUS
CZECH REPUBLIC
DEMOCRATIC REPUBLIC
   OF THE CONGO
DENMARK
DJIBOUTI
DOMINICA
DOMINICAN REPUBLIC
ECUADOR
EGYPT
EL SALVADOR
ERITREA
ESTONIA
ETHIOPIA
FIJI
FINLAND
FRANCE
GABON
GEORGIA
GERMANY

GHANA
GREECE
GUATEMALA
GUYANA
HAITI
HOLY SEE
HONDURAS
HUNGARY
ICELAND
INDIA
INDONESIA
IRAN, ISLAMIC REPUBLIC OF
IRAQ
IRELAND
ISRAEL
ITALY
JAMAICA
JAPAN
JORDAN
KAZAKHSTAN
KENYA
KOREA, REPUBLIC OF
KUWAIT
KYRGYZSTAN
LAO PEOPLE'S DEMOCRATIC
   REPUBLIC
LATVIA
LEBANON
LESOTHO
LIBERIA
LIBYA
LIECHTENSTEIN
LITHUANIA
LUXEMBOURG
MADAGASCAR
MALAWI
MALAYSIA
MALI
MALTA
MARSHALL ISLANDS
MAURITANIA, ISLAMIC
   REPUBLIC OF
MAURITIUS
MEXICO
MONACO
MONGOLIA
MONTENEGRO
MOROCCO
MOZAMBIQUE
MYANMAR
NAMIBIA
NEPAL
NETHERLANDS
NEW ZEALAND
NICARAGUA
NIGER
NIGERIA
NORWAY

OMAN
PAKISTAN
PALAU
PANAMA
PAPUA NEW GUINEA
PARAGUAY
PERU
PHILIPPINES
POLAND
PORTUGAL
QATAR
REPUBLIC OF MOLDOVA
ROMANIA
RUSSIAN FEDERATION
RWANDA
SAN MARINO
SAUDI ARABIA
SENEGAL
SERBIA
SEYCHELLES
SIERRA LEONE
SINGAPORE
SLOVAKIA
SLOVENIA
SOUTH AFRICA
SPAIN
SRI LANKA
SUDAN
SWAZILAND
SWEDEN
SWITZERLAND
SYRIAN ARAB REPUBLIC
TAJIKISTAN
THAILAND
THE FORMER YUGOSLAV
   REPUBLIC OF MACEDONIA
TOGO
TRINIDAD AND TOBAGO
TUNISIA
TURKEY
UGANDA
UKRAINE
UNITED ARAB EMIRATES
UNITED KINGDOM OF
   GREAT BRITAIN AND
   NORTHERN IRELAND
UNITED REPUBLIC
   OF TANZANIA
UNITED STATES OF AMERICA
URUGUAY
UZBEKISTAN
VENEZUELA, BOLIVARIAN
   REPUBLIC OF
VIET NAM
YEMEN
ZAMBIA
ZIMBABWE

RADIOPHARMACEUTICALS FOR SENTINEL LYMPH NODE DETECTION: STATUS AND TRENDS

COPYRIGHT NOTICE

FOREWORD

In a continuous effort to support and promote scientific research in cancer diagnosis and therapy, the IAEA organized a coordinated research project (CRP) on the Development of ^{99m}Tc Radiopharmaceuticals for Sentinel Node Detection and Cancer Diagnosis. This project stemmed from results obtained from a previous IAEA CRP on the Labelling of Small Biomolecules with Novel ^{99m}Tc Cores. The CRP on Development of ^{99m}Tc Radiopharmaceuticals for Sentinel Node Detection and Cancer Diagnosis was followed by a technical meeting on the Current Role and Trends of Hybrid Imaging and Radioguided Surgery, which focused on the use of radioactive imaging agents as a method for identifying diseased tissues that require surgical removal. The most widely recognized example of radioguided surgery, known as sentinel lymph node detection (SLND) or sentinel lymph node biopsy, is currently employed for planning the therapeutic treatment of superficial cancers such as breast cancer and skin melanoma. The basic concept behind this method is that, for this type of cancer, the spread of the metastases from the primary tumour site always occurs through lymphatic drainage, and thus the most proximal (sentinel) lymph node will be the first to receive the metastatic invasion. It follows that, after surgical resection of the primary tumour, the precise localization of this sentinel lymph node allows its removal and biopsy to assess whether the metastatic process has already affected it. This information has proven to be crucial for planning the further therapeutic treatment of the patient. In fact, if histological analysis of the node is negative, i.e. devoid of cancerous cells, there is no need to resort to surgical dissection of the lymph nodes, which is of clear benefit to the patient.

Various types of nanocolloidal particles labelled with ^{99m}Tc are currently used as SLND imaging agents. However, they have suboptimal properties because of their unspecific uptake in the lymph node. An alternative, molecular uptake mechanism for this class of tracers that exploits the presence of receptors for mannose on the outer macrophage's membrane, has recently been proposed. This entails the design of a multifunctional ligand that is able to accommodate a number of mannose residues along with a suitable chelating group for the radiometal. Dextran provides a convenient macromolecular scaffold for appending a relatively large number of functional groups, and its effically has recently been demonstrated through the development of a new ^{99m}Tc radiopharmaceutical for SLND (marketed under the name Lymphoseek) that targets mannose receptors on macrophages hosted in lymph nodes. This new compound can be considered the first outstanding achievement of this novel approach to SLND and provides the basis for developing alternative SLND imaging agents following the same molecular design, but using different and more sophisticated chemical strategies

for incorporating the radiometal into the dextran mannose multifunctional framework.

The first of three research coordination meetings (RCMs) of the CRP was held on 12–16 November 2007 at the IAEA in Vienna, and was attended by 18 participants from 17 countries. The second RCM was held in Athens on 18–22 May 2009, and was attended by 16 participants and 3 observers. The final RCM took place at the IAEA Headquarters in Vienna, on 22–26 November 2010, and was attended by 17 participants and 2 observers.

The technical meeting on radioguided surgery took place on 2–7 September 2012 at the IAEA Headquarters, with the participation of 15 international experts in the field.

The present publication is based on the extensive analysis carried out during the CRP and technical meeting and all the contributing authors were participants at these meetings. It is specifically focused on radiopharmaceuticals for SLND and thus constitutes a unique example of a publication providing an updated description of the status of the field. The invaluable contribution of R. Pasqualini (France) in coordinating the biological work carried out during the CRP and reviewing it in Chapter 8 of this report is gratefully acknowledged.

The IAEA officer responsible for this publication was A. Duatti of the Division of Nuclear Sciences and Applications.

CONTENTS

Chapter 1

INTRODUCTION

1.1. BACKGROUND

A sentinel lymph node (SLN) is defined as the first lymph node to which cancer cells are most likely to spread from a primary tumour. In the case of established cancerous dissemination, it is postulated that SLNs are the target organs primarily reached by metastasizing cancer cells from the tumour. This is because the spread of some forms of cancer usually follows an orderly progression, spreading first to regional lymph nodes because the flow of lymph is unidirectional. In these cases, if the cancer spreads, it will migrate first to lymph nodes (lymph glands) close to the tumour before reaching other parts of the body.

SLN surgery determines if the cancer has spread to the very first draining lymph node or not. Sentinel lymph node biopsy (SLNB) is a procedure in which the SLN is identified, removed and examined to determine whether cancer cells are present. If the SLN does not contain cancerous cells, then there is a high likelihood that the cancer has not spread to any other area of the body. Hence, a negative SLNB result suggests that the cancer has not developed the ability to spread to nearby lymph nodes or other organs. Conversely, a positive SLNB result indicates that the cancer is present in the SLN and may be present in other nearby lymph nodes (called regional lymph nodes) and, possibly, other organs. This information can help a physician determine the stage of the cancer (the extent of the disease within the body) and develop an appropriate treatment plan.

There are various advantages to the SLN procedure. First and foremost, it decreases unnecessary lymph node dissections where this is not necessary, thereby reducing the risk of lymphoedema, which is a common complication of this procedure. Increased attention to the node(s) identified as most likely to contain metastases is also more likely to detect micrometastases and result in staging and treatment changes. The main uses are in breast cancer and malignant melanoma surgery, although the procedure has been used in other tumour types with some degree of success. The average sensitivity of the SLNB is approximately 90%, with a false negative rate of about 10%. A positive histological result indicates that malignant cancer cells have migrated to some of the SLNs. Conversely, SLNs that are not affected by malignant cells will give a negative result.

The basic technique of sentinel node identification involves the injection of a tracer that identifies the lymphatic drainage pathway from a primary tumour. The earliest applications used a vital blue dye (VBD), usually isosulphan blue. Although isosulphan blue is generally safe, anaphylaxis can occur in up

to 1% of patients. Other blue dyes such as methylene blue have had similar success rates in a small series of studies. Subsequent reports describe the use of radioisotopes such as ^{99m}Tc bound colloids for preoperative lymphoscintigraphy and intraoperative localization using a gamma probe. The most commonly used radiolabelled colloid in the United States of America is ^{99m}Tc sulphur colloid, whereas ^{99m}Tc nanocolloid and ^{99m}Tc antimony sulphide are more commonly used in Europe and Australia, respectively.

The ideal radiotracer should show rapid transit towards sentinel nodes, with persistent retention in the nodes. In general, the drainage, distribution and clearance of radioactive colloids by the lymphatic system vary and are dependent on particle size. Small particles are drained and cleared first, and large particles are drained and cleared last, and may be retained virtually indefinitely at the injection site. The distribution of particle sizes within each radioactive colloid preparation is rather diverse, and is a major determinant of the kinetics of tracer clearance and thus SLN visualization. While smaller particles allow quick visualization of SLNs, larger particles have the advantages of longer tracer retention in the SLN, which permits intraoperative detection the following day, and slow transit in the lymphatic system, which minimizes visualization of lymph nodes downstream of the SLN. Additionally, particles smaller than 4–5 nm may penetrate capillary membranes without adequate retention in the lymph nodes. It is believed that a particle size range of 100–200 nm is the best compromise between the conflicting needs for efficient, fast, lymphatic drainage and satisfactory retention in the SLN. Evidently, conventional sentinel lymph node detection (SLND) imaging agents, such as nanocolloids, are non-specific particles or macromolecules because their uptake mechanism is driven by passive diffusion to follow the lymphatic drainage and accumulate within the lymph node. They generally lack the ideal imaging properties of rapid injection site clearance and high SLN extraction.

New radiotracers have been developed for SLND with the aim of improving performance. The molecular imaging (MI) paradigm has guided the design of these new SLND tracers. The ultimate goal of MI is the non-invasive localization and quantification of certain molecular events in vivo. It is the visualization, characterization and measurement of biological processes at the molecular and cellular levels in humans and other living systems. As with other imaging applications, MI requires fixation of a signal emitting molecule (e.g. one containing a radioactive, fluorescent or paramagnetic label) within the cell or tissue where the target is expressed. There are several different mechanisms by which this can be brought about. In the receptor–ligand model, one signal molecule (the ligand) binds with high affinity to a specific site on a target molecule (the receptor), which has a stationary biodistribution over the period of imaging. The key determinants of success for this type of imaging are the specificity and affinity of the receptor–ligand interaction, as well as the receptor

density itself. The receiver–ligand pair does not necessarily have to mimic a naturally occurring interaction, but can be made to bind with high specificity to molecules that are not considered to have any intrinsic biological activity.

Following this receptor targeted molecular approach, the design of new and more specific SLND diagnostic tracers has been undertaken. In Chapter 4, Vera et al. report the synthesis of ^{99m}Tc diethylenetriaminepentaacetic acid (DTPA) mannosyl dextran, which is designed to bind to mannose receptor type C (MRC) within the lymphoid tissues for SLN imaging. The MRC is a 165 kD membrane glycoprotein, and MRC belongs to the C type lectin superfamily. These proteins are involved in mediating phagocytosis of microbes and are highly expressed on the surface of macrophages hosted in lymphoid tissues. The new SLND agent ^{99m}Tc DTPA mannosyl dextran consists of a polysaccharide backbone (dextran) with an average molecular weight (MW) of 9500 g/mol, bearing pendant arms containing 55 mannose glycosides for high affinity binding to MRCs, and 8 DTPA groups for ^{99m}Tc chelation. The resulting linear molecule has a diameter of 7.1 nm.

In this compound, dextran plays the role of a macromolecular scaffold to accommodate a number of different functional groups, each performing a specific chemical or biological function (multifunctional ligand). By applying the same strategy, in the course of the coordinated research project (CRP) entitled Development of ^{99m}Tc Radiopharmaceuticals for Sentinel Node Detection and Cancer Diagnosis, research efforts have been undertaken which the dextran backbone is further functionalized using different types of chelators for binding to different ^{99m}Tc metallic fragments including $[^{99m}Tc(CO)_3]^+$ (^{99m}Tc carbonyl), $[^{99m}Tc \equiv N]^{2+}$ (^{99m}Tc nitrido), $[^{99m}Tc(SNS)]$ (^{99m}Tc 4 + 1) and $[^{99m}$Tc Hydrazinonicotinic acid] cores. These metallic cores allow the use of highly sophisticated chemical methods for labelling the dextran derived multifunctional mannosylated ligand in high specific activity while affording robust ^{99m}Tc conjugates. The resulting multifunctional ligands are essentially similar to DTPA mannosyl dextran, but differ in the coordination mode to the selected ^{99m}Tc fragment.

The MI paradigm is changing the approach of medicine to the treatment of disease, particularly for cancer treatment. A living organism is viewed as a chemical fabric where an intricate and astonishingly complex network of biochemical processes is acting to sustain life. A fundamental switch in the clinical perspective has been brought about by the recognition that treatment of pathological conditions should be approached at the molecular level. Nuclear medicine is always at the forefront of this revolution because its basic approach is intrinsically molecular, as evidenced by the use of single molecule radioactive probes for investigating inner cellular and subcellular processes. Owing to its inherent molecular trait, the progress of nuclear medicine is

tightly bound to the constant development of new radiolabelled agents capable of detecting increasingly smaller details of the underlying molecular substrate. The evolution of radiolabelled diagnostic agents for SLND offers a notable example of this transition towards more specific molecular probes, as witnessed by the development of macrophage-receptor-specific tracers that are expected to improve the sensitivity of this diagnostic modality. The IAEA promptly captured this ongoing scientific advancement by promoting a CRP and a technical meeting on this subject. Therefore, the results of these activities, as presented in this publication, constitute a significant example of real time contribution to the progress of a specific scientific discipline and a highly valuable reference material for operators working with this clinical methodology.

1.2. OBJECTIVE

The scientific objectives of the CRP can be outlined as follows:

— Design and synthesis of dextran multifunctional ligands with pendant mannose residues for interaction with the macrophage's receptors and suitable chelating groups for binding to novel ^{99m}Tc cores;
— Preparation of the corresponding ^{99m}Tc labelled conjugates with high yield and in high specific activity;
— Analytical characterization of the multifunctional ligands and of the corresponding radiolabelled conjugates;
— In vitro evaluation of stability and binding affinity for mannose receptors and in vivo biological evaluation in animal models for sentinel node detection;
— Development of a 'cold kit' formulation for easy and reliable preparation of the new ^{99m}Tc radiopharmaceuticals to be distributed in Member States.

1.3. SCOPE

The main outcomes of the CRP are described in this publication, along with results of the extensive analysis of the status and perspectives of SLND carried out during the technical meeting on Current Role and Trends of Hybrid imaging and radioguided surgery. Thus, the present publication is intended to provide a broad illustration of SLND methodology by covering basic principles, clinically established applications and recent advancements brought about after the advent of the MI paradigm and the development of dextran mannose multifunctional ligands.

1.4. STRUCTURE

In Chapter 2, an overview of the biology and physiology of the lymphatic system and of the basic uptake mechanisms underlying the use of radiolabelled colloids as imaging agents for SLND is presented. Chapter 3 reviews the most important clinical applications of the SLND approach with emphasis, in particular, on radioguided surgery. Chapter 4 reports on application of the novel molecular approach to the development of more specific and selective SLND tracers by illustrating the preparation and diagnostic properties of the first dextran mannose SLND imaging agent ^{99m}Tc tilmanocept (Lymphoseek). Chapters 5–8 describe the most important results of the CRP, with particular emphasis on chemical characterization and preclinical evaluation in animal models of three new SLND MI agents with a similar structure based on the dextran mannose multifunctional platform, but specifically tailored to the chemistry of the novel ^{99m}Tc cores.

Chapter 2

BASIC DESCRIPTION OF THE LYMPHATIC SYSTEM FROM THE PERSPECTIVE OF SLN UPTAKE OF RADIOACTIVE TRACERS

R. PASQUALINI

CIS bio international/IBA, Saclay, RP Innovative,
Clamart, France

E. JANEVIK-IVANOVSKA

Faculty of Medical Sciences,
Goce Delcev University,
Stip, The Former Yugoslav Republic of Macedonia

2.1. SUMMARY

The lymphatic system is part of the circulatory system. It is closely associated with the cardiovascular system because it includes a network of vessels that contributes to liquid transportation throughout the body. This circulatory system is essential for the maintenance of interstitial fluid balance, uptake of dietary fat and for body defence against invasion by disease causing agents.

Lymph nodes, which contain large numbers of B and T lymphocytes and macrophages, are located along lymphatic pathways. They have two primary functions: filtering and digesting potentially harmful particles from lymph before returning it to the bloodstream and contributing to the immune surveillance provided by lymphocytes and macrophages. In their function of filtering particles or cell debris, lymph nodes may collect cancer cells that are breaking and travelling away from the primary tumour. The spread of some forms of cancer usually follows an orderly progression, spreading first to regional lymph nodes, then the next rank of lymph nodes and so on. Therefore, the first lymph node (the SLN) is more likely than other lymph nodes to contain cancer cells. If a suitable radioactive tracer, generally a nanocolloid or a dye, is administrated in the proximity of the tumour site, it will travel through the lymphatic system and be trapped in the SLN, allowing its localization using an appropriate probe or by visual determination. The size and the charge of the radioactive tracer will mainly influence the extent of radioactivity remaining at the site of injection, the rate of diffusion into the lymphatic vessels and the uptake in the SLN. Knowledge of the

physiology of the lymphatic system will help to identify factors influencing the diffusion and uptake mechanism of radioactive tracers in the lymph nodes and will assist in the design of more efficient and selective SLN seeking drugs.

2.2. INTRODUCTION

The purpose of this chapter is to provide readers with a basic description of the structure and function of lymph nodes, with a particular interest in the mechanisms that might mediate the uptake of radioactive tracers in these structures. In this regard, many aspects of the physiology of the lymphatic system, mainly those related to the formation and transport of lymphatic fluid, will not be developed comprehensively. Several excellent articles have appeared recently describing the microstructure and physiology of the lymphatic system [2.1–2.6]. Readers are encouraged to consult these references, which have been of constant help when writing the chapter that follows.

2.3. THE LYMPHATIC SYSTEM: A GENERAL VIEW

The lymphatic system is closely associated with the cardiovascular system. Similar to the latter, it includes a network of vessels that contributes to liquid transportation throughout the body. Lymphatic vessels transport excess fluid away from the interstitial space between cells in most tissues and return it to the bloodstream, as schematically depicted in Fig. 2.1.

The lymphatic system is found throughout the body, with the exception of the central nervous system, where cerebrospinal fluid fulfils the normal role of lymph. This circulatory system is essential for the maintenance of interstitial fluid balance, uptake of dietary fat and the body's defence against invasion by disease causing agents.

2.4. STRUCTURE OF THE LYMPHATIC NETWORK

The lymphatic network begins as lymphatic capillaries merge to form lymphatic vessels, which in turn converge to form large vessels that eventually join the blood stream via the right lymphatic duct [2.7].
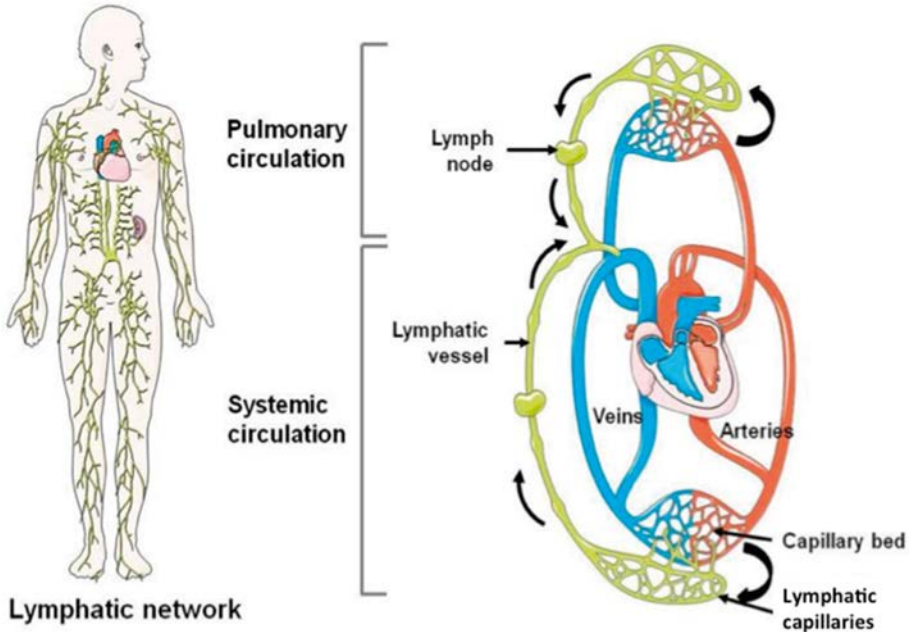
FIG. 2.1. Lymphatic vessels, which are closely associated with blood vessels, transport fluid from interstitial spaces to the bloodstream (graphical material provided by Servier Medical Art).

2.4.1. Lymphatic capillaries

Lymphatic capillaries are closed ended tubes (see Fig. 2.2). They are 10–60 µm in diameter, and, like blood capillaries, are composed of an endothelial cell layer. However, the gaps between the endothelial cells in the lymphatic capillaries are larger than those found in the blood capillaries [2.8, 2.9]. These endothelial clefts can open to dimensions of several micrometres, allowing macromolecules, colloids, cells and cellular debris to pass unhindered, depending on the degree of distension [2.10–2.13]. The lymphatic capillaries are thus more permeable and larger than blood capillaries, allowing for easier entrance of relatively large protein particles. Attached to the lymphatic capillaries are anchoring filaments, which contain elastic fibres. These anchoring filaments extend out from the lymphatic capillary, attaching lymphatic endothelial cells to surrounding collagen, and prevent endothelial cells from collapsing when interstitial fluid pressure increases.
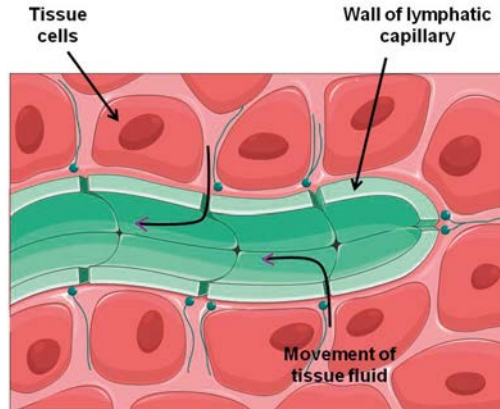
FIG. 2.2. Tissue fluid enters lymphatic capillaries through flap like valves between adjacent cells. Anchoring filaments to tissue cells are not drawn (graphical material provided by Servier Medical Art).

2.4.2. Lymphatic vessels

Lymphatic vessels form as lymph capillaries merge. The walls of lymphatic vessels are similar to those of veins, although thinner. Morphologically, the walls are composed of three layers: an endothelial lining, a middle layer of smooth muscle and elastic fibres, and an outer layer of connective tissue. Like veins, semilunar valves are present to prevent the backward flow of lymph.

2.4.3. Lymphatic trunks and collecting ducts

Lymphatic trunks form from the union of collecting vessels. They are named after the regions they serve: lumbar, jugular, subclavian, bronchomediastinal and intestinal trunks. Except for the latter trunk, each of them occurs in pairs, left and right, for each side of the body. These lymphatic trunks then join one of the two collecting ducts, the thoracic duct or the right lymphatic duct. These ducts empty into the left and right subclavian veins, respectively.

Figure 2.3 is a view of the lymphatic and blood network in the region of fluid interchanges.
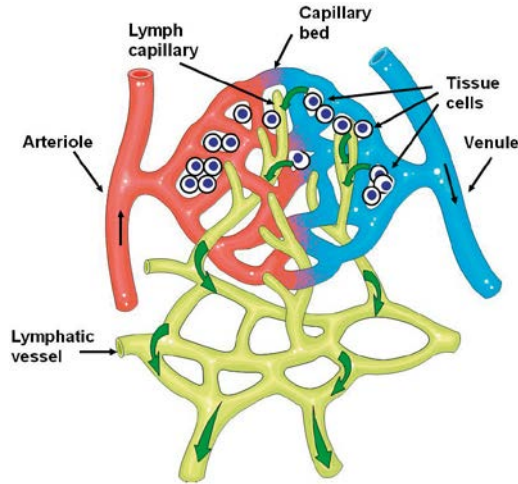
FIG. 2.3. Relationship between the lymphatic and blood capillaries (graphical material provided by Servier Medical Art, modified).

2.5. LYMPH PRODUCTION AND MOVEMENT

2.5.1. Role of the interstitial space

The interstitial space located between the capillary walls and cells is composed of two phases [2.14]:

— An interstitial fluid containing salts and plasma proteins;
— An extracellular matrix (ECM), which is constituted of fibrous protein (predominantly collagen, but also elastin, fibronectin and laminin) and glycosaminoglycans (GAGs) [2.15].

Collagen fibres provide much of the structural framework of the tissue. There are several types of collagen, with type I being predominantly found in the skin. All collagens consist of three polypeptide α chains with high hydroxyproline (Hyp) content and a very common sequence Gly-Pro-X and Gly-X-Hyp (Gly = glycine, Pro = proline, X = proline or 4-hydroxyproline) [2.16]. Collagen I possess a slightly positive charge (pI ∼ 8, where pI = –logI, I = ionic strength) at physiological pH [2.17].

Glycosaminoglycans are unbranched polysaccharide chains composed of repeating disaccharide units. One of the two sugars is always an amino sugar (N-acetylglucosamine or N-acetylgalactosamine), which, with the exception of

hyaluronic acid, is sulphated. The second sugar is usually glucoronic or iduronic acid [2.18]. Because there are sulphate and/or carboxyl groups on most of their sugars, GAGs are highly negatively charged. With the exception of hyaluronic acid, these GAG chains attach to a protein core to make up larger molecules called proteoglycans (PGs), and, in turn, PG subunits are combined to form large aggregates, which can have MWs as large as 10^8 g/mol.

Collagen and PGs will restrict the space available to macromolecules in the interstitial space by steric effects. Additionally, because of their high density negative charge at a physiological pH, PGs will exert an electrostatic exclusion effect on negatively charged macromolecules [2.14]. This results in the presence of narrow aqueous tissue channels of approximately 100 nm diameter, allowing the passage of macromolecules by diffusion [2.19]. Therefore, it seems reasonable to speculate that the size of administered colloids should be less than 100 nm in diameter if good drainage from the injection site has to be achieved.

2.5.2. Formation of lymph

Tissue fluid is composed of water and dissolved substances that migrate from blood capillaries by diffusion and filtration. Tissue fluid contains, among other small molecules and gas, some relatively small proteins. Usually, these small proteins are not reabsorbed when water and dissolved molecules travel back into the venule ends of these capillaries. As a result, the protein concentration of the tissue fluid tends to rise, increasing the osmotic pressure of the fluid in the interstitial space. This increasing interstitial pressure forces some of the tissue fluid into the lymphatic capillaries, where it becomes lymph. Because of the high permeability of lymphatic walls, there is no exclusion of interstitial molecules, irrespective of their size. The protein composition of lymph is nearly equivalent to that of interstitial fluid, which is similar to, albeit less concentrated than, that of blood plasma, from which it originates [2.1]. The only exception occurs for intestinal lymph, which contains a high amount of fat resorbed directly from the intestine.

Lymph, like venous blood, is under relatively low hydrostatic pressure. Flow through the lymphatic vessels cannot occur without the intervention of outside help. These outside forces include contraction of skeletal muscles, pressure changes owing to the action of breathing muscles and, for large lymphatic trunks, contraction of the wall's smooth muscles. Movement of the lymph in the vessels is unidirectional because the presence of valves prevents backflow [2.20].

2.6. LYMPH NODES

Lymph nodes are located along the lymphatic pathways, particularly where lymphatic vessels merge to form trunks. They contain a large number of lymphocytes and macrophages, whose role is to combat against invading microorganisms.

2.6.1. Structure of a lymph node

Lymph nodes may vary in size and shape, ranging from a few millimetres to a maximum of 2.5 cm long in their normal state, and are often bean shaped. Figure 2.4 illustrates a section of a typical lymph node.

Lymph nodes consist of multiple lymphoid lobules. This structure, which is the basic anatomical and functional unit of a lymph node, is surrounded by sinuses, in which lymph flows, and enclosed by a capsule. The smallest lymph nodes may contain very few (or even one single) lymphoid lobules, while the largest ones may comprise a great number of such structures.

Only the principal aspects of the anatomical structure and function of lymph nodes that are related to the mechanism of uptake of radiotracers will be
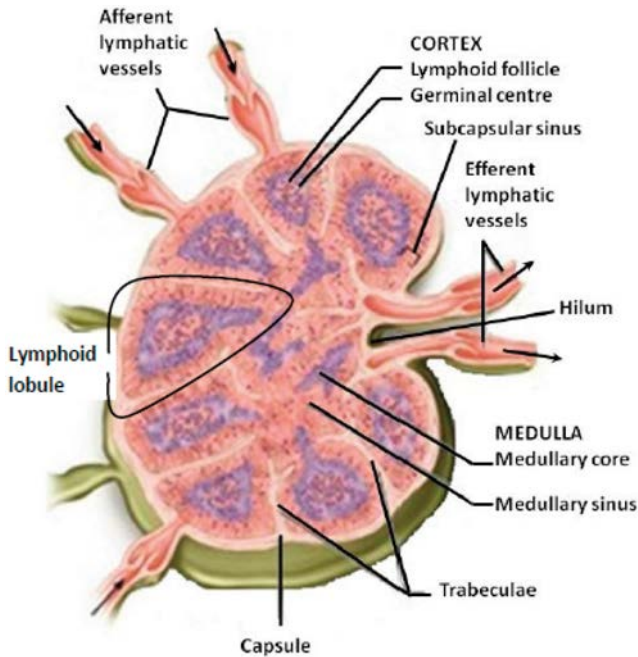
FIG. 2.4. Section of a lymph node.

covered here. For a more detailed description, readers are invited to refer to the previously mentioned references [2.1–2.6].

Schematically, lymphoid lobules are arranged side by side, radiating from the hilum, at the indented region of the lymph node, to which they are anchored, separated from the capsule by the sinuses. The hilum is the portion through which the blood vessels connect with the node. The afferent vessels enter separately at various points of the convex surface, but the efferent lymphatic vessel exits from the hilum. Because lymph nodes have fewer efferent vessels than afferent vessels, the lymph flows slowly and stagnates somewhat within the node. This is important because it allows time for the generation of an immune response and for macrophages to remove debris from the lymph before it re-enters the blood vascular system. Because each afferent vessel collects lymph from a different drainage region, each lymphoid lobule is potentially exposed to different sets of antigens, antigen-presenting cells and inflammatory mediators [2.21]. As a result of this heterogeneous immunological stimulation, lobules within the same lymph node may have different levels of immunological activity.

The entire lymph node is filled with a fine reticular meshwork composed of spindle shaped or elongated fibroblastic reticular cells and their reticular fibres that form the basic supporting structure of the lobules and criss-cross the lumens of the sinuses [2.22]. This causes the lobule to subdivide into a large number of narrow channels and interstices, 10–20 μm wide, which are occupied by lymphocytes, macrophages and antigen-presenting cells.

In the sinuses, the reticular meshwork has thinner branches and correspondingly larger interstices than the lobular reticular meshwork [2.23]. Macrophages, also known as sinus histiocytes, stick to this reticular meshwork and trap bacteria, cell debris, red blood cells and other particulates suspended in the lymph as it flows through the meshes of this biological filter. They tend to occur in clusters; their number increases in response to the need for particle clearance and they may completely fill the sinuses. However, an supportive (reticular) cells in lymphoid tissue can also ingest foreign particles and cell debris, but with less efficiency than macrophages.

Ludwig has shown that two types of structural configurations between lymph vessels and lymph nodes may exist [2.24]. In the first type, as illustrated in Fig. 2.4, the lymph node receives lymph from the afferent duct. The lymphatic liquid passes through the lymph node, which filters it, and then empties into the efferent channel. In the other configuration, the lymphatic vessel develops through the lymph node, or over its surface, without allowing emptying of its contents into that node. As pointed out by Tanis et al. [2.25], if the first lymph node adopts the latter configuration, the tumour cells transported in the lymph will not be trapped in the lymph node. This situation could be one of the explanations of false negative SLND with radiocolloids.

2.6.2. Function of lymph nodes

Lymph nodes have two primary functions:

— They prevent the spread of microorganisms and toxins that enter interstitial fluids by filtering potentially harmful particles from lymph before returning it to the bloodstream. Furthermore, they destroy bacteria, toxins and particulate matter through the phagocytic action of macrophages.
— They operate an immune surveillance, which is provided by lymphocytes and macrophages (the immune system function will not be treated further in this chapter).

2.6.2.1. Filtering function of lymph nodes

The rationale for SLND with radioactive colloids is based on the ability of lymph nodes to retain foreign particles that are present in the lymphatic fluid.

As described earlier, the labyrinthine structure of the reticular meshwork, in which lymph slowly percolates, and the presence of macrophages and reticular cells lined on it, allows sequestration of foreign particles or products from cell degradation. The lymph nodes appear to provide two main types of filtration: the first is a simple mechanical passage through the reticular meshwork and the second involves a biological reaction with the phagocytic elements. Receptors on the phagocytes and reticular cells are able to recognize foreign colloids, either by the nature of the particle surface or by opsonins adsorbed onto the particle surface [2.26]. Removing the lymph of particulate matter is based on an active, saturable phagocytosis process.

2.6.2.2. Receptor based uptake of foreign matters

In the lymph node, phagocytosis is the main process of macrophages. These cells are derived from circulating monocytes, whose phagocytic ability is highly enhanced by this differentiation process [2.27]. Monocytes/macrophages, as well as neutrophils, have been referred to as 'professional phagocytes' because of their high phagocytic capacity and efficiency at internalizing particles [2.28]. This property can probably be ascribed to the presence of an array of dedicated phagocytic receptors that increases the particle range and phagocytic rate [2.29]. It should be outlined that the role of macrophages is not only to ingest and destroy bacteria, viruses, inorganic foreign particles and cellular debris. Some of them also facilitate cross-talk between innate and adaptive immunity by acting as 'antigen presenting cells'. However, the involvement of macrophage in the immune response will not be further developed in this chapter.

Phagocytosis occurs through a complex mechanism that cannot be appropriately explained on the basis of a simple single model. Despite the complexity associated with several phagocytic mechanisms, the basic features of the process can easily be accommodated within the following description. First, particle internalization is initiated by the interaction of specific receptors on the surface of the phagocyte with some ligands on the surface of the particles. Then, a phagocytic cup is formed on the macrophage membrane around the foreign matter, with subsequent engulfment in a vesicle that fuses with cell lysosomes where chemical degradation takes place. Finally, non-digestible residues are ejected from the cell by exocytosis.

Engulfment of invading microorganisms, foreign particles and apoptotic bodies is initiated by the engagement of specialized pattern recognition receptors, which can discriminate among numerous bacterial components such as bacterial carbohydrates (mannose receptor, glucan receptor) and bacterial lipids (lipopolysaccharides receptors), as well as other structures typically found on pathogen surfaces (toll like receptors, scavenger receptors) [2.30]. Additionally, macrophages have molecules on their surface known as Fc receptors, which are capable of binding immunoglobin G through its Fc region onto opsonized pathogens.

The mannose receptor on macrophages recognizes mannose and fucose on the surfaces of pathogens and mediates phagocytosis of the organisms. The mannose receptor is a single chain receptor with a short cytoplasmic tail and an extracellular domain including eight lectin-like carbohydrate binding domains, a fibronectin type II domain and an ending N-terminal cysteine rich domain [2.31]. The three types of domains at the extracellular region have different ligand specificity:

— The C type lectin-like domain binds glycoproteins with exposed mannose, fucose or N-acetyl glucosamine residues [2.32–2.34];
— The fibronectin type II domain binds to collagens I, II, III and IV with high affinity [2.35];
— The cysteine rich domain recognizes sulphated carbohydrates [2.36, 2.37].

In recent years, macrophage specific delivery systems have gained much attention because macrophages act as a natural hideout for several pathogenic microorganisms. Therefore, several research groups have explored the carbohydrate specific glycoprotein uptake system of macrophages for specifically targeting these drug delivery systems [2.38–2.42]. Among different carriers, liposomes have been extensively investigated as delivery systems for phagocyte targeted therapies because of their advantages which include low immunogenicity, biocompatibility, cell specificity and drug protection [2.43].

2.7. THE SLN

2.7.1. The SLN concept

The SLN is the hypothetical first lymph node, or group of nodes, that receives lymph collected from a primary tumour mass. If cancerous dissemination occurs, it is postulated that the SLN will trap any metastasizing cells leaving the tumour. If the SLN is negative for tumour metastasis, the presence of cancerous cells in all other lymph nodes in the same lymphatic chain is highly improbable [2.44–2.49].

Sentinel lymph node mapping (SLNM) can be performed using a dye (patent blue or isosulphan blue), a radioactive tracer or both. The radioactive tracers currently used in clinical routine are based on ^{99m}Tc labelled colloids (either inorganic or of albumin origin) [2.50]. However, the new approved dextran based tracer, ^{99m}Tc tilmanocept (see Section 2.7.3) is expected to be gradually adopted by the nuclear medicine community.

Ideally, an SLN imaging agent would rapidly clear from the injection site to allow easy detection of nodes that are located close to the injection site. Residence of the activity in the SLN should be selective and high enough to allow different protocols for detection (external acquisition or radioguided surgery). It should be obtained with high specific activity to avoid saturation of the phagocytic process, with consequent leakage of radioactivity to the higher echelon nodes of the region, and should be safe.

2.7.2. Physicochemical aspects of lymph node delivery of biologically inert agents

Basically, to be taken up by the SLN, large molecules or colloids administered by subdermal injection should first travel into the interstitial space, cross the membrane of lymphatic capillaries, flow freely into the lymphatic vessels and, finally, be phagocytized by macrophages of the first lymph node encountered on their travel.

There is no unanimous consent in defining the order of importance of the parameters affecting the overall localization process of foreign material into lymph nodes. However, characteristics related to the size, shape and charge of particles are generally mentioned as the most relevant ones [2.2, 2.51, 2.52].

2.7.2.1. Particle size

Size is the major factor determining the behaviour of particulate materials after subcutaneous injection. Particles that are smaller than a few nanometres will mostly penetrate the blood capillary membrane, whereas larger particles (up to about 100 nm) can enter the lymphatic capillaries and be transported to lymph nodes. Larger particles will be trapped in the interstitial space for a long time [2.53]. Additionally, particle size also governs endocyte uptake by macrophages. However, the upper size limit for lymphatic uptake has not been strictly defined. The optimal colloidal size for lymphoscintigraphy is believed to be approximately 50–70 nm [2.54], but the range 10–100 nm has also been proposed [2.50–2.55]. The results of recent studies correlating the particle profile of ^{99m}Tc labelled inorganic colloids with lymph node uptake suggest that colloids with nanometric dimensions are the best suited for a high node uptake [2.56]. As a general rule, it can be assumed that very small nanoparticles (<10 nm) are best suited for lymphoscintigraphy or rapid SLND, whereas large particles (>100 nm) display a longer retention in the first encountered lymph node.

The earliest lymphoscintigraphic methods used colloidal (^{198}Au) gold (9–15 nm in size) [2.57]. Although promising results were obtained, confirming the suitability of small sized colloids, the absorbed dose at the injection site was judged to be unacceptably high (13–27 Gy/MBq) to allow safe use of this radiocolloid. These dosimetric concerns were removed by the introduction of the less irradiating ^{99m}Tc based radiocolloids.

There is variation in the nature and size of ^{99m}Tc labelled colloids used worldwide for the detection of SLNs [2.2, 2.58]. Studies in the USA were initiated with ^{99m}Tc sulphur colloid, which is a radiopharmaceutical that was initially approved for liver and spleen scintigraphy. This radiocolloid (administered 0.22 µm filtered or unfiltered) is still used nowadays, with the US Food and Drug Administration (FDA) approving its indication for SLNM only very recently. In Europe, albumin colloids and a preformed rhenium sulphide colloid are the approved agents. Of the two, albumin colloid is the most frequently used tracer. Technetium-99m labelled antimony trisulphide is the colloid of choice in Australia, whereas ^{99m}Tc calcium phytate is the tracer used in Japan.

The size ranges of some radiocolloids currently used in clinical practice are shown in Table 2.1 [2.58–2.62].

TABLE 2.1. SIZE OF SOME APPROVED ^{99m}Tc RADIOCOLLOIDS

Colloid composition	Size range (nm)	Comments	References
Human serum albumin	7–23[a] 3–16[a]	Registered in different countries in Europe; not approved in USA	[2.59, 2.60]
Human serum albumin	100–600[b] <100[b]	Registered in different countries in Europe; not approved in USA	Refer to supplier brochures
Stannous/stannic hydroxide	30–200[a]	Approved in some European countries	[2.60]
Rhenium sulphide	8–68[a]	Registered in different countries in Europe	[2.61]
Sulphur colloid 0.1 µm filtered sulphur colloid	50–1000[c] 30–50[c]	Registered in USA	[2.50, 2.61]
Antimony trisulphide	2–16[d] 17–23[a]	Registered in Australia	[2.58]
Calcium phytate	150–200[a] 150–1500[a]	Mainly used in Japan; size depends on Ca^{2+} concentration	[2.62]

[a] Particle size measurement using dynamic light scattering.
[b] Particle size measurement method not disclosed.
[c] Particle size measurement using membrane filtration.
[d] Particle size measurement using transmission electron microscopy.

As illustrated in Table 2.1, approved radiocolloids span quite a large size range. Although in some guidelines, it is reported that a preparation with the majority of particles ranging between 100 nm and 200 nm in size can be considered the best compromise between fast lymphatic drainage and optimal retention in the SLN [2.52], the influence of the colloid size on diagnostic performance (sensitivity and specificity) has not yet been evaluated in large prospective studies. Probably, one of the largest comparative studies is that reported by Paganelli et al., in which 215 patients with operable breast carcinoma were assigned to three different diagnostic procedures [2.63]. Group A was treated with ^{99m}Tc antimony sulphide (particle size < 50 nm), group B was

treated with ^{99m}Tc colloidal albumin (particle size < 80 nm) and group C was treated with ^{99m}Tc colloidal albumin (particle size 200 –1000 nm). In each group, two methods of administration (peritumoural and subdermal) were evaluated. The conclusion of this study was that larger particle sized colloids were most successful in detecting only one or two sentinel nodes, even 14–16 h after injection, and that subdermal administration was the preferred route. However, the choice of the best radiocolloid has been dictated to a great extent, and still is, by its availability as an approved radiopharmaceutical.

It must be emphasized, however, that great care must be taken to not simply compare the size of radiocolloids measured with different sizing techniques, mainly because most particles are not regularly shaped, accentuating the inherent limitations of each technique. For instance, transmission electron microscopy will give the size of inorganic cores, but often not the coating (e.g. gelatine layers). Moreover, particles are heated by the electron beam, possibly causing sublimation of some components of the particle (e.g. sulphur in the case of metal sulphide), therefore altering the original size (the freeze–fracture technique should be used). Dynamic light scattering (DLS), also referred to as photon correlation spectroscopy, is able to give the hydrodynamic diameter of particles, but the diameter that is obtained using this technique is the diameter of a sphere that would have the same translational diffusion coefficient as the particle. As the translational diffusion coefficient depends not only on the size of the particle 'core', but also on any surface structure, as well as the concentration and type of ions in the medium, meaningful results are obtained only with strict control of the experimental parameters. Additionally, the use of DLS becomes more and more problematic when the size distribution of the sample broadens.

2.7.2.2. Particle shape

Recently, particle shape has been identified as playing an important role in the ability of macrophages to internalize particles [2.64, 265]. Theoretical models based on cellular internalization have already underlined the benefit of using non-spherical particles for drug delivery [2.66]. Experimental studies have confirmed this prediction, showing, in an alveolar macrophage model, that the local geometry of the particle at the point of cell attachment, not the overall particle shape, can dictate whether macrophages initiate internalization [2.67].

The effect of shape on phagocytosis has also been observed for CdTe quantum dot cystine composites with sphere, rod and needle particle shapes. In mouse leukaemic monocyte macrophage, the microspheres exhibit the highest degree of internalization and the fastest phagocytosis rate, while almost no internalization of the needle shaped species occurs, clearly indicating a significant effect of the shape on the macrophage phagocytosis [2.68]. Therefore, the size

of particles will affect the completion of phagocytosis, especially when the particle volume exceeds the cell volume, and particle shape remains important in initiating engulfment of a particle by macrophages.

2.7.2.3. Particle charge

Although this has been less frequently investigated, there is evidence that modifications of the surface charge of particles can influence transport in the interstitial space and uptake by lymph node macrophages.

While for particles the size is the predominant factor governing movement in the interstitial space, the effect of charge becomes significant for proteins and small sized polymers. In the interstitial space, fixed negative charges, principally because of GAGs, are expected to contribute significantly to interstitial exclusion of charged macromolecules. In an ex vivo model of mouse tail skin, Reddy et al. [2.69] investigated the rate of interstitial convective transport of anionic and uncharged 3 kg/mol dextran. It was found that the anionic dextran moved with a higher average velocity through the interstitium than the neutral dextran, suggesting that electrostatic repulsion may serve to reduce the interactions between a negatively charged solute and the ECM.

The influence of the surface charge on macrophage phagocytosis is less clear. From a literature survey, general trends cannot be reliably developed that would apply to any kind of particle, as the chemical composition of the surface may also play a role in the phagocytic process. Two classes of synthetic particles have been extensively used to study phagocytosis: liposomes (vesicles composed of a lipid bilayer) and polymerized microspheres (e.g. polystyrene). These particles offer a large flexibility for tailoring their size, shape, charge and hydrophobicity.

Liposomes have been extensively used as a particulate model because of their potential for carrying and delivering drugs to cells and because of the relative ease with which their charge and size can be shaped. The drainage of negatively charged liposomes has been shown to be faster than that for positive liposomes [2.70]. It has also been shown that the rate of liposome localization in the lymph nodes after subcutaneous injections to rats was in the order negative > positive > neutral liposomes [2.71].

In a recent review article on drug delivery to monocytes and macrophages with liposomes, Kelly et al. [2.43] report that negatively charged lipids such as phosphatidylserine and phosphatidylglycerol are preferentially recognized by macrophages [2.72]. Studies comparing phosphotidylcholine (neutral) and phosphatidylserine (anionic) composed liposomes have established negative liposome formulations to have enhanced macrophage internalization in lung

macrophages of mice after intravenous administration of liposomes to the animals [2.73].

Experiments using polystyrene microspheres with macromolecule modified surfaces produced different clearance and organ deposition patterns for negatively or positively charged particles [2.74], suggesting that positive charges increase phagocytic uptake while negative charges reduce uptake [2.75]. These findings were not confirmed by the work of Tabata et al. [2.76], who studied uptake by mouse peritoneal macrophages of modified cellulose microspheres with different surface charges. It was found that there was no significant difference in phagocytosis between cationic and anionic surfaces when compared at a zeta potential of the same absolute value.

2.7.2.4. Surface hydrophobicity/hydrophilicity

Opsonins prefer to associate with hydrophobic rather than hydrophilic surfaces [2.77]. Indeed, the phagocytosis of hydrophobic polystyrene nanospheres was shown to be drastically reduced by the adsorption of hydrophilic block copolymers prior to intravenous administration [2.78]. Conversely, nanospheres conditioned with block copolymers of polyoxyethylene chains of 5–15 ethylene oxide units are effectively opsonized in lymphatics, which is a process that dramatically enhances sequestration by regional lymph nodes [2.79]. However, because hydrophobicity exerts a negative effect on particle drainage from the injection site, an appropriate coating should be found that allows optimization between the extent of drainage and the uptake process by macrophages.

2.7.2.5. Molecular weight

As the MW increases, there is a decreased ability for the molecule to penetrate blood capillaries, with a consequent increase in preference to enter into lymphatic vessels.

It has been shown that for water soluble compounds with MWs ranging from 246 g/mol to 19 000 g/mol, a linear relationship exists between the MW of a compound administered subcutaneously and the fraction of the dose absorbed by the lymphatic draining. Compounds with a MW greater than 16 000 g/mol are absorbed mainly by the lymphatics that drain the application site [2.80]. This was the rationale for the use, either for lymphoscintigraphy or for SLND, of non-particulate agents such as ^{99m}Tc human serum albumin (HSA) (MW = 67 000 g/mol) [2.81], ^{99m}Tc dextran (average MW = 110 000 g/mol) [2.82] and ^{99m}Tc hydroxyethyl starch (average MW = 450 000 g/mol) [2.83].

The suitability of ^{99m}Tc dextran (average MW = 82 000 g/mol) as a lymph node imaging agent was determined in rabbits and dogs by comparison with ^{99m}Tc antimony sulphide colloid. In both species, in spite of a rapid uptake rate, total popliteal lymph node sequestration of ^{99m}Tc dextran was significantly lower than that observed for colloidal ^{99m}Tc antimony sulphide [2.84]. These results were confirmed in a more recent study in which mice were used as the animal model. SLN uptake of ^{99m}Tc dextran (average MW = 70 000 g/mol) was lower than that observed for ^{99m}Tc albumin colloid and ^{99m}Tc antimony sulphide [2.85].

Despite these findings in animal models, ^{99m}Tc dextran has been used, with apparent success, to detect SLN in small cohorts of patients with breast carcinoma [2.86–2.88]. Promising results were also reported with ^{99m}Tc hydroxyethyl starch in a small group of normal volunteers and in patients with breast carcinoma [2.83].

The labelling process of dextran and hydroxyethyl starch with stannous-reduced ^{99m}Tc deserves comment. The two compounds are equally made of a large number of glucose units, although they are differently assembled. Because only weak chelating hydroxyl groups are present on the molecules, colloidal Tc may form during the labelling step, thus contaminating the preparation with radioactive particulate species. In addition, loss of labelling may also take place ex vivo, inducing alteration of the expected radioactivity distribution. Moreover, because the labelling process of dextran is performed in the presence of high amounts of stannous chloride, concomitant formation of ^{99m}Tc-labelled tin colloid cannot be totally excluded. To obviate these limitations, a modified dextran, incorporating cysteamine as the chelator for ^{99m}Tc, has been synthesized and tested in animals. This dextran derivative has shown higher chelation stability against DTPA than ^{99m}Tc dextran, enabling clear visualization of axillary lymph nodes after intradermal injection in rats [2.89].

Technetium-99m HSA has also been proposed as a radioactive non-particulate agent for the detection of SLNs. Comparative studies with other lymphoscintigraphic agents (^{99m}Tc sulphur colloid, ^{99m}Tc albumin colloid and ^{99m}Tc phytate) have been performed in animals and in humans. In mice, ^{99m}Tc HSA tends to accumulate in the SLN less efficiently than ^{99m}Tc sulphur colloid and disperses more rapidly to the next echelon nodes and to the systemic circulation [2.90].

The diagnostic performance of ^{99m}Tc HSA has been compared to that of ^{99m}Tc albumin colloid and filtered ^{99m}Tc sulphur colloid. In one clinical study, 51 patients with stage I or stage II melanoma were equally assigned to one of the three treatment groups. Early images with all three agents provided reliable identification of SLNs. As expected, ^{99m}Tc HSA demonstrated faster washout rates from injection sites and better definition of lymph channels than either

particulate agent, whereas the particulate agents were retained longer in nodes and demonstrated more nodes in delayed images than in early images [2.91].

A similar study was conducted in patients with cutaneous melanoma (CM) using unfiltered ^{99m}Tc sulphur colloid as the comparator. In this study, the majority of patients (85 out of 106) received ^{99m}Tc albumin. A few of them (4) received both tracers. In this study, SLNM was similar in both HSA and sulphur colloid cohorts. However, it should be pointed out that acquisition of images was limited to 1 h after administration of tracers, which is a relatively short period of time, in which the ^{99m}Tc HSA activity has not yet migrated from the node [2.92].

The analysis of a retrospective study including 533 patients with breast carcinoma, with half of them explored with ^{99m}Tc HSA and the remainder with ^{99m}Tc phytate, showed that the identification rate of SLNs was significantly higher in the phytate group than in the HSA group. Most importantly, the highest radioactivity of SLNs per case was more than five times higher in the phytate group than in the HSA group, demonstrating a better diagnostic performance of ^{99m}Tc phytate [2.93].

Therefore, although no rigorous studies can be advocated to confirm the inferior performance of ^{99m}Tc HSA and ^{99m}Tc dextran, it seems unlikely that these two tracers would, in the near future, replace the well established radiocolloids for SLND.

2.7.3. Receptor based radiotracers for SLND

Very recently, cell mannose receptors have been used to target resident lymph node macrophages with a radioactive agent for SLND. The radiotracer is a synthetic macromolecule composed of a dextran backbone and multiple subunits of DTPA (for ^{99m}Tc chelation) and mannose (for receptor binding) [2.94]. This receptor based approach has shown excellent results in animals and humans for detecting SLNs [2.95, 2.96]. This dextran derivative, named ^{99m}Tc labelled tilmanocept, has been approved by the FDA for use in patients with breast cancer or melanoma who are undergoing surgery to remove tumour draining lymph nodes. At the time of writing, the drug had recently been approved by the European Medicines Agency. An extensive discussion of this new tracer is given by Vera et al. in Chapter 4.

Receptor mediated uptake by lymph nodes has also been reported by Takagi et al. [2.97], who have compared ^{99m}Tc-labelled HSA and ^{99m}Tc-labelled mannosyl neoglycoalbumin to a commercial ^{99m}Tc rhenium sulphide colloid in mice. Similar to the results obtained with the mannosyl dextran derivatives [2.94], the introduction of mannose residues on albumin increases the uptake and the residence time of this radiotracer in the lymph nodes. Indeed, the added mannose

residues allow the protein to be recognized and internalized by macrophages, thus confirming the efficacy of the receptor mediated process of phagocytosis.

2.8. CONCLUSIONS

Having a basic understanding of what is occurring at the microscopic level in the lymphatic system may allow for better appreciation of the parameters that influence the biological properties of current SLND tracers and, eventually, help to raise suggestions for the design of an ideal agent. This chapter has therefore attempted to briefly outline the anatomy and physiology of the lymphatic system and to illustrate how the functioning of this circulatory system can affect the fate of exogenous materials in the body. Some oversimplifications of the complex mechanism underlying transport in the lymph and phagocytosis have been necessary, but hopefully without affecting the scientific value of the text.

For biological inert radiocolloids, not only size, but also shape and charge, play important roles in the overall uptake process by lymph nodes. It is interesting to note that most of the radiocolloids that are now approved for SLND were developed either for lymphoscintigraphy or for liver and spleen imaging. From a scientific perspective, these radiocolloids do not display the optimal characteristics required for a diagnostic agent.

Impressive progress has been achieved in very recent years in designing new agents whose uptake by lymph nodes is mediated by a receptor–ligand interaction mechanism. With the use of this kind of new agent, nuclear medicine has further strengthened its leading position as an MI discipline.

REFERENCES TO CHAPTER 2

[2.1] SWARTZ, M.A., The physiology of the lymphatic system, Adv. Drug. Deliv. Rev. **50** (2001) 3–20.

[2.2] SZUBA, A., SHIN, W.S., STRAUSS, H.W., ROCKSON, S., The third circulation: radionuclide lymphoscintigraphy in the evaluation of lymphoedema, J. Nucl. Med. **44** (2003) 43–57.

[2.3] SCHULTE-MERKER, S., SABINE, A., PETROVA, T.V., Lymphatic vascular morphogenesis in development, physiology, and disease, J. Cell Biol. **1193** (2011) 607–618.

[2.4] ALITALO, K., The lymphatic vasculature in disease, Nat. Med. **17** (2011) 1371–1380.

[2.5] SKOBE, M., DETMAR, M., Structure, function, and molecular control of the skin lymphatic system, J. Investig. Dermatol. Symp. Proc. **5** (2000) 14–9.

[2.6] WILLARD-MACK, C.L., Normal structure, function, and histology of lymph nodes, Toxicol. Pathol. **34** (2006) 409–424.

[2.7] SHIER, D., BUTLER, J., LEWIS, R., Holes's Human Anatomy and Physiology, 12th edn, McGraw-Hill Science/Engineering/Math, New York (2009).

[2.8] BALUK, P., et al., Functionally specialized junctions between endothelial cells of lymphatic vessels, J. Exp. Med. **204** (2007) 2349–2362.

[2.9] DEJANA, E., ORSENIGO, F., MOLENDINI, C., BALUK, P., McDONALD, D.M., Organization and signaling of endothelial cell-to-cell junctions in various regions of the blood and lymphatic vascular trees, Cell Tissue Res. **335 (**2009) 17–25.

[2.10] CASTENHOLZ, A., "Structure of initial and collecting lymphatic vessels", Lymph Stasis: Pathophysiology, Diagnosis and Treatment (OLSZEWSKI, W.L., Ed.), CRC Press, Boca Raton, FL (1991), 15–41.

[2.11] IKOMI, F., SCHMID-SCHONBEIN, G., Lymph transport in the skin, Clin. Dermatol. **13** (1995) 419–427.

[2.12] LEAK, L.V., Lymphatic removal of fluids and particles in the mammalian lung, Environ. Health Perspect. **35** (1980) 55–76.

[2.13] CASTENHOLZ, A., Strukturbild und Wirkungsweise der "initialen lymphbahn", Z. Lymphol. **81** (1984) 55–64.

[2.14] WIIG, H., SWARTZ, M.A., Interstitial fluid and lymph formation and transport: physiological regulation and roles in inflammation and cancer, Physiol. Rev. **92** (2012) 1005–1060.

[2.15] FRANTZ, C., STEWART, K.M., WEAVER, V.M., The extracellular matrix at a glance, J. Cell Sci. **123** (2010) 4195–4200.

[2.16] KADLER, K.E., BALDOCK, C., BELLA, J., BOOT-HANDFORD, R.P., Collagens at a glance, J. Cell. Sci. **120** (2007) 1955–1958.

[2.17] LI, S.T., KATZ, E.P., An electrostatic model for collagen fibrils. The interaction of reconstituted collagen with Ca^{2+}, Na^+, and Cl^-, Biopolymers **15** (1976) 1439–1460.

[2.18] SCOTT, J.E., Structure and function in extracellular matrices depend on interactions between anionic glycosaminoglycans, Pathol. Biol. **49** (2001) 284–289.

[2.19] CASLEY-SMITH, J.R., The fine structure and functioning of tissue channels and lymphatics, Lymphology **13** (1980) 120–129.

[2.20] ZAWIEJA, D.C., Contractile physiology of lymphatics, Lymphat. Res. Biol. **7** (2009) 87–96.

[2.21] SAINTE-MARIE, G., PENG, F.S., BELISLE, C., Overall architecture and pattern of lymph flow in the rat lymph node, Am. J. Anat. **164** (1982) 275–309.

[2.22] CLARK, S.L., Jr., The reticulum of lymph nodes in mice studied with the electron microscope. Am. J. Anat. **110** (1962) 217–257.

[2.23] LUK, S.C., NOPAJAROONSRI, C., SIMON, G.T., The architecture of the normal lymph node and hemolymph node. A scanning and transmission electron microscopic study, Lab. Invest. **29** (1973) 258–265.

[2.24] LUDWIG, J., Über Kurschlusswege der Lymphbahnen und ihre Beziehungen zur lymphogen Krebsmetastasierung, Pathol. Microbiol. **25** (1962) 329–334.

[2.25] TANIS, P.J., NIEWEG, O.E., VALDÉS OLMOS, R.A., KROON, B.B., Anatomy and physiology of lymphatic drainage of the breast from the perspective of sentinel node biopsy, J. Am. Coll. Surg. **192** (2001) 399–409.

[2.26] FRIER, M., "Phagocytosis", Progress in Radiopharmacology (COX, P.H., Ed.), Elsevier, Amsterdam (1981) 249–260.

[2.27] GUYTON, A.C., Textbook of Medical Physiology, 7th edn, W.B. Saunders (1986).

[2.28] RABINOVITCH, M., Professional and non-professional phagocytes: an introduction, Trends Cell. Biol. **5** (1995) 85–87.

[2.29] ADEREM, A., UNDERHILL, D.M., Mechanisms of phagocytosis in macrophages, Ann. Rev. Immunol. **17** (1999) 593–623.

[2.30] TAYLOR, P.R., et al., Macrophage receptors and immune recognition, Ann. Rev. Immunol. **23** (2005) 901–944.

[2.31] TAHL, P.D., EZEKOWITZ, R.A., The mannose receptor is a pattern recognition receptor involved in host defense, Curr. Opin. Immunol. **10** (1998) 50–55.

[2.32] STAHL, P.D., RODMAN, J.S., MILLER, M.J., SCHLESINGER, P.H., Evidence for receptor-mediated binding of glycoproteins, glycoconjugates, and lysosomal glycosidases by alveolar macrophages, Proc. Natl. Acad. Sci. USA **75** (1978) 1399–1403.

[2.33] SHEPHERD, V.L., LEE, Y.C., SCHLESINGER, P.H., STAHL, P.D., L-Fucose-terminated glycoconjugates are recognized by pinocytosis receptors on macrophages, Proc. Natl. Acad. Sci. USA **78** (1981) 1019–1022.

[2.34] HUBBARD, A.L., WILSON, G., ASHWELL, G., STUKENBROK, H., An electron microscope autoradiographic study of the carbohydrate recognition systems in rat liver. I. Distribution of ^{125}I-ligands among the liver cell types, Cell Biol. **83** (1979) 47–64.

[2.35] MARTINEZ-POMARES, L., et al., Carbohydrate-independent recognition of collagens by the macrophage mannose receptor. Eur. J. Immunol. **36** (2006) 1074–1082.

[2.36] FIETE, D.J., BERANEK, M.C., BAENZIGER, J.U., A cysteine-rich domain of the "mannose" receptor mediates GalNAc-4-SO$_4$ binding, Proc. Natl. Acad. Sci. USA **95** (1998) 2089–2093.

[2.37] LETEUX, C., et al., The cysteine-rich domain of the macrophage mannose receptor is a multispecific lectin that recognizes chondroitin sulfates A and B and sulfated oligosaccharides of blood group Lewis(a) and Lewis(x) types in addition to the sulfated N-glycans of lutropin, J. Exp. Med. **191** (2000) 1117–1126.

[2.38] YOO, M.K., et al., Superparamagnetic iron oxide nanoparticles coated with mannan for macrophage targeting. J. Nanosci. Nanotechnol. **8** (2008) 5196–5202.

[2.39] NAHAR, M., JAIN, N.K., Preparation, characterization and evaluation of targeting potential of amphotericin B-loaded engineered PLGA nanoparticles, Pharm. Res. **26** (2009) 2588–2598.

[2.40] NIMJE, N., et al., Mannosylated nanoparticulate carriers of rifabutin for alveolar targeting, J. Drug Target. **17** (2009) 777–787.

[2.41] PRAKASH, J., et al., Tumor-targeted intracellular delivery of anticancer drugs through the mannose-6-phosphate/insulin-like growth factor II receptor, Int. J. Cancer **126** (2010) 1966–1981.

[2.42] JAIN, N.K., MISHRA, V., MEHRA, N.K., Targeted drug delivery to macrophages, Expert Opin. Drug Deliv. **10** (2013) 353–367.

[2.43] KELLY, C., JEFFERIES, C., CRYAN, S.A., Targeted liposomal drug delivery to monocytes and macrophages. J. Drug Deliv. **2011** (2011), 727241.

[2.44] CABANAS, R.M., An approach for the treatment of penile carcinoma, Cancer **39 (**1977) 456–466.

[2.45] ALAZRAKI, N.P., et al., Lymphoscintigraphy, the sentinel node concept, and the intraoperative gamma probe in melanoma, breast cancer, and other potential cancers, Semin. Nucl. Med. **27** (1997) 55–67.

[2.46] VERONESI, U., et al., Sentinel-node biopsy to avoid axillary dissection in breast cancer with clinically negative lymph nodes, Lancet **349** (1997) 1864–1867.

[2.47] KESHTGAR, M.R.S., ELL, P.J., Sentinel lymph node detection and imaging, Eur. J. Nucl. Med. **26 (**1999) 57–67.

[2.48] MARIANI, G., et al., Radioguided sentinel lymph node biopsy in breast cancer surgery, J. Nucl. Med. **42** (2001) 1198–1215.

[2.49] BUSCOMBE, J., et al., Sentinel node in breast cancer procedural guidelines, Eur. J. Nucl. Med. Mol. Imaging **34** (2007) 2154–2159.

[2.50] WILHELM, A.J., MIJNHOUT, G.S., FRANSSEN, E.J., Radiopharmaceuticals in sentinel lymph-node detection: an overview, Eur. J. Nucl. Med. **26** (1999) S36–S42.

[2.51] HAWLEY, A.E., DAVIS, S.S., ILLUM, L., Targeting of colloids to lymph nodes: influence of lymphatic physiology and colloidal characteristics, Adv. Drug Deliv. Rev. **17** (1995) 129–148.

[2.52] MITRAGOTRI, S., LAHANN, J., Physical approaches to biomaterial design, Nat. Mater. **8** (2009) 15–23.

[2.53] MOGHIMI, S.M., BONNEMAIN, B., Subcutaneous and intravenous delivery of diagnostic agents to the lymphatic system: applications in lymphoscintigraphy and indirect lymphography, Adv. Drug Deliv. Rev. **37** (1999) 295–312.

[2.54] BERGQVIST, L., STRAND, S.E., PERSSON, B.R., Particle sizing and biokinetics of interstitial lymphoscintigraphic agents, Semin. Nucl. Med. **13** (1983) 9–19.

[2.55] UREN, R.F., HOWMAN-GILES, R.B., THOMPSON, J.F., Regarding sentinel lymph node localization in early breast cancer, J. Nucl. Med. **40** (1999) 1403–1406.

[2.56] NÚÑEZ, E.G., et al., Influence of colloid particle profile on sentinel lymph node uptake, Nucl. Med. Biol. **36** (2009) 741–747.

[2.57] HULTBORN, K.A., LARSSO, L.-G., RAGNHULT, I., The lymphodrainage from the breast to the axillary and parasternal lymph nodes, studied with the aid of colloidal Au^{198}, Acta Radiol. **43** (1955) 52–64.

[2.58] TSOPELAS, C., Particle size analysis of ^{99m}Tc-labeled and unlabeled antimony trisulfide and rhenium sulfide colloids intended for lymphoscintigraphic application, J. Nucl. Med. **42** (2001) 460–466.

[2.59] GOMMANS, G.M.M., et al., Further optimisation of ^{99m}Tc-Nanocoll sentinel node localisation in carcinoma of the breast by improved labeling, Eur. J. Nucl. Med. **28 (**2001) 1450–1455.

[2.60] JIMENEZ, I.R., et al., Particle sizes of colloids to be used in sentinel lymph node radiolocalization, Nucl. Med. Commun. **29** (2008) 166–172.

[2.61] HUNG, J.C., et al., Filtered technetium-99m-sulfur colloid evaluated for lymphoscintigraphy, J. Nucl. Med. **36** (1995) 1895–1901.

[2.62] HIGASHI, H., et al., Particle size of tin and phytate colloid in sentinel node identification, J. Surg. Res. **121** (2004) 1–4.

[2.63] PAGANELLI, G., et al., Optimized sentinel node scintigraphy, Q. J. Nucl. Med. **42** (1998) 49–53.

[2.64] CHAMPION, J.A., KATARE, Y.K., MITRAGOTRI, S., Particle shape: a new design parameter for micro- and nanoscale drug delivery carriers, J. Control. Rel. **121** (2007) 3–9.

[2.65] MITRAGOTRI, S., In drug delivery, shape does matter, Pharm. Res. **26** (2009) 232–234.

[2.66] DECUZZI, P., PASQUALINI, R., ARAP, W., FERRARI, M., Intravascular delivery of particulate systems: does geometry really matter? Pharm. Res. **26** (2009) 235–243.

[2.67] CHAMPION, J.A., MITRAGOTRI, S., Role of target geometry in phagocytosis, Proc. Natl. Acad. Sci. USA **103** (2006) 4930–4934.

[2.68] LU, Z., QIAO, Y., ZHENG, X.T., CHAN-PARKA, M.B., LI, C.M., Effect of particle shape on phagocytosis of CdTe quantum dot–cystine composites, Med. Chem. Commun. **1** (2010) 84–86.

[2.69] REDDY, S.T., BERK, D.A., JAIN, R.K, SWARTZ, M.A., A sensitive in vivo model for quantifying interstitial convective transport of injected macromolecules and nanoparticles, J. Appl. Physiol. **101** (2006) 1162–1169.

[2.70] HIRANO, K., HUNT, C.A., STRUBBE, A., MacGREGOR, R.D., Lymphatic transport of liposome encapsulated drugs following intraperitoneal administration-effect of liposome composition, Pharm. Res. **6** (1985) 271–278.

[2.71] PATEL, H.M., BOODLE, K.M., VAUGHAN-JONES, R., Assessment of the potential uses of liposomes for lymphoscintigraphy and lymphatic drug delivery: failure of [99m]technetium marker to represent intact liposomes in lymph nodes, Biochim. Biophys. Acta **801** (1984) 76–86.

[2.72] AHSAN, F., RIVAS, I.P., KHAN, M.A., TORRES SUAREZ, A.I., Targeting to macrophages: role of physicochemical properties of particulate carriers – liposomes and microspheres – on the phagocytosis by macrophages, J. Control. Rel. **79** (2002) 29–40.

[2.73] FIDLER, I.J., RAZ, A., FOGLER, W.E., Design of liposomes to improve delivery of macrophage-augmenting agents to alveolar macrophages, Cancer Res. **40** (1980) 4460–4466.

[2.74] WILKINS, D.J., MYERS, P.A., Studies on the relationship between the electrophoretic properties of colloids and their blood clearance and organ distribution in the rat, Br. J. Exp. Pathol. **47** (1966) 568–576.

[2.75] AYHAN, H., TUNCEL, A., BOR, N., PISKIN, E., Phagocytosis of monosize polystyrene-based microspheres having different size and surface properties, J. Biomater. Sci. Polym. **7** (1995) 329–342.

[2.76] TABATA, Y., IKADA, Y., Effect of the size and surface charge of polymer microspheres on their phagocytosis by macrophage, Biomaterials **9** (1988) 356–362.

[2.77] PATEL, H.M., Serum opsonins and liposomes: their interaction and opsonophagocytosis, Crit. Rev. Ther. Drug Carrier Syst. **9** (1992) 39–90.

[2.78] ILLUM, L., DAVIS, S.S., The organ uptake of intravenously administered colloidal particles can be altered using a non-ionic surfactant (Poloxamcr 338), FEBS Lett. **167** (1984) 79–82.

[2.79] MOGHIMI, S.M., et al., Surface engineered nanospheres with enhanced drainage into lymphatics and uptake by macrophages of the regional lymph nodes, FEBS Lett. **344** (1994) 25–30.

[2.80] SUPERSAXO, A., HEIN, W.R., STEFFEN, H., Effect of molecular weight on the lymphatic absorption of water-soluble compounds following subcutaneous administration, Pharm. Res. **7** (1990) 167–169.

[2.81] McNEILL, G.C., et al., Whole-body lymphangioscintigraphy: preferred method for initial assessment of the peripheral lymphatic system, Radiology **172** (1989) 495–502.

[2.82] HENZE, E., et al., Lymphoscintigraphy with Tc-99m-labeled dextran, J. Nucl. Med. **23** (1982) 923–929.

[2.83] SADEK, S., OWUNWANNE, A., ABDEL-DAYEM, H.M., YACOUB, T., Preparation and evaluation of Tc-99m hydroxyethyl starch as a potential radiopharmaceutical for lymphoscintigraphy: comparison with Tc-99m human serum albumin, Tc-99m dextran, and Tc-99m sulfur microcolloid, Lymphology **22** (1989) 157–166.

[2.84] JUMA, N., ANDREY, T., EGE, G.N., Comparison as a lymphoscintigraphic agent between $^{99}Tc^m$ dextran and $^{99}Tc^m$ antimony sulphide colloid, Br. J. Radiol. **58** (1985) 325–330.

[2.85] EDREIRA, M.M., COLOMBO, L.L., PEREZ, J.H., SAJAROFF, E.O., DE CASTIGLIA, S.G., In vivo evaluation of three different ^{99m}Tc-labelled radiopharmaceuticals for sentinel lymph node identification, Nucl. Med. Commun. **22** (2001) 499–504.

[2.86] KARAYALCIN, B., ARAS, G., ERBAY, G., ERCAN, M.T., Parasternal lymphoscintigraphy using $^{99}Tc^m$-dextran, Nucl. Med. Commun. **9** (1988) 657–662.

[2.87] OFFODILE, R., et al., Minimally invasive breast carcinoma staging using lymphatic mapping with radiolabeled dextran, Cancer **82** (1998) 1704–1708.

[2.88] BARROS, A., CARDOSO, M.A., SHENG, P.Y., COSTA, P.A., PELIZON, C., Radioguided localisation of non-palpable breast lesions and simultaneous sentinel lymph node mapping, Eur. J. Nucl. Med. Mol. Imaging. **29** (2002) 1561–1565.

[2.89] MATSUNAGA, K., et al., Technetium labeling of dextran incorporating cysteamine as a ligand, Nucl. Med. Biol. **32** (2005) 279–285.

[2.90] NATHANSON, S.D., ANAYA, P., KARVELIS, K.C., ECK, L., HAVSTAD, S., Sentinel lymph node uptake of two different technetium-labeled radiocolloids, Ann. Surg. Oncol. **4** (1997) 104–110.

[2.91] GLASS, E.C., ESSNER, R., MORTON, D.L., Kinetics of three lymphoscintigraphic agents in patients with cutaneous melanoma, J. Nucl. Med. **39** (1998) 1185–1190.

[2.92] BEDROSIAN, I., et al., ^{99m}Tc-human serum albumin: an effective radiotracer for identifying sentinel lymph nodes in melanoma, J. Nucl. Med. **40** (1999) 1143–1148.

[2.93] TAKEI, H., et al., ^{99m}Tc-phytate is better than ^{99m}Tc-human serum albumin as a radioactive tracer for sentinel lymph node biopsy in breast cancer, Surg. Today **36** (2006) 219–224.

[2.94] VERA, D.R., WALLACE, A.M., HOH, C.K., MATTREY, R.F., A synthetic macromolecule for sentinel node detection: (^{99m})Tc-DTPA-mannosyl-dextran, J. Nucl. Med. **42** (2001) 951–959.

[2.95] SONDAK, V.K., et al., Combined analysis of phase III trials evaluating [^{99m}Tc] tilmanocept and vital blue dye for identification of sentinel lymph nodes in clinically node-negative cutaneous melanoma, Ann. Surg. Oncol. **20** (2013) 680–688.

[2.96] WALLACE, A.M., et al., Comparative evaluation of [(^{99m})Tc]tilmanocept for sentinel lymph node mapping in breast cancer patients: results of two phase 3 trials, Ann. Surg. Oncol. **20** (2013) 2590–2599.

[2.97] TAKAGI, K., et al., ^{99m}Tc-labeled mannosyl-neoglycoalbumin for sentinel lymph node identification, Nucl. Med. Biol. **31** (2004) 893–900.

Chapter 3

CLINICAL APPLICATIONS OF RADIOGUIDED SLNB

F. ORSINI, G. MARIANI
Regional Center of Nuclear Medicine,
University of Pisa Medical School,
Pisa, Italy

3.1. SUMMARY

A survey of the most important clinical applications of SLNB, which is accomplished using radiolabelled nanocolloidal particles, is presented in this chapter. In particular, emphasis is given to the diagnostic value of this procedure for the treatment of various degenerative diseases.

3.2. INTRODUCTION

The most advanced diagnostic techniques of preoperative imaging (computed tomography (CT), magnetic resonance imaging, ultrasound, single photon emission tomography (SPECT), positron emission tomography (PET) and PET/CT) provide information of increasing quality regarding topographical location and extent of neoplastic disease. The surgeon can thus rely on such information for planning the optimal surgical approach tailored to each individual patient, with the final goal of radically removing the tumour, while, at the same time, limiting the aggressiveness of surgery, within the increasingly common scenario for oncological surgery to become less and less mutilating and to adopt minimally invasive surgical procedures.

Intraoperatively, radioguidance provides the surgeon with an additional interaction modality that enables exploration of the surgical field by relying not only on the traditional modalities of direct visual inspection and palpation, but also on the possibility of identifying the tissue to be removed by preoperative labelling of the target tissue with a proper radiopharmaceutical. This additional guidance requires the use of an intraoperative gamma probe for detecting and localizing the site of accumulation of a radioactive compound (the radiopharmaceutical) at the target tissue, guiding the surgeon through an acoustic signal that is proportional to the amount of radioactivity detected by the probe. This combined procedure is termed radioguided surgery, and is sometimes also aided by the acquisition of intraoperative scintigraphic images using a dedicated, small-field-of-view

portable gamma camera. Although several different approaches based on radioguided surgery have been developed or are in various phases of clinical validation, the most widely utilized applications of this procedure concern SLNB in patients with solid epithelial cancers [3.1].

The popularity of radioguided surgery is increasing, not only in highly specialized and/or academic environments, but also in peripheral hospitals; this trend is especially obvious in the case of SLNB, or alternatively SLND, in patients with breast cancer or malignant CM, which are the two applications where the effectiveness of radioguided surgery has most definitely been proven. For these two cancers, the validity of the SLN concept is now also recognized by the most recent version of the manual for tumour staging developed by the American Joint Committee on Cancer, the so-called TNM system (where T stands for status of the primary tumour, N for status of locoregional lymph nodes and M for distant metastases) [3.2]. In fact, both for breast cancer and for melanoma, the N parameter includes specific notations for the presence of macrometastasis, micrometastasis or isolated tumour cells in the SLN. In this regard, because no imaging modality is able to detect microscopic metastasis (nor the presence of isolated tumour cells), such information must be based on histopathological analysis of the SLN. Therefore, SLNB emerges as the only reliable method for identifying micrometastatic disease in regional lymph nodes, and is now the accepted standard of care in various clinical conditions, in particular, for patients with early stage breast cancer and CM. Nevertheless, despite its established benefits as a minimally invasive approach for nodal staging, SLNB is still relatively underutilized in patients with tumours other than breast cancer and CM.

In the past 5 years, there has been momentum in technology and in clinical research, thus opening new avenues to novel strategies for radioguided surgery. In this setting, the ongoing integration of 'virtual reality' approaches with standard approaches in some well defined conditions is increasing, facilitating the use of minimally invasive surgeries. Indeed, MI—in particular, radionuclide imaging — is becoming essential for optimizing surgical approaches that are tailored to the disease-specific conditions encountered. This synergy has fostered growing interactions between surgical specialties (mostly oncological surgery) and nuclear medicine. In this new perspective, different medical specialties cooperate to achieve a common goal of improved patient management and overall benefit [3.3].

Key concepts of SLNB include the following:

— SLNB is a specific application of radioguided surgery.
— Labelling a tissue with a radioactive compound provides the surgeon with the opportunity to identify the target tissue to be removed.

— A gamma probe is able to localize the site of accumulation of the radiopharmaceutical at the target tissue, guiding the surgeon through an acoustic signal.
— SLNB can be applied to solid epithelial cancers and, in particular, SLNB has been validated in breast cancer and melanoma.
— SLNB allows detection of micrometastases and isolated tumour cells by detailed histopathological analysis.

3.3. SLNB IN BREAST CANCER

Breast cancer is the most frequent type of cancer diagnosed in women worldwide. In the USA, more than 209 000 new cases were diagnosed in 2009, with more than 40 000 deaths from this malignancy [3.4].

The rationale for SLNB in the surgical treatment of breast cancer is based on the fact that, in the case of lymphatic metastasis, the tumour spreads through the lymphatic system following an orderly progression, from the first level to higher levels (Fig. 3.1). Therefore, the first lymph node encountered by the lymph in its route from the site of the primary tumour to the basin of lymphatic drainage (i.e. the SLN) is the most likely to be the first site of metastasis, and is therefore to be considered as the 'lymph nodal sentinel' for the detection of early lymphatic metastasis; conversely, the absence of metastasis in the SLN stands for absent metastatic involvement of all other lymph nodes in the same lymphatic chain.

Thus, in breast cancer as in other solid tumours, the SLN is a lymph node that first receives direct lymphatic drainage from the breast neoplasm. Usually, there are one or two SLNs, but occasionally, more nodes can be identified by lymphoscintigraphic mapping and during an intraoperative search with a gamma probe. International meetings on SLNB have reached consensus over the procedures to be employed, and many national and international scientific societies have published their own recommendations [3.5−3.20].

Once identified (either pre- or intraoperatively through lymphoscintigraphy), the SLN can be surgically removed and histologically analysed for prognostic and therapeutic strategy purposes. In fact, when the SLN does not harbour metastasis, this procedure avoids unnecessary radical axillary lymph node dissection. Only when metastasis is found in the SLN should radical lymph node dissection be performed.

Preoperatively, the axillary lymph node status can be assessed by clinical examination (with rather low sensitivity), by ultrasound (more sensitive, especially if including fine needle aspiration cytology, if necessary) [3.21] and by ^{18}F fluorodeoxyglucose PET/CT (>95% specificity, but low sensitivity for lymph nodes < 5–8 mm in size). Detection of axillary lymph node metastasis by
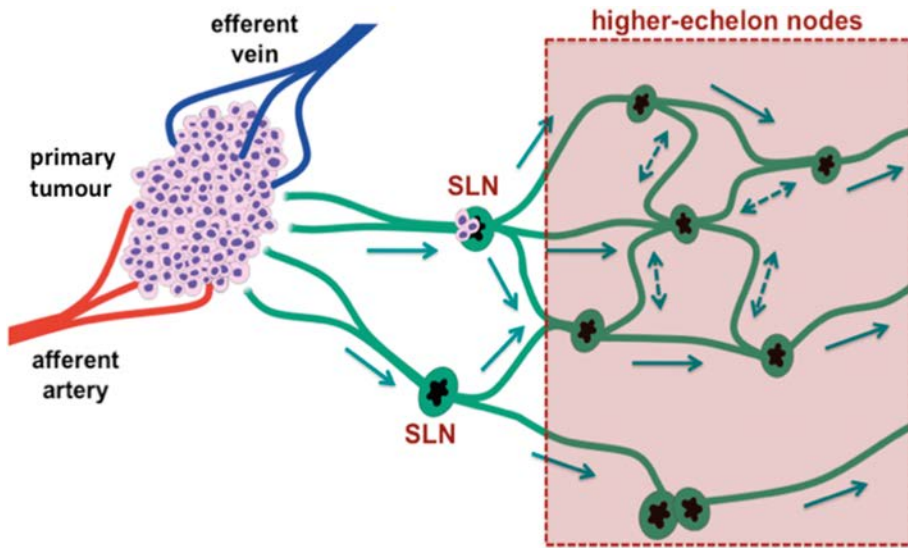
FIG. 3.1. Schematic representation of the migration of cancerous cells from primary lesion to SLNs following lymphatic flow.

any of the above evaluation techniques mandates de novo axillary lymph node dissection. Therefore, these patients are not candidates for SLNB.

Nevertheless, given the limited sensitivity of imaging techniques for evaluating the axillary lymph node status, the axillary lymphatic basin must be explored surgically. In fact, according to the TNM approach, the locoregional lymph node status is an essential component for prognostic purposes and for selecting the most appropriate treatment strategy; in this regard, the status of axillary lymph nodes remains the most important prognostic factor for survival [3.22].

Depending on the status of the axilla, different therapeutic strategies are adopted in terms of surgery, adjuvant chemotherapy, radiotherapy and hormonal therapy. In addition, axillary lymph node dissection provides excellent locoregional control of disease in the case of metastasis.

About 30%–40% of patients without palpable lymph nodes will develop macroscopic axillary recurrence if axillary lymph node dissection is not performed, regardless of adjuvant chemotherapy. However, it should be noted that in prospective randomized trials, a significant increase of overall survival has never been demonstrated for patients treated with axillary dissection compared to those who have not undergone the procedure.

Radical de novo axillary lymph node dissection, in addition to excision of the primary tumour, has, for some decades, represented the standard surgical

procedure for patients with breast cancer. However, this surgical procedure has considerable impact on the wellbeing of patients because a non-negligible proportion of them (5%–20%) suffer from significant complications such as prolonged wound healing, pain, lymphoedema and motor sensory impairment.

On the other hand, the fraction of patients who, after lymph node axillary dissection, are found to actually have axillary metastasis at the time of lumpectomy is directly related to the diameter of the primary tumour, and only amounts to approximately 20%–30% of the cases in early stage breast cancer. Thus, on average, at least 70% of these patients undergo radical axillary dissection without proof that they actually need such an aggressive procedure (yet with the same associated morbidity experienced by patients for whom axillary dissection is potentially beneficial). In this regard, it should be noted that the SLNB procedure entails significantly reduced morbidity compared to radical axillary dissection [3.23].

In the perspective of reducing the number of such unnecessary de novo axillary dissections, Giuliano et al. [3.6, 3.7] first described, in 1994, their experience with the use of a vital dye (Evans blue) injected around the primary tumour site to find SLNs in patients with breast cancer. This technique of intraoperative lymphatic mapping then evolved (and actually improved) with the adoption of ^{99m}Tc labelled colloids for lymphatic mapping, and with the introduction of an intraoperative gamma probe for identifying the source of radioactivity (the SLN(s) that had trapped the radiocolloid injected interstitially at the tumour site) in the surgical field.

SLNM and SLNB can be performed using the blue dye, the radiocolloid or both. SLNM with radiocolloids alone leads to successful SLN identification in more than 97% of cases; the blue dye technique alone has a lower success rate (75%–80%). The use of both techniques can further increase the success rate to 99%, especially when associated with lymphoscintigraphy. The combined procedure has the advantage of also identifying massively metastatic SLNs, an occurrence where extensive replacement of the normal tissue (in particular, macrophages) with tumour cells may prevent efficient radiocolloid accumulation in the affected lymph node [3.24, 3.25].

When lymphatic mapping is not successful, full axillary lymphadenectomy is generally necessary to allow assessment of the status of the axillary lymph nodes.

It should be emphasized that adequate training of a multidisciplinary team is required to reduce the number of unsuccessful SLNM procedures, as well as the potentially associated morbidity. In fact, correctly performing radioguided SLNB is based on the collaboration of different specialists, including surgeons, nuclear physicians and pathologists. Incorporation of radiologists and radiotherapists into such a multidisciplinary team should also be encouraged [3.18, 3.26].

Key concepts of SLNB include the following:

— Radical axillary lymph node dissection has, for some decades, represented the standard surgical procedure for patients with breast cancer.
— Only in 20%–30% of cases of early stage breast cancer is lymphatic metastasis detected by radical axillary dissection.
— Approximately 5%–20% of patients undergoing radical axillary dissection suffer from disabling complications.
— SLNB is a procedure for identifying those lymph nodes that are most likely to be the first sites of lymphatic metastasis.
— The absence of metastasis in the SLNs represents absent metastatic involvement of all other lymph nodes in the same lymphatic chain.
— Only when metastasis is found in the SLN should radical axillary lymph node dissection be performed.
— The false negative rate (i.e. tumour recurrence in an axilla that had been classified as negative for metastasis based on SLNB) is 3%–5%.
— Histopathological analysis is more accurate when focused on only one (or a few) lymph node(s) and combined with complete sectioning and staining of the whole lymph node, rather than only two to three sections per node.
— The rates of detection and intraoperative harvesting of internal mammary chain SLNs are much lower than those for axillary SLNs, and the clinical significance and impact of internal mammary chain SLNB on outcome are still being debated.

When the SLNB procedure is correctly performed and the SLN is found to be free from metastasis, the negative predictive value of this finding for metastatic involvement of other axillary lymph nodes is very high, ~95%–97%. This means that only in a low percentage of cases (3%–5%) may the SLNB technique yield false negative results. In this regard, the false negative rate can be defined as the proportion of patients with negative SLNB who actually have disease in the axillary lymph nodes, as shown either by completion axillary lymphadenectomy (as was initially done in early clinical validation studies) or during follow-up. The current gold standard to assess the false negative rate for SLN axillary staging is long term follow-up (assessing for appearance of axillary metastasis in an axilla that had been classified as negative on the basis of the SLNB). In fact, sufficient experience has now been published to compare the axilla disease-free survival time after SLNB and after lymphadenectomy [3.27]. More recently, the survival benefit of SLNB was addressed in the National Surgical Adjuvant Breast and Bowel Project trial B-32 (NSABP-32) that randomized 5611 women to SLNB versus SLNB + axillary lymphadenectomy. After a mean follow-up of

95.6 months, the SLNB arm displayed a 90.3% survival rate at 8 years versus 91.8% in the axillary lymphadenectomy arm (with the difference being not statistically significant) [3.28]. These findings, based on long term follow-up, therefore confirm earlier data from the same clinical protocol suggesting that, in the case of negative SLNB, there are no significant differences regarding disease-free survival, overall survival and local control of disease between patients undergoing de novo axillary lymph node dissection and those not undergoing axillary dissection because of a negative SLNB [3.29].

Nevertheless, it should be noted that false negative SLNB procedures are higher in patients with higher pathological grading of the tumour (grade 3), as well as in patients in whom only one SLN was retrieved intraoperatively, compared to patients in whom multiple SLNs were retrieved [3.30]. Regarding analysis of the SLN, it should be emphasized that with this approach, the attention of the pathologist is focused on only one (or a few) SLN(s), rather than on the up to 20–25 lymph nodes that are typically retrieved during full axillary dissection. Therefore, this low nuber of SLNs can be analysed more accurately, for instance, with complete sectioning and staining of the whole lymph node rather than with only two to three sections per node. Immunohistochemistry (and, to a greater degree, molecular analysis using the technique of reverse transcriptase polymerase chain reaction (RT-PCR)), further improves the sensitivity of analysis, possibly leading to the identification of micrometastases and even isolated tumour cells, which cannot be assessed with conventional haematoxylin eosin staining. In this regard, micrometastasis, which is observed in approximately 10%–20% of the SLNs so extensively analysed, entails a certain risk of metastatic involvement of upper echelon lymph nodes. Therefore, SLNB has improved the overall accuracy of the histopathological staging of the axilla in breast cancer patients because it enables the detection of minimal nodal metastatic involvement (micrometastases) in patients with clinically negative axilla.

More recently, the results of a multicentric randomized study have suggested that radical axillary lymph node dissection may even be unnecessary for women with early breast cancer (T1 and T2) and axillary isolated tumour cells or micrometastases in the SLN (detected by haematoxylin eosin staining). In fact, the local recurrence rate was 2.5% in the SLNB-only group (i.e. patients who had not been submitted to axillary lymph node dissection despite having had a positive SLNB) versus 3.6% in the group of patients who had been submitted to axillary lymphadenectomy because of the positive SLNB finding. These results demonstrate that SLNB offers an excellent regional control in early breast cancer patients, even without axillary lymphadenectomy, as well as sufficient information to select adequate adjuvant therapy [3.31].

Another issue that deserves consideration concerns the patterns of radiocolloid migration to the internal mammary chain (IMN) observed in different patients. Although early studies showed great variation in the frequency of scintigraphic IMN visualization, it was later found that the detection rate of IMN SLNs is significantly affected by the depth of radiocolloid injection, in that lymphoscintigraphic mapping of the IMN requires deep injection of the radiocolloid, either peritumourally or intratumourally [3.32].

The rates of detection and intraoperative harvesting of IMN SLNs are much lower than those for axillary SLNs. In particular, IMN SLNs have been detected in about one third of patients with breast cancer, of which approximately 63%–92% could be harvested during surgery, and, of those, 11%–27% were metastatic [3.33–3.36].

However, the clinical significance and the impact of IMN SLNB on outcome are still being debated. In fact, even if there is some evidence that IMN mapping can lead to upstage migration and modification of treatment planning for radiotherapy and systemic therapy, there is no evidence supporting that SLNM of the IMN will improve the outcome of treatment and survival [3.37].

3.3.1. Indications and contraindications for SLNB in breast cancer

Basic recommendations for SLNB include an early stage biopsy of proven breast cancer (T1 and T2, up to 5 cm in maximum diameter) and appropriate selection of patients to undergo the SLNB procedure. In particular, preoperative diagnostic imaging of the axilla must be negative, and must include fine needle aspiration cytology in the case of suspicious lymph nodes [3.20]. In the case of preoperative findings indicating metastatic involvement of axillary lymph nodes, the patient should not undergo SLNB but rather full axillary lymph node dissection.

The emergence of molecular biology techniques for SLN analysis and the introduction of newer imaging techniques during SLNM, although posing new challenges, also enable the resolution of conditions that had been initially defined as contraindications for performing SLNB in patients with breast cancer. In fact, several meta-analyses and guidelines have been presented, and have led to general acceptance of the SLNB procedure in a wider spectrum of cases than initially accepted, such as in cases of multicentric/multifocal tumours, prior diagnostic or excisional breast biopsy, ductal carcinoma in situ, after neoadjuvant therapy or after previous breast surgery (including plastic surgery) [3.38−3.40].

For patients who have had previous breast surgery, lymph drainage may be changed (and follow unexpected patterns) in patients who have undergone prior breast or axillary surgical procedures, because non-axillary drainage has been identified more often in reoperative SLNB than in primary SLNB. In

73% of patients, migration to the regional nodal drainage basins has been noted in ipsilateral axillary, supraclavicular, internal mammary, interpectoral and contralateral axillary nodes [3.41].

Multifocal breast cancer is defined as separate foci of ductal carcinoma more than 2 cm apart within the same quadrant, while multicentric breast cancer indicates the presence of separate independent foci of carcinoma in different quadrants [3.42]. Until a few years ago, SLNB was considered to be contraindicated in patients with multicentric and multifocal breast cancer because it was believed that it was difficult to localize the true SLN, and a negative SLNB result would not exclude, in these cases, the possibility of metastasis being present in a lymph node draining from other regions of the breast. However, the majority of the breast can actually be considered as a single unit with lymph drainage to only a few designated lymph nodes in the axilla [3.43, 3.44].

Several studies have demonstrated an efficacy of radioguided SLNB in these patients equal to that commonly observed in patients with unicentric breast cancer. The presence of lymph node metastasis is significantly higher in SLNs, as well as in non-SLNs in patients with multicentric breast cancer; however, the sensitivity, false negative rate and overall accuracy of SLNB are similar in both conditions, although there are some discrepancies between the results reported by different groups [3.45−3.47].

Debate is still ongoing as to whether SLNB is accurate enough after neoadjuvant chemotherapy, or whether it should be performed before starting chemotherapy in patients with locally advanced breast cancer. Performing SLNB before or after neoadjuvant systemic treatment has advantages and disadvantages in each case. Before neoadjuvant chemotherapy (as accepted by American Society of Clinical Oncology guidelines), SLNB yields a more precise axillary, staging reliable information about the axillary lymph node status. However, it can delay the beginning of the treatment, and two surgeries can be needed in the same patient (i.e. SLNB before starting neoadjuvant chemotherapy, then surgery of the primary tumour). On the other hand, SLNB performed after such primary chemotherapy can assess the response at lymphatic level, but may lead to the underestimation of the initial stage [3.48]. Furthermore, after neoadjuvant chemotherapy, the SLND rate decreases, the rate of false negative cases increases and the long term local recurrence rate in patients in whom lymphadenectomy has not been performed because of a negative SLNB has yet to be determined. This group of patients was previously regarded as ineligible for SLNB, under the assumption that, after neoadjuvant chemotherapy, the lymph drainage pattern may not represent the pattern occurring in the tumour basin before chemotherapy, therefore possibly leading to false negative results. The available data show that there are no significant differences in the success rate of SLNB according to clinical tumour size or clinical nodal status, and that the false negative rate is

not affected by tumour response to chemotherapy. Recently, a systematic review of 24 clinical SLNB trials in patients with breast carcinoma after neoadjuvant chemotherapy was undertaken. The global SLN identification rate was 89.6%, with metastatic lymph node involvement being observed in 37% of the patients; the overall false negative rate was 8.4% [3.49−3.51].

Although pregnancy has traditionally been considered as a contraindication to performing radioguided SLNB, the radiodosimetric burden to patients is very low, and the benefit should be considered in those presenting early lesions. In pregnant patients with early lesions and clinically/ultrasound negative axilla, the possibility of performing a 1 day procedure including breast surgery and radioguided SLNB with administration of a low dose of radiocolloid should be considered. In fact, the available data indicate that radioguided SLNB can be performed safely and successfully in pregnant women with breast cancer, as it entails minimum risk to the fetus [3.52−3.54].

Radiation exposure of the fetus from the administered radiocolloid is very low and does not increase the risk of prenatal death, congenital malformation or mental impairment. On the other hand, blue dyes should not be used in pregnant patients [3.20].

Finally, some conditions that were previously considered as formal contraindications to SLNB have changed to possible applications, on a patient by patient basis [3.2, 3.18, 3.38]. These conditions include large or locally advanced invasive breast cancers (T3), ex situ ductal carcinoma, prior non-oncological breast surgery or axillary surgery, and the presence of suspicious palpable axillary lymph nodes.

Key concepts of SLNB include the following:

— Indications for SLNB consist of tumour diameters of less than 5 cm and a negative preoperative diagnostic imaging of the axilla (including fine needle aspiration in suspected axillary lymph nodes).
— Absolute contraindications of SLNB include clinical evidence of lymph node metastasis.
— Other relative contraindications such as pregnancy, multicentric/multifocal tumours, prior diagnostic or excisional breast biopsy, ductal carcinoma in situ, previous neoadjuvant therapy or previous breast surgery (including plastic surgery) are now not completely accepted, and each case has to be discussed individually.

3.3.2. SLNB procedures in breast cancer

The SLNB procedure consists of several sequential phases: radiocolloid injection, lymphoscintigraphy, intraoperative detection using a gamma probe

(aided or not by intraoperative imaging) and, finally, pathological analysis of the resected SLNs.

Lymphoscintigraphy for SLNM is usually performed approximately 3 h to 24 h before surgery, depending on logistics and/or the scheduled time of surgery. The radiopharmaceutical most commonly used in Europe consists of colloidal particles of HSA, ranging in size between 20 nm and 80 nm (Nanocoll), labelled with ^{99m}Tc. A radiocolloid activity of 7–30 MBq is generally injected in a volume of 0.2–0.8 mL, by means of a 25 gauge needle. In the case of obese patients, the activity to be administered is increased to 15–55 MBq. Following administration, the patient is invited to gently massage the breast for a few minutes to facilitate and accelerate lymphatic drainage.

There are different modalities of radiocolloid administration: intratumoural, peritumoural, intradermal, subdermal or perisubareolar.

Intratumoural injection requires higher volumes and activities of the radiopharmaceutical to overcome the high intratumoural pressure owing to abnormal lymphoneoangiogenesis; such high volumes of the radiocolloid cause some extravasation towards the peritumoural lymphatic vessels, thus initiating migration of the radiocolloid, which can be depicted by lymphoscintigraphy. Because of the reduced efficiency of lymphatic drainage within the tumour mass, the SLN is often visualized quite late after intratumoural radiocolloid injection.

Peritumoural (or intraparenchymal) administration consists of multiple injections of the radiocolloid around the tumour, under mammographic or ultrasound guidance in the event of non-palpable lesions. As observed after intratumoural injection, this technique results in good visualization of the axillary lymphatic drainage, but also of the IMN displaying the internal mammary lymph nodes (in 10%–30% of cases); however, the rate of radiocolloid migration from the injection site to the SLN is still quite slow.

Subdermal or intradermal injection of the radiocolloid on the skin projection of the breast tumour allows fast SLN visualization, by virtue of the remarkable development of the lymphatic network at that level. In fact, under physiological conditions, most of the lymphatic flow of the breast converges into the subareolar plexus of Sappey; lymph flow then proceeds from the deep zones to the more superficial subcutaneous plexus, which drains mostly to the anterior (or pectoral) group of axillary lymph nodes. With this technique, lymphoscintigraphic visualization of IMN SLNs is very rare (~1%–2%).

Finally, perisubareolar injection has more recently been proposed, based on the presence of the lymphatic plexus of Sappey, towards which lymph from virtually the entire breast seems to drain. It is the simplest method of injection and could be particularly appropriate in specific cases, such as non-palpable or multicentric/multifocal tumours, or in the case of previous lumpectomy.

Numerous studies have shown that, irrespective of the different modalities of radiocolloid injection described above (peritumoural, intradermal, subareolar), in virtually all patients, lymphoscintigraphy shows migration to the same SLN or group of SLNs. These findings therefore suggest that lymph from different regions of the breast reaches the same axillary lymph nodes.

Lymphoscintigraphy can be performed the day before surgery, or at least 2–3 h prior to surgery. A gamma camera equipped with a parallel hole, low energy, high resolution collimator is generally used. The patient is positioned supine, with the arms abducted (in the same position as during surgery), placing the collimator as close as possible to the axillary region. A ^{57}Co flood source can be positioned underneath the patient's body, to obtain some reference anatomical landmarks in the scintigraphic image. Alternatively, the body contour can be identified by moving a ^{57}Co point source along the patient's body during scintigraphic acquisition.

In the current protocol, a sequence of three static planar scans (in the oblique anterior, lateral and anterior projections) is acquired at least 5–10 min after radiocolloid administration (Figs 3.2 and 3.3). Dynamic acquisition can also be performed, starting immediately after radiocolloid injection, and it usually consists of sequential sets of a few minutes each. Such a dynamic imaging mode can be useful (although not always strictly required) to assess the initial kinetics of radiocolloid migration and to visualize the lymphatic routes leading to the SLNs. Using a point source of ^{57}Co, it is possible to mark the cutaneous projection of the SLN, to help the surgeon identify the best surgical approach. In the case of low/absent migration of the radiocolloid, late acquisitions are performed at 3 h or 18 h postinjection. In addition to identifying the SLNs, lymphoscintigraphy is also useful for identification of any unusual lymph draining basins, as well as radiocolloid migration to IMN SLNs, or even to intramammary, interpectoral or infraclavicular lymph nodes.

Major advances in the whole process of SLNM in the preoperative phase have been made possible by the use of SPECT/CT imaging [3.55, 3.56]. This is generally performed after acquiring delayed planar imaging (mostly 2–4 h after radiocolloid administration). SPECT/CT does not replace planar lymphoscintigraphy, but should rather be considered as a complementary imaging modality. The use of SPECT/CT acquisitions is particularly important for the identification of uptake 'foci' in cases of unusual lymph node draining basins, thus obviating the problem of identifying anatomical landmarks as a reference for anatomotopographic localization of the SLN(s) [3.57–3.59].
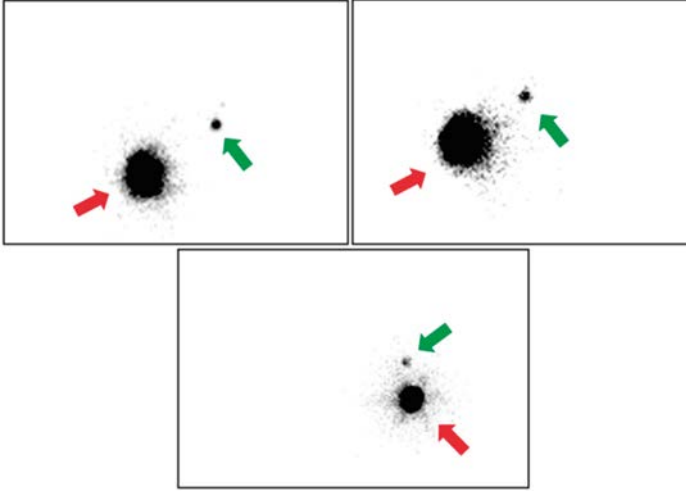
FIG. 3.2. Oblique anterior (top, left), lateral (top, right) and anterior (bottom) static projections, acquired 5–10 min after radiocolloid administration, showing exclusive migration to the first SLN (larger spot corresponds to the injection site).
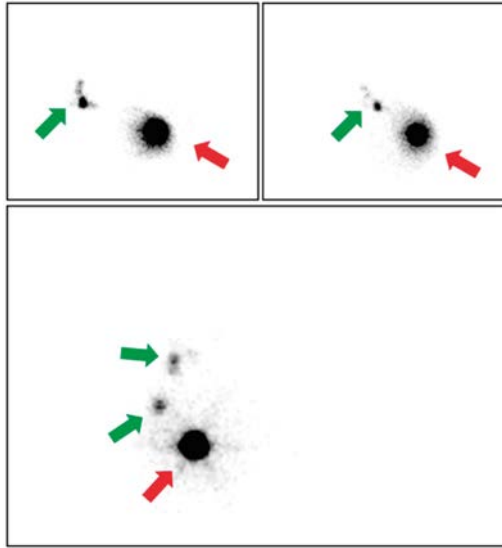
FIG. 3.3. Oblique anterior (top, left), lateral (top, right) and anterior (bottom) static projections, acquired 5–10 min after radiocolloid administration, also showing migration of radioactivity to lymph nodes adjacent to the first SLN (larger spot corresponds to the injection site).

An additional useful application of SPECT/CT imaging is in patients in whom the SLN is not visualized on planar imaging. Multiplanar reconstruction (MPR) enables two dimensional display of fusion images in relation to CT and SPECT, with the use of cross-reference lines allowing navigation between axial, coronal and sagittal views. At the same time, this tool enables correlation of the radioactive SLNs seen on the fused SPECT/CT images with the lymph nodes seen on CT images. This information may be helpful during the intraoperative procedure, as well as for assessing the completeness of excision using portable gamma cameras or probes. Fused SPECT/CT images may also be displayed using maximum intensity projection. This tool enables three dimensional (3-D) display, and improves anatomical localization of SLNs by summing up various slices. When using volume rendering for 3-D display, different colours are assigned to anatomical structures such as muscle, bone and skin (Figs 3.4 and 3.5). This facilitates better identification of anatomical reference points and incorporates an additional dimension in the recognition of SLNs.
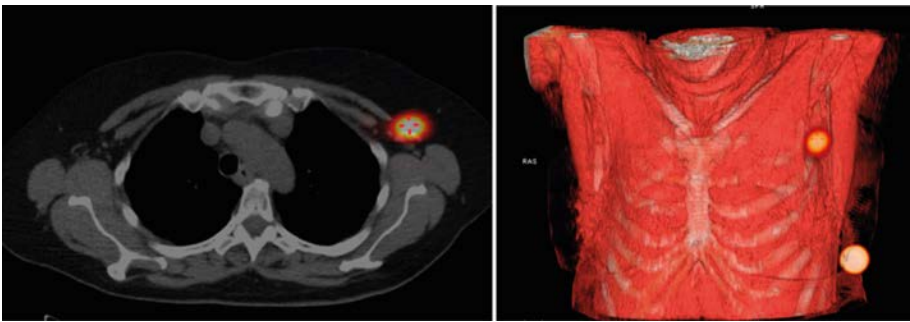
FIG. 3.4. Fused SPECT/CT image showing a thoracic lymph node (left) and the corresponding 3-D volume and colour rendering (right) showing bone and muscle anatomical structures.
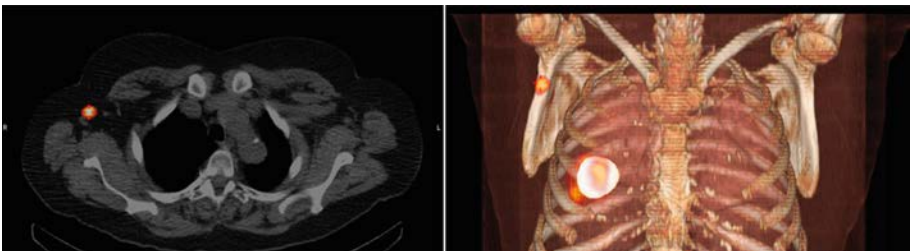
FIG. 3.5. Fused SPECT/CT image showing an axillary lymph node (left) and the corresponding 3-D volume and colour rendering (right) showing bone anatomical structures.

Intraoperative SLND is facilitated by a preliminary exploration of the axilla, with a gamma probe, to confirm the correct location of the skin mark placed on the skin projection of the SLN during lymphoscintigraphy. The gamma probe does not produce any scintigraphic image, but it yields both a numerical readout and an audible signal that is proportional to the counting rate, thus guiding the surgeon to the foci with the highest target/background ratios. A small incision is then performed in the skin region with maximum radioactive counts, along the ideal line for axillary dissection. When the tumour is located in the upper outer quadrant, access to the SLN can occur through the same surgical incision used for tumour excision. An intraoperative search of the SLN is performed by moving the gamma probe in different directions to precisely localize areas of maximum radioactivity accumulation, corresponding to the SLN [3.60].

Once the SLN has been removed, the gamma probe is utilized to obtain an ex vivo counting rate (to confirm that it is actually the SLN), and the surgical field is explored again with the probe, assessing residual radioactivity to confirm removal of the hot node(s). If necessary, the search continues for possible further radioactive lymph nodes. The SLN and any other nodes so identified are then sent for complete histopathological analysis.

During the past decade, dedicated portable gamma cameras for real time intraoperative imaging probes have become commercially available; they are generally employed not for actual radioguidance during surgery, but to confirm completeness of SLN removal [3.61−3.63]. Several recent reports outline the added value of imaging with portable gamma cameras in clinical and experimental settings for radioguided SLNB [3.64−3.69].

There is no delay between image acquisition and display (real time imaging), with the possibility of continuous monitoring and spatial orientation on the screen. However, because non-imaging gamma probes are still the standard equipment for radioguided surgery, the role of intraoperative imaging is generally limited, at least so far, to that of an additional aid to the surgeon for SLN identification. In particular, the usefulness of non-imaging probes in patients with breast cancer has been ascertained in particular cases with difficult lymphatic drainage or extra-axillary drainage, in cases with only faint lymph node radiocolloid uptake, when the SLN is located very close to the injection site, or finally, when no conventional gamma camera is available.

Novel technological advances have also made it possible to combine a spatial localization system and two tracking targets to be fixed on the patient's body and on a conventional hand held gamma probe, resulting in a new modality of 3-D localization of the traditional acoustic signal of the gamma probe. This feature, together with the real time information on depth that the system may provide, expands the application of radioguided SLNB in oncology, particularly for malignancies with deep lymphatic drainage patterns [3.70, 3.71].

On the other hand, the possibility of combining the current radiopharmaceuticals with other agents opens new avenues for exploration in SLNB. In this regard, a radiolabelled nanocolloid agent has been combined with indocyanine green, a fluorescent agent, for sentinel node detection in robot assisted lymphadenectomy [3.72–3.74].

For all these new intraoperatives modalities, the preoperative anatomical SPECT/CT acquisition remains the crucial starting point for optimal surgical planning.

Key concepts of SLNB include the following:

— The SLNB procedure consists of several sequential phases: radiocolloid injection, lymphoscintigraphy (aided by SPECT/CT or not), intraoperative detection with a gamma probe (aided by intraoperative imaging or not) and, finally, pathological analysis of the resected SLNs.
— Radiocolloid administration can be performed with different modalities: intratumoural, peritumoural, intradermal, subdermal or perisubareolar.
— Lymphoscintigraphy is a mandatory step of SLNM performed by a gamma camera to visualize the lymphatic route and to mark the skin projection of SLNs with a cutaneous marker.
— SPECT/CT, MPR and volume rendering for 3-D display allows better identification of anatomical landmarks as a reference for anatomotopographic localization of the SLN(s).

3.4. SLNB IN CM

CM, which is potentially the most dangerous form of skin tumour, causes 90% of skin cancer mortality, and it can present rather differently from patient to patient. It is often highly aggressive, and usually fatal if diagnosed in an advanced stage. Better prognosis is observed in the early stages, when the probability of distant metastasis is low and resection of the primary tumour and regional lymph nodes may be curative. The 5 year mortality is approximately 20% in patients with stages I–II CM, but it is dramatically higher in stage III (35%) and stage IV (90%) [3.75, 3.76].

The incidence of CM has increased about threefold over the last 30–40 years. The main risk factors are represented by age, family history, immunosuppression and exposure to the sun. In the very early stages of disease (with a Breslow thickness of 0.76–1.5 mm), the incidence of metastatic involvement of the SLNs is only about 5%, but it increases up to 20% for melanomas with a thickness between 1.5 mm and 4 mm. With a Breslow thickness greater than 4 mm, the incidence of metastases in SLNs rises to about 50% [3.77]. The presence of

lymph node metastases decreases the survival rate by about half, with the 5 year mortality being around 70%–75% in the case of nodal metastasis. Furthermore, for patients with N1 disease, the number of involved lymph nodes and the extension of lymph nodal metastatic involvement (microscopic or macroscopic) are the two most important prognostic factors. Regardless of the Breslow thickness, the 5 year survival of patients with non-ulcerated melanoma and a single lymph nodal metastasis is significantly higher than in patients with four or more lymph nodal metastases (70% versus 27%).

The radioguided SLNB procedure in malignant CM was first reported in 1993 [3.78] using intradermally injected ^{99m}Tc sulphur colloid. Since that time, the use of radioguided SLNB has largely surpassed the use of VBD alone for the surgical evaluation of at-risk nodal basins in patients with malignant CM [3.79].

The SLN status is included in the latest version of the TNM staging system for CM, reflecting its importance for staging and treatment [3.80, 3.81]. The procedure can, in fact, identify patients who may benefit from postoperative adjuvant therapy and also provides a means of homogeneous stratification of patients for and within randomized clinical trials [3.12].

Similar to breast cancer patients, in patients with CM, the presence of an SLN that is free from metastasis obviates the need for lymphadenectomy, while the presence of metastasis mandates it [3.82, 3.83]. Radical lymph node dissection is also recommended when SLNB shows micrometastasis, because approximately 5%–12% of these patients will have metastatic involvement of non-sentinel nodes. At variance with breast cancer, locoregional lymph node dissection in the case of a positive SLNB is performed not only for staging/ prognostic stratification, but also for improving overall survival of patients.

Overall, SLNB identifies those 20%–25% of patients who present with clinically occult regional disease, by guiding the pathologist to perform extensive analysis of the lymph node(s) most likely to contain metastatic disease. It can also minimize the morbidity associated with elective lymphadenectomy (e.g. lymphoedema), by identifying those patients most likely to benefit from lymphadenectomy after a minor procedure. Moreover, similar to breast cancer, SLNB in patients with melanoma allows the pathologist to analyse the SLN, using multiple sections and different staining techniques, much more accurately than is possible when analysing the numerous lymph nodes retrieved during locoregional lymph node dissection. After conventional staining with haematoxylin eosin, it is important to perform immunohistochemistry employing specific antibodies against the melanoma associated S-100 and human melanoma black 45 antigens [3.84–3.90].

Molecular biology RT-PCR techniques to detect the messenger ribonucleic acid of melanoma related molecules such as tyrosinase (the key enzyme in the synthesis of melanin) and the melanoma antigens recognized by T lymphocytes

(melanoma antigen recognized by T cells 1 (MART-1 and MART-2) are also gaining popularity [3.91]. These techniques are characterized by high sensitivity and specificity, and have high prognostic values. In particular, they allow identification of patients who, despite a negative SLN by conventional histopathology, have a tumour recurrence risk between that of patients with negative molecular analysis and those whose sentinel nodes contain metastasis by conventional histopathological evaluation [3.92–3.97].

Metastatic spread through the lymphatic system starts with the infiltration of neoplastic cells through the basal lamina in the connective tissue. After infiltrating the endothelium of lymphatic vessels, cancer cells follow the lymphatic flow and home in on the first lymph node encountered (the SLN), proliferating in the sinusoids and remaining confined in the subcapsular space to subvert the normal lymph node structure. Accurate staging of lymph node status is therefore of paramount importance in the management of patients with early stage melanoma (clinical stages I and II). In fact, SLNB probably has maximum clinical impact in the early to intermediate stages of the disease (with a Breslow thickness of less than 4 mm) [3.98–3.101].

Prophylactic lymph nodal dissection in the basin where a metastatic SLN was found and postoperative adjuvant therapy with interferon type 2β result in increasing overall survival (especially in the case of micrometastasis).

The success of SLN identification with gamma probe guidance is very high in patients with CM (~98%), higher than that obtained using the blue dye technique alone (75%–80%). When combining these two techniques (radiocolloid and blue dye), the success rate for SLN identification is higher than 99% [3.75, 3.76, 3.102].

While in breast cancer patients, axillary lymphadenectomy performed in the case of positive SLNB is mainly used to better stratify patients for prognostic purposes, in CM patients, locoregional lymphadenectomy represents per se an effective therapy for patients with SLN metastasis. In fact, lymphadenectomy reduces mortality from about 70% to about 50% in these patients.

In early studies on SLNB in CM patients, complete lymphadenectomy was performed, regardless of the presence or absence of SLN metastasis, to determine the accuracy of SLNB. In these early studies, false negative results were observed in as few as 2% of patients [3.103]. Subsequent studies based on the appearance of metastasis in lymphatic basins that had been classified as negative by SLNB, and in which, therefore, lymphadenectomy had not been performed, have instead reported higher false negative values of between 4% and 16% [3.104]. However, in these studies, the SLN had only been analysed with intraoperative frozen section histology, which is now known to have a low sensitivity. In some studies, only haematoxylin eosin staining (without immunohistochemistry or without multiple sections) had been performed. Therefore, such apparently

high false negative rates of SLNB may have been related to the accuracy of the histopathological analysis of SLNs [3.84]. On the other hand, molecular analysis may ensure maximum accuracy of the technique, and in fact reduces false negative SLNB rates [3.97].

Key concepts of SLNB include the following:

— SLNB is also employed in patients with melanoma to ascertain TNM staging.
— SLNB identifies those 20%–25% of patients who present with clinically occult lymph node disease.
— The presence of an SLN that is free from metastasis obviates the need for lymphadenectomy, while the presence of metastasis mandates it.
— In the case of a positive SLNB, locoregional lymph node dissection is performed, not only for staging/prognostic stratification, but also for improving the overall survival of patients.
— Similar to breast cancer, SLNB in patients with melanoma allows the pathologist to analyse accurately the SLN using multiple sections and different staining techniques.
— The success of SLN identification with gamma probe guidance is very high (~98%), and is greater than that obtained with the blue dye technique alone (75%–80%).

3.4.1. Indications and contraindications to SLNB in melanoma

Patients with high risk lesions between 0.75 mm and 0.99 mm in thickness should be considered for SLNB if their melanoma is Clark level IV or V, ulcerated, shows a vertical growth phase, or has lymphatic invasion or a high mitotic rate. On the other hand, a contraindication to SLNB in CM is a lesion of Breslow thickness greater than 4 mm, because in these cases, the probability of locoregional lymph node metastasis is high, therefore, regional lymphadenectomy may be indicated, regardless of the SLN status. However, even in these cases, lymphoscintigraphy can identify unexpected patterns of lymphatic drainage, for instance, towards distant or contralateral lymph node basins, and SLNB may identify patients who are node negative and may be spared dissection [3.76].

Prior wide excision with large skin flaps, which may distort the pattern of lymphatic drainage, may be a contraindication to radioguided SLNB because lymphoscintigraphy could show unreliable lymphatic drainage, which is different from that followed by cancer cells prior to surgery.

Lymph from CM lesions localized in the extremities flows from the site of the primary tumour predictably to the ipsilateral axilla or to the ipsilateral inguinal lymphatic basins; nevertheless, SLNs may also be found in aberrant

areas of drainage, such as the epitrochlear nodal basin in the upper extremities and the popliteal nodal basin in the lower extremities.

On the contrary, the patterns and direction of lymphatic drainage are very variable and often unpredictable for melanomas in the median and paramedian regions of the trunk, as well as in the head and neck regions. In these locations, lymphatic drainage is often ambiguous, with drainage being possible to both axillary and inguinal regions, or to the contralateral neck [3.105–3.109].

Several studies have demonstrated that lymphatic drainage from melanomas of the head, neck and trunk cannot be reliably predicted based on the classic anatomical notions of Sappey. Instead, lymphoscintigraphy directly visualizes drainage from these sites to SLNs in aberrant locations. This possibility highlights the importance of preoperative lymphoscintigraphy for performing radioguided SLNB in these patients.

For melanomas of the trunk, preoperative lymphoscintigraphic localization to multiple nodal basins has been demonstrated in 17%–32% of patients undergoing radioguided SLNB [3.110−3.112].

Likewise, preoperative lymphoscintigraphy identifies in-transit (interval, aberrant) SLNs in 3%–10% of patients. Metastatic disease is found in approximately 18% of these in-transit SLNs, which is similar to the rate found in conventional lymph node basins, and the status of one basin does not predict the status of the other basin [3.113−3.115].

Key concepts of SLNB include the following:

— Indications for SLNB in melanoma are patients with a Breslow thickness ranging between 1 mm and 4 mm, or high risk lesions with a Breslow thickness between 0.75 mm and 0.99 mm (with Clark levels IV or V, ulcerated, showing a vertical growth phase, or with lymphatic invasion or a high mitotic rate).
— An absolute contraindication is a lesion of Breslow thickness greater than 4 mm, because in these cases, the probability of locoregional lymph node metastasis is high (therefore, lymph node dissection should be performed de novo).
— A relative contraindication is prior wide excision with large skin flaps because lymphoscintigraphy could show unreliable lymphatic drainage, which is different from that followed by cancer cells prior to surgery.

3.4.2. SLNB procedures in melanoma

There is general consensus that the optimal modality of radiocolloid administration in patients with melanoma is intra/subdermal injection. This is usually performed as multiple administrations around the primary tumour or

around the recent surgical scar, which is the most common occurrence because the diagnosis and thickness of melanomas are usually determined by excisional biopsy. In order not to alter the lymphatic drainage pattern or kinetics, as could be caused by an excessive increase in interstitial pressure, it is generally recommended to inject small volumes of radiocolloid, about 0.05–0.2 mL per aliquot, with each aliquot containing approximately 5 MBq of ^{99m}Tc radiocolloid. The total administered activity is generally higher, usually between 74 MBq and 100 MBq, than that used for breast cancer [3.102, 3.104]. For melanomas of the extremities, a single injection could be performed perilesionally on the side towards the axilla or groin.

Lymphoscintigraphy is generally performed using a wide-field-of-view gamma camera, equipped with a high resolution collimator. Unlike lymphoscintigraphy for breast cancer, dynamic scintigraphic acquisition should always be performed for melanoma [3.116]. The dynamic images (one every 30 s or 60 s) are usually acquired during the first 20–30 min from injection, after which static images of the lymphatic basin reached by the radiocolloid are usually acquired. Planar static images are acquired in different projections, depending on the pattern of lymphatic drainage and location of the SLN(s), to identify and mark with a dermographic pen the skin projection of the SLNs. Lymphoscintigraphy frequently shows more than one SLN. The most radioactive node may not be the first one visualized along the pathway(s) of lymphatic drainage, i.e. the SLN. Dynamic acquisition is especially useful to highlight lymphatic drainage and to visualize the correct progressive order of lymph nodes along the drainage pathway (Figs 3.6 and 3.7).

Tomographic imaging with hybrid SPECT/CT equipment is especially useful when performing lymphoscintigraphy for patients with CM because it allows better evaluation of the anatomic topographical coordinates of the lymph nodes and of the surrounding structures. As in breast cancer, SPECT/CT constitutes a valuable aid to the surgeon for more rapid intraoperative localization of the SLNs (Fig. 3.8) [3.56, 3.117]. It is useful for providing important additional information to planar imaging, especially when the sentinel node is located in uncommon locations that require unusual surgical access.
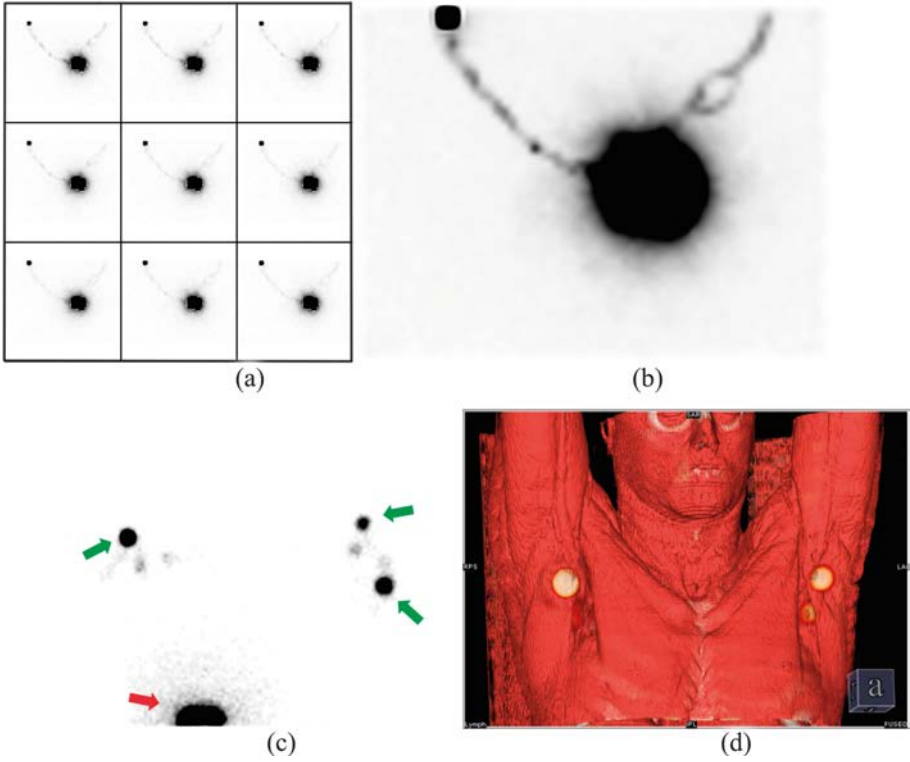
FIG. 3.6.   Planar SPECT dynamic images showing the drainage flow connecting adjacent lymph nodes (a–b); an enlarged view of a single frame (c) and the corresponding SPECT-CT 3-D volume rendering display showing bone and muscle anatomical structures (d).
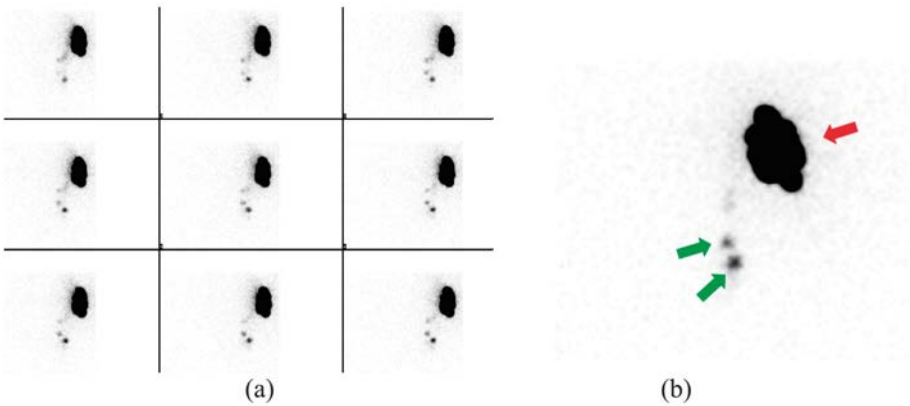
FIG. 3.7. Planar dynamic acquisition showing the migration of radioactivity from the injection site to the lymph nodes (a). Enlarged view of a single dynamic frame (b).

54
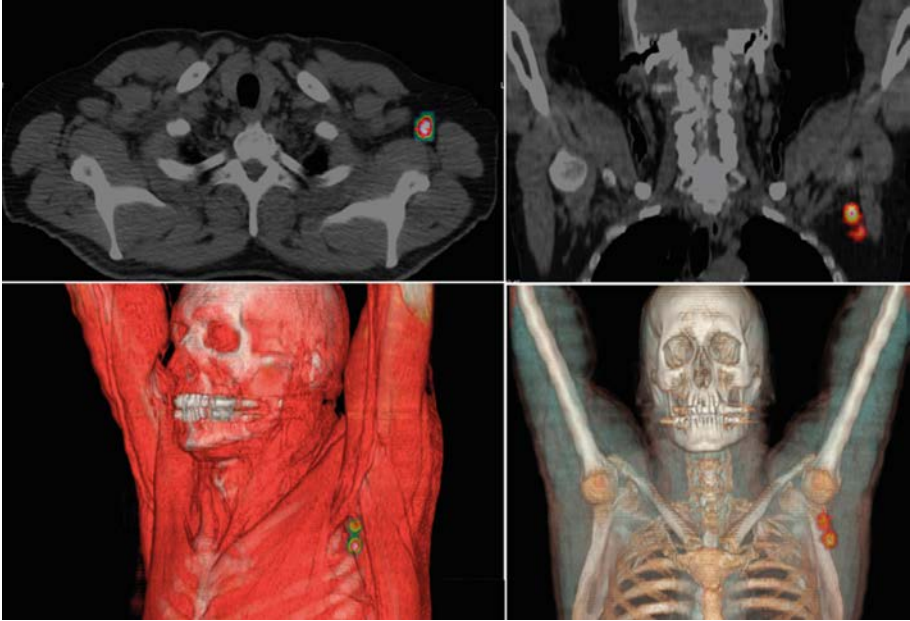
FIG. 3.8. SPECT/CT lymphoscintigraphy of a patient with breast cancer showing uptake in axillary lymph nodes.

SLNB in CM patients is performed within a few hours of lymphoscintigraphy, on the same day or on the next day, depending on the institutional preference. The gamma probe is inserted through the incision made on the cutaneous marker, and it is slowly moved to explore the entire lymphatic basin. After identification and excision, the SLN should be counted ex vivo with the gamma probe. The resulting counts are important to confirm that the excised node is the SLN. Furthermore, the counts constitute a reference for other radioactive lymph nodes in the basin. The basin should be explored again with the gamma probe, looking for any other radioactive lymph nodes. These should be removed if their ex vivo counting rate is higher than 10%–20% of the ex vivo counting rate of the SLN [3.118, 3.119].

The role of SPECT/CT imaging for SLNB in melanomas is similar to that already mentioned for breast cancer. Conventional planar lymphoscintigraphy offers a clear visualization of SLNs, providing practical information on their number and location for skin marking and showing unexpected, aberrant and deeper nodes. However, some important aspects, such as depth and anatomical relationship of the SLNs with surrounding tissues, cannot be obtained using planar imaging alone. There are also instances where false negative interpretation can occur, for instance, when one SLN is obscured by another, or by the nearby

radiocolloid injection site, when the SLN contains too little radioactivity or when two adjacent lymph nodes are thought to be a single node [3.120]. In this regard, the introduction of SPECT/CT [3.121–3.124] has overcome some of the limitations of planar scintigraphic mapping. SPECT/CT fused images show SLNs in an anatomical 3-D volume rendering scenario, thus providing a real anatomical map through which the surgeon can navigate for searching the SLNs more easily [3.56, 3.125]. Accurate SLN localization leads to improved patient management owing to changes in treatment or surgical approach. SPECT/CT is particularly helpful for localizing SLNs draining from primary tumours high on the trunk, or in the head and neck region.

Key concepts of SLNB include the following:

— The SLNB procedure consists of several sequential phases: radiocolloid injection, lymphoscintigraphy (aided or not by SPECT/CT), intraoperative detection with a gamma probe (aided or not by intraoperative imaging) and, finally, pathological analysis of the resected SLNs.
— Radiocolloid administration is generally performed peritumourally or around the surgical scar, with at least four aliquots of radiocolloid.
— Lymphoscintigraphy is a mandatory step of SLNM, performed using a gamma camera to visualize lymphatic routes and to identify the SLNs of each lymphatic basin.
— SPECT/CT, MPR and volume rendering for 3-D display allow better identification of anatomical landmarks as a reference for anatomotopographic localization of the SLN(s).
— In the intraoperative phase, the surgeon is radioguided to localize the SLNs by a gamma probe (with an acoustic sound) or by a portable gamma camera (with real time images).

3.5. OTHER APPLICATIONS OF RADIOGUIDED SLNB

As mentioned earlier, SLNB procedures in patients with either breast cancer or CM have already achieved the status of standard of care for N-staging purposes, so that further management of cancer patients after primary surgery can adequately be planned. Nevertheless, potential benefits of this approach can also be envisaged for other solid cancers, with the rationale of accurately mapping the status of locoregional lymph nodes while avoiding aggressive procedures based on extensive lymph node dissection.

Numerous clinical trials have explored the feasibility and accuracy of SLNB in several oncological conditions, including, among others, tumours of the head and neck region, the gastrointestinal tract and the genitourinary apparatus.

Nevertheless, in all these fields, SLNM should still be considered within well designed experimental clinical trials, as further investigations are required for defining the clinical impact of this procedure. In this section, the main potential applications of SLNB in tumours other than breast cancer and melanoma are briefly listed.

3.5.1. SLNB in head and neck cancers

In addition to melanomas located in the head and neck, the most important applications of SLNB for tumours of this region concern cancers of the oral cavity. In these patients, radioguided SLNB is emerging as a highly promising modality to stage the clinical and radiological N0 neck, considering the poor sensitivity of other commonly used radiological and nuclear medicine staging modalities. A positive SLN is considered to be an unfavourable prognostic factor [3.126].

However, the role of SLNB in oral cancer is not as well established as it is for breast cancer and melanoma, and some controversy still persists regarding the appropriate indication. The procedure has been used for stage T1 or T2 lesions [3.127, 3.128], although several investigators have found selective neck dissection more appropriate in view of the high risk of nodal metastasis [3.129]. In general, patients with transorally resectable T1–T2 tumours and with negative lymph node assessment on clinical and radiological examination (including fine needle aspiration cytology) are considered for SLNB.

SLNB in the head and neck region may be complex owing to difficult anatomical relations and unpredictable lymphatic drainage. Generally, lymphatic drainage is expected to occur towards the homolateral lymph nodes of the neck, but in cancers of the oral cavity, lymphatic drainage can be highly unpredictable, and contralateral drainage is often seen, even in well lateralized malignancies of the tongue or floor of the mouth [3.130, 3.131].

Early results regarding the accuracy of SLNB in patients with oral cavity malignancies, in which both the SLNB procedure and a complete selective neck dissection were performed, showed accurate staging of regional lymph nodes, with a 96% negative predictive value [3.132].

Lymphoscintigraphy for SLNM is generally performed some hours before the scheduled time for surgery. After peritumoural or intratumoural radiocolloid injection, both planar lymphoscintigraphy and SPECT/CT images are generally acquired. Intraoperatively, the search for the radioactive SLN is usually performed using a conventional hand held gamma probe. However, the advent of new techniques such as the use of a portable gamma camera for intraoperative SLND or the concomitant injection of radiolabelled and fluorescent colloidal agents may improve the accuracy of SLNB in head and neck cancers, especially when the injection site is close to the SLN basin; such combined imaging may, in

fact, help the surgeon to localize the SLNs in relation to the anatomical level in the neck [3.133, 3.134].

For thyroid cancer, SLNB may display some benefits for accurate nodal staging, particularly for detecting metastatic lymph nodes outside the central neck, and for selecting patients who would benefit from complete neck dissection and optimized radioiodine ablation therapy. Currently, however, there is no direct evidence that SLNB is associated with long term clinical and survival benefits in patients with thyroid cancer. The procedure includes peritumoural or intratumoural radiocolloid administration and accurate preoperative imaging to optimally plan lymph node dissection. Well controlled prospective clinical trials will determine the clinical significance of occult metastases and their early detection by SLNB in patients with thyroid cancer [3.134].

3.5.2. SLNB in gastrointestinal cancers

Procedures for SLNM and SLNB in gastrointestinal cancers have gradually expanded in recent years. Lymphatic drainage of the gastrointestinal tract is much more complicated than other sites, with skip metastasis being rather frequent because of aberrant lymphatic drainage outside the basin [3.135]. At present, the applicability of the SLN concept in cancers of the gastrointestinal tract has still to be established through well designed prospective multicentre studies. The aim of SLNB varies according to the tumour site.

In cases of oesophageal cancer, SLNB can minimize surgical invasiveness, but still allow accurate analysis of the lymph node status. In fact, considering that cancers of the distal oesophagus can metastasize to cervical lymph nodes, while cancers of the cervical oesophagus can metastasize to celiac lymph nodes, SLNB is expected to allow for a more selective approach [3.136].

The extent of lymphadenectomy in gastric cancer has been a source of controversy for decades. Because of a lack of consensus regarding the surgical approach to lymph node dissection, individualized approaches based on SLNB are still being debated, and could represent an opportunity worth exploring, especially in patients with early gastric cancer (T1–T2). In this regard, laparoscopic function, preserving resection of the primary gastric tumour, in conjunction with lymphatic basin dissection, guided by SLNB, could become the standard for treating early gastric cancer. In the event of uninvolved SLNs, transabdominal surgery could be avoided [3.137].

The most accurate SLNB approach combines both blue dye and radiocolloid administration (i.e. endoscopic submucosal injection of radiocolloid the day prior to surgery and endoscopic submucosal injection of 1% isosulphan blue intraoperatively) [3.138].

Moreover, SLNB can disclose unexpected and/or aberrant sites of drainage, thus guiding surgeons to perform a regional dissection approach tailored to the individual patient [3.139−3.142].

The potential advantages of SLNM in the case of colorectal cancer consist of the identification of aberrant lymphatic drainage leading to modification of the intended surgical approach (an event occurring in 5%–8% of patients). Moreover, following standardized surgical procedure (including selective lymphadenectomy), SLNB can identify the crucial node(s) to be submitted to extensive analysis with immunohistochemistry to search for micrometastases.

The overall success rate for radioguided SLNB is generally high. Most of the failures reported in patients with rectal cancer are most likely because of local submucosal lymphatic fibrosis induced by neoadjuvant radiation therapy administered prior to surgery [3.143]. Furthermore, the overall accuracy for predicting lymph node metastasis is generally high (~95%), and the false negative rate is low.

The modality of radiocolloid administration varies according to the tumour site, although in most cases, it can be performed during preoperative endoscopy; as is the case for other tumours, the blue dye is instead injected intraoperatively. Use of the two agents in combination is reported to lead to better results. Usually, radiocolloid injection is performed between 2 h and 24 h before surgery, either submucosally around the tumour (during endoscopy prior to surgery) or subserosally (during open or laparoscopic surgery) [3.144].

Because of a recurrence rate as high as 30% in node negative colon cancer patients treated only with surgery and locoregional lymphadenectomy, SLNB could more appropriately allow for selective focused sampling techniques to ultrastage patients and ultimately identify a subset of patients who will benefit from adjuvant chemotherapy [3.145, 3.146]. With this approach, lymph nodal upstaging occurs in about 20% of the cases. Nevertheless, the clinical impact of micrometastasis in terms of prognosis and need for adjuvant chemotherapy has still to be clarified.

In rectal cancer, SLNM could be useful to select patients who would benefit, after standard surgery, from a selective approach with lateral pelvic lymph node dissection, which becomes necessary in about 15% of the cases [3.146, 3.147].

Radioguided SLNB has also been applied to patients with anal cancer [3.148−3.154]. SLN visualization is generally demonstrated in 75%–100% of the patients. There are three common pathways of lymphatic drainage from anal cancers (i.e. drainage to the inguinal, iliac and mesorectal lymphatic basins). The very frequent finding of bilateral lymphatic drainage emphasizes the importance of preoperative lymphoscintigraphy for most effectively performing radioguided SLNB. The inguinal region is the predominant lymphatic drainage pathway, representing the site of localization most accessible to perform a

minimally invasive radioguided SLNB. However, large scale prospective clinical trials assessing the clinical impact of radioguided SLNB in patients with anal cancer are still lacking.

3.5.3. SLNB in tumours of the female reproductive system

There has also been increasing interest in the use of radioguided SLNB in gynaecological cancers, because this procedure has been shown to be accurate for evaluating nodal basins for metastatic disease and is associated with reduced short term and long term morbidity when compared with complete lymph node dissection.

Because of the high morbidity rates of lymph nodal dissection, recent literature continues to support the safety and feasibility of SLNB for early stage vulvar cancer because the procedure is associated with low recurrence rates, excellent survival, lower morbidity and shorter hospital stay compared to classical inguinal dissection. SLNB therefore promises to provide adequate staging with less treatment related morbidity, especially in selected vulvar cancer patients in whom it can be considered an alternative surgical approach to full lymph node dissection [3.155].

For endometrial and cervical cancer, SLNB has been described with encouraging results, although this application requires further investigation, given some ambiguity in published reports. In particular, reports on SLNB only include small groups of patients, and the SLND rates vary depending on the injection sites/modalities and the agents employed [3.156]. For endometrial cancer, most studies have reported low false negative rates, with variable sensitivities and generally low SLND rates. Radioguided SLNB is also promising in early stage cervical cancer, with detection rates and sensitivities greater than 90%.

3.5.4. SLNB in tumours of the male reproductive system

For cancers of the male reproductive system, the feasibility of radioguided SLNB is increasingly being explored because of the high incidence of morbidity, such as lymphoedema and infections, after standard surgery with full lymph node dissection. Moreover, the introduction of microinvasive surgical techniques implies the possibility to achieve proper evaluation of the lymph node status, even with a small surgical incision. This goal can be reached by analysing SLNs with serial sectioning and extensive histopathological analysis, including immunohistochemical staining.

There is no consensus on the management of patients with clinically node negative penile carcinoma, in whom radical inguinal lymph node dissection is routinely performed, although it turns out to be unnecessary in approximately

75%–80% of patients [3.157]. In addition, this procedure is associated with substantial morbidity. However, since its clinical introduction, there have been reservations about the use of SLNB for penile cancer because of the supposedly long learning curve associated with the procedure and because of possible false negative cases (up to 21% of procedures) [3.158]. After analysis of the possible causes of false negative cases, several modifications were introduced to increase the sensitivity of the SLNB procedure [3.159]. Thus, radioguided SLNB has currently evolved into a reliable minimally invasive staging technique with an associated high sensitivity (90%–95%) and low morbidity in experienced centres [3.160]. However, there are still important differences in the clinical protocols employed worldwide; harmonization of the different phases of the SLNB procedure in patients with penile cancer (including how to implement the learning curve) is therefore needed.

For prostate cancer, where the incidence of complications post lymph node dissection rises up to 25% with 20 lymph nodes dissected, the main advantage of SLNB is the possibility to reduce the incidence of such unnecessary complications [3.161]. Accurate laparoscopic radioguided localization of SLNs in the pelvis can be challenging, especially when the SLNs are located near the intraprostatic injection site (because of the high radioactive background) or in the case of aberrantly located SLNs [3.162]. Original validation of radioguided SLNB for prostate cancer was based on open surgery and on the use of a gamma probe to guide detection of the radioactive SLNs (with only 5.5% false negative cases being reported) [3.163]. SLNB has recently been validated using a laparoscopic gamma probe during minimally invasive surgery with a similarly high detection rate (94%) and sensitivity (~95%) [3.164].

Large scale randomized clinical studies are necessary to assess and validate the added benefit of SLNB in patients with testicular cancers. In this regard, only a few studies [3.165–3.167] have been published, all with small size populations (<25 patients per study), which are therefore without the statistical power and follow-up data to assess sensitivity/false negative rates. On the other hand, in these patients, radioguided SLNM and SLNB was found to be potentially useful to detect aberrant lymphatic drainage [3.165–3.167] and to identify those selected patients who would benefit from adjuvant treatment after orchidectomy.

REFERENCES TO CHAPTER 3

[3.1] MARIANI, G., GIULIANO, A.E., STRAUSS, H.W., Radioguided Surgery: A Comprehensive Team Approach, Springer, New York (2008).
[3.2] EDGE, S.B., et al. (Eds), AJCC Cancer Staging Manual, 7th edn, Springer, New York (2009) 347–369.

[3.3] ZAKNUN, J.J, et al., Changing paradigms in radioguided surgery and intraoperative imaging: the GOSTT concept, Eur. J. Nucl. Med. Mol. Imaging **39** (2012) 1–3.

[3.4] SIEGEL, R., NAISHADHAM, D., JEMAL, A., Cancer statistics 2012, CA Cancer J. Clin. **62** 1 (2012) 10–29.

[3.5] KRAG, D.N., et al., Surgical resection and radiolocalization of sentinel lymph node in breast cancer using a gamma probe, Surg. Oncol. **2** (1993) 335–339.

[3.6] GIULIANO, A.E., KIRGAN, D., GUENTHER, J.M., Lymphatic mapping and sentinel lymphadenectomy for breast cancer, Ann. Surg. **220** (1994) 391–401.

[3.7] GIULIANO, A.E., et al., Improved axillary staging of breast cancer with sentinel lymphadenectomy, Ann. Surg. **222** (1995) 394–401.

[3.8] NOGUCHI, M., KATEV, N., MIYAZAKI, I., Diagnosis of axillary lymph node metastases in patients with breast cancer, Breast Cancer Res. Treat. **40** (1996) 283–293.

[3.9] TAYLOR, A., Jr., et al., Dynamic lymphoscintigraphy to identify the sentinel and satellite nodes, Clin. Nucl. Med. **21** (1996) 755–758.

[3.10] MEIJER, S., et al., Less axillary dissection necessary due to sentinel node biopsy in patients with breast carcinoma, Ned. Tijdschr. Geneeskd. **140** (1996) 2239–2243.

[3.11] ALBERTINI, J.J., et al., Lymphatic mapping and sentinel node biopsy in the patient with breast cancer, JAMA **276** (1996) 1818–1822.

[3.12] ALAZRAKI, N.P., et al., Lymphoscintigraphy, the sentinel node concept, and the intraoperative gamma probe in melanoma, breast cancer, and other potential cancers, Semin. Nucl. Med. **27** (1997) 55–67.

[3.13] PIJPERS, R., et al., Impact of lymphoscintigraphy on sentinel node identification with technetium-99m-colloidal albumin in breast cancer, J. Nucl. Med. **38** (1997) 366–368.

[3.14] GIULIANO, A.E., Lymphatic mapping and sentinel node biopsy in breast cancer. JAMA **277** (1997) 791–792.

[3.15] REINTGEN, D., et al., The role of selective lymphadenectomy in breast cancer, Cancer Control **4** (1997) 211–219.

[3.16] VERONESI, U., et al., Sentinel-node biopsy to avoid axillary dissection in breast cancer with clinically negative lymph-nodes. Lancet **349** (1997) 1864–1867.

[3.17] MARIANI, G., et al., Radioguided sentinel lymph node biopsy in breast cancer surgery, J. Nucl. Med. **42** (2001) 1198–1215.

[3.18] LYMAN, G.H., et al., American Society of Clinical Oncology guideline recommendations for sentinel lymph node biopsy in early-stage breast cancer, J. Clin. Oncol. **23** (2005) 7703–7720.

[3.19] BENSON, J.R., DELLA ROVERE, G.Q., AXILLA MANAGEMENT CONSENSUS GROUP, Management of the axilla in women with breast cancer, Lancet Oncol **8** (2007) 331–348.

[3.20] BUSCOMBE, J., et al., Sentinel node in breast cancer procedural guidelines, Eur. J. Nucl. Med. Mol. Imaging **34** (2007) 2154–2159.

[3.21] BONNEMA, J., et al., Ultrasound guided aspiration biopsy for detection of non palpable axillary node metastases in breast cancer patients: new diagnostic method, World J. Surg. **21** (1997) 270–274.

[3.22] CARLSON, R.W., et al., Breast cancer: clinical practice guidelines in oncology, J. Natl. Compr. Canc. Netw. **7** (2009) 122–192.

[3.23] PURUSHOTHAM, A.D., et al., Morbidity after sentinel node biopsy in primary breast cancer: results from a randomized controlled trial, J. Clin. Oncol. **23** (2005) 4312–4321.

[3.24] ESTOURGIE, S.H., et al., Eight false negative sentinel lymph node procedures in breast cancer: what went wrong? Eur. J. Surg. Oncol. **29** (2003) 336–340.

[3.25] LEIJTE, J., et al., Visualization of tumor blockage and rerouting of lymphatic drainage in penile cancer patients by use of SPECT/CT, J. Nucl. Med. **50** (2009) 364–367.

[3.26] NATIONAL COMPREHENSIVE CANCER NETWORK, Clinical Practice Guidelines in Oncology. Breast Cancer VI (2010), www.nccn.org /professionals/physician_gls/f_guidelines.asp

[3.27] VERONESI, U., et al., A randomized comparison of sentinel-node biopsy with routine axillary dissection in breast cancer, New Engl. J. Med. **349** (2003) 546–553.

[3.28] KRAG, D.N., et al., Sentinel lymph node resection compared with conventional axillary-lymph node dissection in clinically node-negative patients with breast cancer: overall survival findings from the NSABP-32 randomised phase 3 trial, Lancet Oncol. **11** (2010) 927–933.

[3.29] KRAG, D.N., et al., Technical outcomes of sentinel-lymph node resection and conventional axillary lymph-node dissection in patients with node-negative breast cancer: results from the NSABP B32 randomised phase III trial, Lancet Oncol. **8** (2007) 881–888.

[3.30] GOYAL, A., NEWCOMBE, R.G., CHABRA, A., MANSEL, R.E., ALMANAC TRIALISTS GROUP, Factors affecting failed localization and false-negative rates of sentinel node biopsy in breast cancer–results of the ALMANAC validation phase, Breast Cancer Res. Treat. **99** (2006) 203–208.

[3.31] GIULIANO, A.E., et al., Axillary dissection versus no axillary dissection in women with invasive breast cancer and sentinel node metastasis. A randomized clinical trial, JAMA **305** (2011) 569–575.

[3.32] KRYNYCKYI, B.R., et al., Factors affecting visualization rates of internal mammary sentinel nodes during lymphoscintigraphy, J. Nucl. Med. **44** (2003) 1387–1393.

[3.33] PAREDES, P., et al., Clinical relevance of sentinel lymph nodes in the internal mammary chain in breast cancer patients, Eur. J. Nucl. Med. Mol. Imaging **32** (2005) 1283–1287.

[3.34] ESTOURGIE, S.H., et al., Should the hunt for internal mammary chain sentinel nodes begin? An evaluation of 150 breast cancer patients, Ann. Surg. Oncol. **10** (2003) 935–941.

[3.35] VAN DER ENT, F.W., et al., Halsted revisited: internal mammary sentinel lymph node biopsy in breast cancer, Ann. Surg. **234** (2001) 79–84.

[3.36] BOURRE, J.C., et al., Can the sentinel lymph node technique affect decisions to offer internal mammary chain irradiation? Eur. J. Nucl. Med. Mol. Imaging **36** (2009) 758–764.

[3.37] VERONESI, U., MARUBINI, E., MARIANI, L., VALAGUSSA, P., ZUCALI, R., The dissection of internal mammary nodes does not improve the survival of breast cancer patients. 30-year results of a randomised trial, Eur. J. Cancer **35** (1999) 1320–1325.

[3.38] GOLDHIRSCH, A., et al., Thresholds for therapies: highlights of the St Gallen International expert consensus on the primary therapy of early breast cancer 2009, Ann. Oncol. **20** (2009) 1219–1229.

[3.39] KAUFMANN, M., Locoregional treatment of primary breast cancer, Cancer **116** (2010) 1184–1191.

[3.40] RODRIGUEZ-FERNANDEZ, J., et al., Sentinel node biopsy in patients with previous breast aesthetic surgery, Ann. Surg. Oncol. **16** (2009) 989–992.

[3.41] TABACK, B., et al., Sentinel lymph node biopsy for local recurrence of breast cancer after breast-conserving therapy, Ann. Surg. Oncol. **13** (2006) 1099–1104.

[3.42] KUMAR, R., et al., Retrospective analysis of sentinel node localization in multifocal, multicentric, palpable, or nonpalpable breast cancer, J. Nucl. Med. **44** (2003) 7–10.

[3.43] KLIMBERG, V.S., et al., Subareolar versus peritumoral injection for location of the sentinel lymph node, Ann. Surg. **229** (1999) 860–864.

[3.44] NIEWEG, O.E., ESTOURGIE, S.H., VAN RIJK, M.C., KROON, B.B., Rationale for superficial injection techniques in lymphatic mapping in breast cancer patients, J. Surg. Oncol. **87** (2004) 153–156.

[3.45] KNAUER, M., et al., Multicentric breast cancer: a new indication for sentinel node biopsy – a multi-institutional validation study, J. Clin. Oncol. **24** (2006) 3374–3380.

[3.46] GOYAL, A., et al., Sentinel lymph node biopsy in patients with multifocal breast cancer, Eur. J. Surg. Oncol. **30** (2004) 475–479.

[3.47] GIARD, S., et al., Feasibility of sentinel lymph node biopsy in multiple unilateral synchronous breast cancer: results of a French prospective multi-institutional study (IGASSU 0502), Ann. Oncol. **21** (2010) 1630–1635.

[3.48] VERONESI, P., GENTILINI, O., RODRÍGUEZ-FERNANDEZ, J., MAGNONI, F., Breast conservation and sentinel lymph node after neoadjuvant systemic therapy, Breast **18** (2009) 590–592.

[3.49] MAMOUNAS, E.P., et al., Sentinel node biopsy after neoadjuvant chemotherapy in breast cancer: results from National Surgical Adjuvant Breast and Bowel Project Protocol B-27, J. Clin. Oncol. **23** (2005) 2694–2702.

[3.50] KELLY, A.M., DWAMENA, B., CRONIN, P., CARLOS, R.C., Breast cancer sentinel node identification and classification after neoadjuvant chemotherapy — systematic review and metaanalysis, Acad. Radiol. **16** (2009) 551–563.

[3.51] PIÑERO, A., GIMENEZ, J., VIDAL-SICART, S., INTRA, M., Selective sentinel lymph node biopsy and primary systemic therapy in breast cancer, Tumori **96** (2010) 17–23.

[3.52] PANDIT-TASKAR, N., DAUER, L.T., MONTGOMERY, L., et al., Organ and fetal absorbed dose estimates from ^{99m}Tc-sulfur colloid lymphoscintigraphy and sentinel node localization in breast cancer patients, J. Nucl. Med. **47** (2006) 1202–1208.

[3.53] KHERA, S.Y., et al., Pregnancy-associated breast cancer patients can safely undergo lymphatic mapping, Breast J. **14** (2008) 250–254.

[3.54] GENTILINI, O., et al., Sentinel lymph node biopsy in pregnant patients with breast cancer, Eur. J. Nucl. Med. Mol. Imaging **37** (2010) 78–83.

[3.55] MARIANI, G., BRUSELLI, L., KUWERT, T., et al., A review on the clinical uses of SPECT/CT, Eur. J. Nucl. Med. Mol. Imaging **37** (2010) 1959–1985.

[3.56] VERMEEREN, L., VAN DER PLOEG, I.M., VALDES-OLMOS, R.A., et al., SPECT/CT for preoperative sentinel node localization, J. Surg. Oncol. **101** (2010) 184–190.

[3.57] EVEN-SAPIR, E., et al., Lymphoscintigraphy for sentinel node mapping using a hybrid SPECT/CT system, J. Nucl. Med. **44** (2003) 1413–1420.

[3.58] LERMAN, H., et al., Lymphoscintigraphic sentinel node identification in patients with breast cancer: the role of SPECT/CT, Eur. J. Nucl. Med. Mol. Imaging **33** (2006) 329–337.

[3.59] LERMAN, H., et al., Improved sentinel node identification by SPECT/CT in overweight patients with breast cancer, J. Nucl. Med. **48** (2007) 201–206.

[3.60] MATHELIN, C.E., GUYONNET, J.L., Scintillation crystal or semiconductor gamma-probes: an open debate, J. Nucl. Med. **47** (2006) 373.

[3.61] HOFFMAN, E.J., et al., Intra-operative probes and imaging probes, Eur. J. Nucl. Med. **26** (1999) 913–935.

[3.62] SCOPINARO, F., et al., High-resolution, hand-held camera for sentinel-node detection, Cancer Biother. Radiopharm. **23** (2008) 43–52.

[3.63] MATHELIN, C., et al., Precise localization of sentinel lymph nodes and estimation of their depth using a prototype intraoperative mini gamma-camera in patients with breast cancer, J. Nucl. Med. **48** (2007) 623–629.

[3.64] DUCH, J., Portable gamma cameras: the real value of an additional view in the operating theatre, Eur. J. Nucl. Med. Mol. Imaging **38** (2011) 633–635.

[3.65] VIDAL-SICART, S., Added value of intraoperative real-time imaging in searches for difficult-to-locate sentinel nodes, J. Nucl. Med. **51** (2010) 1219–1225.

[3.66] CARDONA-ARBONIES, J., et al., Contribution of the portable gamma camera to detect the sentinel node in breast cancer during surgery, Rev. Esp. Med. Nucl. **31** (2012) 130–134.

[3.67] VIDAL-SICART, S., BROUWER, O.R., VALDES-OLMOS, R.A., Evaluation of the sentinel lymph node combining SPECT/CT with the planar image and its importance for the surgical act, Rev. Esp. Med. Nucl. **30** (2011) 331–337.

[3.68] VIDAL-SICART, S., et al., The use of a portable gamma camera for preoperative lymphatic mapping: a comparison with a conventional gamma camera, Eur. J. Nucl. Med. Mol. Imaging **38** (2011) 636–641.

[3.69] WENDLER, T., et al., First demonstration of 3-D lymphatic mapping in breast cancer using freehand SPECT, Eur. J. Nucl. Med. Mol. Imaging **37** (2010) 1452–1461.

[3.70] RIEGER, A., et al., First experiences with navigated radio-guided surgery using freehand SPECT, Case Rep. Oncol. **4** (2011) 420–425.

[3.71] VAN DER POEL, H.G., et al., Intraoperative laparoscopic fluorescence guidance to the sentinel lymph node in prostate cancer patients: clinical proof of concept of an integrated functional imaging approach using a multimodal tracer, Eur. Urol. **60** (2011) 826–833.

[3.72] KEEREWEER, S., et al., Optical image-guided surgery – where do we stand? Mol. Imaging Biol. **13** (2011) 199–207.

[3.73] POLOM, K., et al., Current trends and emerging future of indocyanine green usage in surgery and oncology: a literature review, Cancer **117** (2011) 4812–4822.

[3.74] THOMPSON, J.F., SCOLYER, R.A., KEFFORD, R.F., Cutaneous melanoma, Lancet **365** (2005) 687–701.

[3.75] GERSHENWALD, J.E., et al., "Sentinel lymph node biopsy in cutaneous melanoma", Radioguided Surgery: A Comprehensive Team Approach (MARIANI, G., GIULIANO, A.E., STRAUSS, H.W., Eds), Springer, New York (2008) 92–110.

[3.76] ROSS, M., "Sentinel node mapping for early-stage melanoma", Educational Book (PERRY, M.C., Ed.), American Society of Clinical Oncology, Alexandria, VA (1997) 326–330.

[3.77] ALEX, J.C., KRAG, D.N., The gamma-probe-guided resection of radiolabeled primary lymph nodes, Surg. Oncol. Clin. North Am. **5** (1996) 33–41.

[3.78] TAYLOR, A., Jr., et al., Dynamic lymphoscintigraphy to identify the sentinel and satellite nodes, Clin. Nucl. Med. **21** (1996) 755–758.

[3.79] EDGE, S.B. (Eds), AJCC Cancer Staging Manual, 7th edn, Springer, New York (2009) 325–340.

[3.80] GERSHENWALD, J.E., SOONG, S.J., BALCH, C.M., AMERICAN JOINT COMMITTEE ON CANCER (AJCC) MELANOMA STAGING COMMITTEE. 2010 TNM staging system for cutaneous melanoma and beyond, Ann. Surg. Oncol. **17** (2010) 1475–1477.

[3.81] ALOIA, T.A., GERSHENWALD, J.E., Management of early-stage cutaneous melanoma, Curr. Probl. Surg. **42** (2005) 460–534.

[3.82] BELHOCINE, T.Z., et al., Role of nuclear medicine in the management of cutaneous malignant melanoma, J. Nucl. Med. **47** (2006) 957–967.

[3.83] GIBBS, J.F., et al., Accuracy of pathologic techniques for the diagnosis of metastatic melanoma in sentinel lymph nodes, Ann. Surg. Oncol. **6** (1999) 699–704.

[3.84] COCHRAN, A.J., The pathologist's role in sentinel lymph node evaluation, Semin. Nucl. Med. **30** (2000) 11–17.

[3.85] KOOPAL, S.A., TIEBOSH, A.T., ALBERTUS PIERS, D., Frozen section analysis of sentinel lymph nodes in melanoma patients, Cancer **89** (2000) 1720–1725.

[3.86] COCHRAN, A.J., et al., Current practice and future directions in pathology and laboratory evaluation of the sentinel node, Ann. Surg. Oncol. **8** (2001) 13–17.

[3.87] PRIETO, V.G., CLARK, S., Processing of sentinel lymph nodes or detection of metastatic melanoma, Ann. Diagn. Pathol. **6** (2002) 257–264.

[3.88] COOK, M.G., et al., The development of optimal pathological assessment of sentinel lymph nodes for melanoma, J. Pathol. **200** (2003) 314–319.

[3.89] SCOLYER, R.A., THOMPSON, J.F., McCARTHY, S.W., Sentinel lymph nodes in malignant melanoma: extended histopathologic evaluation improves diagnostic precision, Cancer **1** (2004) 2141–2142 (author reply: 2142–2143).

[3.90] VIALE, G., MAZZAROL, G., MAIORANO, E., "Histopathology of sentinel lymph nodes", Radioguided Surgery: A Comprehensive Team Approach (MARIANI, G., GIULIANO, A.E., STRAUSS, H.W., Eds), Springer, New York (2008) 190–200.

[3.91] GOYDOS, J.S., et al., Minimally invasive staging of patients with melanoma: sentinel lymphadenectomy and detection of the melanoma specific proteins MART-1 and tyrosinase by reverse transcriptase polymerase chain reaction, J. Am. Coll. Surg. **187** (1998) 182–188.

[3.92] GOYDOS, J.S., et al., Patterns of recurrence in patients with melanoma and histologically negative but RT-PCR-positive sentinel lymph nodes, J. Am. Coll. Surg. **196** (2003) 196–204.

[3.93] RIBUFFO, D., et al., Prognostic significance of reverse transcriptase-polymerase chain reaction-negative sentinel nodes in malignant melanoma, Ann. Surg. Oncol. **10** (2003) 396–402.

[3.94] KAMMULA, U.S., et al., Serial follow-up and the prognostic significance of reverse transcriptase-polymerase chain reaction-staged sentinel lymph nodes from melanoma patients, J. Clin. Oncol. **22** (2004) 3989–3996.

[3.95] ROMANINI, A., et al., Molecular staging of the sentinel lymph node in melanoma patients: correlation with clinical outcome, Ann. Oncol. **16** (2005) 1832–1840.

[3.96] MOCELLIN, S., et al., Sentinel lymph node molecular ultrastaging in patients with melanoma: a systematic review and meta-analysis of prognosis, J. Clin. Oncol. **25** (2007) 1588–1595.

[3.97] BALCH, C.M., et al., A comparison of prognostic factors and surgical results in 1,786 patients with localized (stage I) melanoma treated in Alabama, USA, and New South Wales, Australia, Ann. Surg. **196** (1982) 677–684.

[3.98] REINTGEN, D.S., et al., Efficacy of elective lymph node dissection in patients with intermediate thickness primary melanoma, Ann. Surg. **198** (1983) 379–385.

[3.99] BALCH, C.M., et al., Efficacy of an elective regional lymph node dissection of 1 to 4 mm thick melanomas for patients 60 years of age and younger, Ann. Surg. **224** (1996) 255–263.

[3.100] LENS, M., Sentinel lymph node biopsy in melanoma patients, J. Eur. Acad. Dermatol. Venereol. **24** (2010) 1005–1012.

[3.101] CHAKERA, A.H., et al., EANM-EORTC general recommendations for sentinel node diagnostics in melanoma, Eur. J. Nucl. Med. Mol. Imaging **36** (2009) 1713–1742.

[3.102] THOMPSON, J.F., et al., Sentinel node biopsy for melanoma: where have we been and where are we going? Ann. Surg. Oncol. **11** (2004) 147S–151S.

[3.103] MARIANI, G., et al., Radioguided sentinel lymph node biopsy in malignant cutaneous melanoma, J. Nucl. Med. **43** (2002) 811–827.

[3.104] UREN, R.F., HOWMAN-GILES, R., THOMPSON, J.F., Lymphatic drainage to triangular intermuscular space lymph nodes in melanoma on the back, J. Nucl. Med. **37** (1996) 964–966.

[3.105] UREN, R.F., HOWMAN-GILES, R., THOMPSON, J.F., Lymphatic drainage from the skin of the back to retroperitoneal and paravertebral lymph nodes in melanoma patients, Ann. Surg. Oncol. **5** (1998) 384–387.

[3.106] UREN, R.F., THOMPSON, J.F., HOWMAN-GILES, R., Sentinel nodes, interval nodes, lymphatic lakes, and accurate sentinel node identification, Clin. Nucl. Med. **25** (2000) 234–236.

[3.107] THOMPSON, J.F., UREN, R.F., Anomalous lymphatic drainage patterns in patients with cutaneous melanoma, Tumori **87** (2001) 54–56.

[3.108] UREN, R.F., HOWMAN-GILES, R., THOMPSON, J.F., Patterns of lymphatic drainage from the skin in patients with melanoma, J. Nucl. Med. **44** (2003) 570–582.

[3.109] ALAZRAKI, N., et al., Procedure guideline for lymphoscintigraphy and the use of intraoperative gamma probe for sentinel lymph node localization in melanoma of intermediate thickness, J. Nucl. Med. **43** (2002) 1414–1418.

[3.110] LEONG, S.P., et al., Heterogeneous patterns of lymphatic drainage to sentinel lymph nodes by primary melanoma from different anatomic sites, Clin. Nucl. Med. **30** (2005) 150–158.

[3.111] FEDERICO, A.C., et al., Effect of multiple-nodal basin drainage on cutaneous melanoma, Arch. Surg. **143** (2008) 632–637.

[3.112] VIDAL-SICART, S., et al., Is the identification of in-transit sentinel lymph nodes in malignant melanoma patients really necessary? Eur. J. Nucl. Med. Mol. Imaging **31** (2004) 945–949.

[3.113] THOMPSON, J.F., et al., Location of sentinel lymph nodes in patients with cutaneous melanoma: new insights into lymphatic anatomy, J. Am. Coll. Surg. **189** (1999) 195–204.

[3.114] SCARSBROOK, A.F., GANESHAN, A., BRADLEY, K.M., Pearls and pitfalls of radionuclide imaging of the lymphatic system. Part 1: sentinel node lymphoscintigraphy in malignant melanoma, Br. J. Radiol. **80** (2007) 132–139.

[3.115] MARIANI, P., et al., Radioguided sentinel lymph node biopsy in patients with malignant cutaneous melanoma: the nuclear medicine contribution, J. Surg. Oncol. **85** (2004) 141–151.

[3.116] UREN, R.F., SPECT/CT lymphoscintigraphy to locate the sentinel lymph node in patients with melanoma, Ann. Surg. Oncol. **16** (2009) 1459–1460.

[3.117] McMASTERS, K.M., et al., Sentinel lymph node biopsy for melanoma: how many radioactive nodes should be removed? Ann. Surg. Oncol. **8** (2001) 192–197.

[3.118] MANCA, G., et al., Optimal detection of sentinel lymph node metastases by intraoperative radioactive threshold and molecular analysis in patients with melanoma, J. Nucl. Med. **49** (2008) 1769–1775.

[3.119] UREN, R.F., Lymphatic drainage of the skin, Ann. Surg. Oncol. **11** (2004) 179S–185S.

[3.120] STATIUS MULLER, M.G., et al., Unpredictability of lymphatic drainage patterns in melanoma patients, Eur. J. Nucl. Med. Mol. Imaging **29** (2002) 255–261.

[3.121] VALDES-OLMOS, R., VIDAL-SICART, S., NIEWEG, O., SPECT-CT and real-time intraoperative imaging: new tools for sentinel node localization and radioguided surgery? Eur. J. Nucl. Med. Mol. Imaging **36** (2009) 1–5.

[3.122] EVEN-SAPIR, E., et al., Lymphoscintigraphy for sentinel node mapping using a hybrid SPECT/CT system, J. Nucl. Med. **44** (2003) 1413–1420.

[3.123] ISHIHARA, T., et al., Management of sentinel lymph nodes in malignant skin tumors using dynamic lymphoscintigraphy and the single-photon-emission computed tomography/computed tomography combined system, Int. J. Clin. Oncol. **11** (2006) 214–220.

[3.124] MAR, M.V., et al., Evaluation and localization of lymphatic drainage and sentinel lymph nodes in patients with head and neck melanomas by hybrid SPECT/CT lymphoscintigraphic imaging, J. Nucl. Med. Technol. **35** (2007) 10–16.

[3.125] KOVÁCS, A.F., et al., Positive sentinel lymph nodes are a negative prognostic factor for survival in T1-2 oral/oropharyngeal cancer — a long-term study on 103 patients, Ann. Surg. Oncol. **16** (2009) 233–239.

[3.126] CIVANTOS, F., et al., Sentinel node biopsy for squamous cell carcinoma of the head and neck, J. Surg. Oncol. **97** (2008) 683–690.

[3.127] PALERI, V., et al., Sentinel node biopsy in squamous cell cancer of the oral cavity and oral pharynx: a diagnostic meta-analysis, Head Neck **27** (2005) 739–747.

[3.128] FERLITO, A., SILVER, A., RINALDO, A., Elective management of the neck in oral cavity squamous carcinoma: current concepts supported by prospective studies, Br. J. Oral Maxillofac. Surg. **47** (2009) 5–9.

[3.129] SHOAIB, T., et al., The nodal neck level of sentinel lymph nodes in mucosal head and neck cancer, Br. J. Plast. Surg. **58** (2005) 790–794.

[3.130] CALABRESE, L., et al., "Sentinel lymph node biopsy in cancer of the head and neck", Radioguided Surgery: A Comprehensive Team Approach (MARIANI, G., GIULIANO, A.E., STRAUSS, W.H., Eds), Springer, New York (2008) 120–129.

[3.131] CIVANTOS, F.J., et al., Sentinel lymph node biopsy accurately stages the regional lymph nodes for T1-T2 oral squamous cell carcinomas: results of a prospective multi-institutional trial, J. Clin. Oncol. **28** (2010) 1395–1400.

[3.132] VERMEEREN, L., et al., A portable gamma-camera for intraoperative detection of sentinel nodes in the head and neck region, J. Nucl. Med. **51** (2010) 700–703.

[3.133] VAN DEN BERG, N.S., et al., Concomitant radio- and fluorescence-guided sentinel lymph node biopsy in squamous cell carcinoma of the oral cavity using ICG-^{99m}Tc-nanocolloid, Eur. J. Nucl. Med. Mol. Imaging **39** (2012) 1128–1136.

[3.134] ROH, J.L., KOCH, W.M., Role of sentinel lymph node biopsy in thyroid cancer, Expert Rev. Anticancer. Ther. **10** (2010) 1429–1437.

[3.135] KOSAKA, T., et al., Lymphatic routes of the stomach demonstrated by gastric carcinomas with solitary lymph node metastasis, Surg. Today **29** (1999) 695–700.

[3.136] TAKEUCHI, H., KITAGAWA, Y., Sentinel node navigation surgery for esophageal cancer, Gen. Thorac Cardiovasc. Surg. **56** (2008) 393–396.

[3.137] OTANI, Y., et al., New method of laparoscopy-assisted function-preserving surgery for early gastric cancer: vagus-sparing segmental gastrectomy under sentinel node navigation, J. Am. Coll. Surg. **198** (2004) 1026–1031.

[3.138] KITAGAWA, Y., SAHA, S., KUBO, A., Sentinel node for gastrointestinal malignancies, Surg. Oncol. Clin. North Am. **16** (2007) 71–80.

[3.139] HAYASHI, H., et al., Sentinel lymph node mapping for gastric cancer using a dual procedure with dye- and gamma probe-guided techniques, J. Am. Coll. Surg. **196** (2003) 68–74.

[3.140] GRETSCHEL, S., et al., Efficacy of different technical procedures for sentinel lymph node biopsy in gastric cancer staging, Ann. Surg. Oncol. **14** (2007) 2028–2035.

[3.141] KITAGAWA, Y., et al., Radioguided sentinel node detection for gastric cancer, Br. J. Surg. **89** (2002) 604–608.

[3.142] EUNOSONO, Y., et al., Detection of sentinel nodes and micrometastases using radioisotope navigation and immunohistochemistry in patients with gastric cancer, Br. J. Surg. **92** (2005) 886–889.

[3.143] BILCHIK, A., et al., Aberrant drainage of missed micrometastases: the value of lymphatic mapping and focused analysis of sentinel lymph nodes in gastrointestinal neoplasms, Ann. Surg. Oncol. **8** (2001) 82–85.

[3.144] KITAGAWA, Y., et al., "Sentinel lymph node mapping in esophageal and gastric cancer — impact on individualized minimally invasive surgery", Selective Sentinel Lymphadenectomy for Human Solid Cancer (LEONG, S., KITAJIMA, M., KITAGAWA, Y., Eds), Springer, New York (2005) 123–139.

[3.145] STOJADINOVIC, A., et al., Prospective randomized study comparing sentinel lymph node evaluation with standard pathologic evaluation for the staging of colon carcinoma: results from the United States Military Cancer Institute Clinical Trials Group Study GI-01, Ann. Surg. **245** (2007) 846–857.

[3.146] BEMBENEK, A.E., et al., Sentinel lymph node biopsy in colon cancer: a prospective multicenter trial, Ann. Surg. **245** (2007) 858–863.

[3.147] KITAGAWA, Y., et al., Sentinel node mapping for colorectal cancer with radioactive tracer, Dis. Colon Rectum **45** (2002) 1476–1480.

[3.148] FUJITA, S., YAMAMOTO, S., AKASU, T., Lateral pelvic lymph node dissection for advanced lower rectal cancer, Br. J. Surg. **90** (2003) 1580–1585.

[3.149] KESHTGAR, M.R., et al., The sentinel node in anal carcinoma, Eur. J. Surg. Oncol. **27** (2001) 113–114.

[3.150] PÉLEY, G., et al., Inguinal sentinel lymph node biopsy for staging anal cancer, Scand. J. Surg. **91** (2002) 336–338.

[3.151] PERERA, D., et al., Sentinel node biopsy for squamous-cell carcinoma of the anus and anal margin, Dis. Colon Rectum **46** (2003) 1027–1031.

[3.152] ULMER, C., BEMBENEK, A., GRETSCHEL, S., Sentinel node biopsy in anal cancer — a promising strategy to individualize therapy, Onkologie **26** (2003) 456–460.

[3.153] DAMIN, D.C., ROSITO, M.A., SCHWARTSMANN, G., Sentinel lymph node in carcinoma of the anal canal: a review, Eur. J. Surg. Oncol. **32** (2006) 247–252.

[3.154] GRETSCHEL, S., et al., Lymphatic mapping and sentinel lymph node biopsy in epidermoid carcinoma of the anal canal, Eur. J. Surg. Oncol. **34** (2008) 890–894.

[3.155] MISTRANGELO, M., et al., Feasibility of the sentinel node biopsy in anal cancer, Q. J. Nucl. Med. Mol. Imaging **53** (2009) 3–8.

[3.156] RABBITI, P., et al., Sentinel lymph node biopsy for squamous cell carcinoma of the anal canal, ANZ J. Surg. **72** (2002) 651–654.

[3.157] AKRIVOS, N., et al., Detection and credibility of sentinel node in vulvar cancer: a single institutional study and short review of literature, Arch. Gynecol. Obstet. **284** (2011) 1551–1556.

[3.158] ROBISON, K., HOLMAN, L.L., MOORE, R.G., Update on sentinel lymph node evaluation in gynecologic malignancies, Curr. Opin. Obstet. Gynecol. **23** (2011) 8–12.

[3.159] WESPES, E., The management of regional lymph nodes in patients with penile carcinoma and reliability of sentinel node biopsy, Eur. Urol. **52** (2007) 5–6.

[3.160] SADEGHI, R., et al., Accuracy of sentinel lymph node biopsy for inguinal lymph node staging of penile squamous cell carcinoma: systematic review and meta-analysis of the literature, J. Urol. **187** (2012) 25–31.

[3.161] KROON, B.K., et al., How to avoid false-negative dynamic sentinel node procedures in penile carcinoma, J. Urol. **171** (2004) 2191–2194.

[3.162] LEIJTE, J.A.P., et al., Reliability and safety of current dynamic sentinel node biopsy for penile carcinoma, Eur. Urol. **52** (2007) 170–177.

[3.163] MEINHARDT, W., et al., Laparoscopic sentinel lymph node biopsy for prostate cancer: the relevance of locations outside the extended dissection area, Prostate Cancer **2012** (2012) 751753.

[3.164] VERMEEREN, L., et al., Intraoperative imaging for sentinel node identification in prostate carcinoma: its use in combination with other techniques, J. Nucl. Med. **52** (2011) 741–744.

[3.165] HOLL, G., et al., Validation of sentinel lymph node dissection in prostate cancer: experience in more than 2,000 patients, Eur. J. Nucl. Med. Mol. Imaging **36** (2009) 1377–1382.

[3.166] SADEGHI, R., et al., Sentinel node mapping in the prostate cancer, Nuklearmedizin **50** (2011) 107–115.

[3.167] BROUWER, O.R., et al., SPECT/CT and a portable gamma-camera for image-guided laparoscopic sentinel node biopsy in testicular cancer, J. Nucl. Med. **52** (2011) 551–554.

Chapter 4

TECHNETIUM-99m TILMANOCEPT:
A SYNTHETIC RECEPTOR TARGETED MOLECULE
FOR SLNM

D.R. VERA, C.K. HOH, D.J. HALL
UCSD Molecular Imaging Program,
Division of Nuclear Medicine, Department of Radiology

C.A. TOKIN, A.M. WALLACE
Divisions of Oncologic Surgery and Plastic and Reconstructive Surgery,
Department of Surgery
UCSD Moores Cancer Center, University of California,
San Diego, La Jolla, California, USA

4.1. SUMMARY

Tilmanocept is a synthetic molecular radiopharmaceutical that was designed to minimize the limitations of currently used agents for SLN identification. Optimal size and specific binding properties allow for improved lymphatic uptake and high retention in the sentinel node, ultimately allowing for an improvement in the accuracy of cancer staging in diseases that utilize SLNM. The use of tilmanocept avoids dangers associated with the use of human or animal derived substances, and has a superior safety profile, avoiding the adverse reactions associated with many of the other agents used today. Furthermore, its chemical properties allow for the attachment of additional imaging reporters, permitting future multimodal imaging of the SLN via a molecular target.

4.2. INTRODUCTION

The SLN is the first draining lymph node in a lymphatic basin and is, therefore, the most likely lymph node to harbour metastatic disease. The concept of the SLN was first introduced by Cabanas in 1977 [4.1]. In 1992, Morton et al. [4.2] developed a dye based technique for intraoperatively finding the SLN. If the SLN is negative for tumour metastasis, the procedure can be used in lieu of complete regional lymphadenectomy [4.3], minimizing morbidity.

SLNB has been used for many solid tumours and has been validated in breast cancer and melanoma as a strong predictor of lymph node status and

long term patient outcome [4.4, 4.5]. While SLNB has been proven to be feasible and reliable, there is still a question as to the optimal agent for SLN identification. The procedure was conceived using VBD that could enter and image lymphatics, and has been validated and improved upon by combining the VBD with a radiopharmaceutical [4.1, 4.6].

Current radiotracers were not specifically designed for SLN imaging and rely on passive uptake. Technetium-99m tilmanocept has been designed to address the shortcomings of the older lymphatic radiopharmaceuticals. On 13 March 2013, the FDA approved ^{99m}Tc tilmanocept for intraoperative lymph node mapping for breast cancer or melanoma.

4.2.1.   Background

Identifying the SLN with high precision is crucial for accurate staging and for monitoring disease progression. It is most commonly used in breast cancer and melanoma; however, it has also been used in various gastrointestinal [4.7] and gynaecological cancers [4.8], as well as in cancers of the head and neck [4.9]. The current technique of SLNB involves the injection of a lymphatic mapping agent, which is most commonly a combination of a VBD and a radiopharmaceutical Tc labelled colloid [4.10]. Dissection is carried out until the SLN is identified intraoperatively via visualization of a blue hue or an acoustic signal from a hand held gamma probe.

Blue dye and colloid based radiotracers are not specifically designed for rapid and specific uptake into the lymphatic system, or for retention in the sentinel node. Their biological properties are largely dependent on passive diffusion governed by particle size. The speed at which a particle enters and stays within a lymph node is related to the size of the particle [4.6]. While particles less than 4–5 nm easily enter lymph channels, their small sizes do not permit long SLN retention times. Larger colloids are taken up by lymphatics at a slower rate, but are retained in lymph nodes for longer periods of time, presumably via phagocytosis by recticuloendothelial macrophages [4.6].

Technetium-99m labelled sulphur colloid was introduced in the mid-1960s for use in hepatic imaging, but has become the most commonly used colloidal SLN imaging agent in the USA [4.11]. A filter can be applied to theoretically limit the particle size to 50–200 nm; however, its relatively large overall size results in slow entry into the lymphatic system, as well as slow injection site clearance. Other preferred radiotracers are Nanocoll (GE Healthcare, Milan, Italy) and ^{99m}Tc HSA nanocolloid (4–80 nm), which are most commonly used in Europe, and Lymph-Flo (Royal Adelaide Hospital, Adelaide, Australia) and ^{99m}Tc colloidal antimony sulphide (~10 nm), which are most commonly used in Australia [4.12, 4.13].

Blue dyes also rely on passive diffusion to enter the lymphatic system, and, owing to their small molecular size, they clear quickly from the lymph nodes [4.6, 4.14]. Isosulphan blue (Lymphazurin) is the most commonly used VBD for intraoperative lymphatic mapping in the USA. It is injected intraoperatively, with visualization of the afferent lymphatics possible within minutes. VBDs have been associated with rare, but significant adverse reactions, including anaphylaxis and cardiopulmonary arrest [4.15, 4.16].

4.2.2.   Ideal sentinel node imaging agent

An ideal SLN imaging agent would exhibit rapid injection site clearance, while not interfering with detection of sentinel nodes in close proximity to the injection site. The tracer should exhibit rapid SLN accumulation with sustained SLN retention. High SLN uptake with low leakage to higher echelon nodes allows for more flexibility in the scheduling of imaging. The agent must also have a favourable safety profile, specifically, with no associated adverse reactions.

In addition, the agent must be synthetic and provide for future development. These features are not exhibited by the current agents, which are colloidal forms of albumin, sulphur and/or antimony. Nanocoll is composed of albumin, which is derived from human blood. This has a serious disadvantage during production, when the chemistry manufacturing and control protocols must be constantly updated for continuous monitoring of viral contamination. Although the probability of a viral 'breakthrough' into the final radiopharmaceutical kit is extremely low, the cost of screening the donated blood and the associated regulatory compliance is very high [4.17]. Currently, the donated blood used to produce Nanocoll is tested for hepatitis B surface antigen, HIV antibodies and antibodies to the hepatitis C virus [4.18]. The sulphur and antimony sulphide colloids do not offer a path for future development. These agents consist of chemical constituents that are not amenable to chemical modification. Examples, which are not possible for these agents, would be the attachment of fluorophores for hybrid imaging or chelation systems, to which PET or therapeutic radioisotopes can be attached.

4.2.3.   Technetium-99m tilmanocept

Technetium-99m tilmanocept (Fig. 4.1) [4.19] is a synthetic receptor binding radiopharmaceutical that was designed [4.20] to address the shortcomings of commonly used SLNM agents. Tilmanocept is the generic name for DTPA mannosyl dextran. It is a macromolecule composed of a dextran backbone and multiple subunits of DTPA and mannose. Figures 4.2–4.4 illustrate the chemical synthesis of tilmanocept, which culminates in the attachment of DTPA and
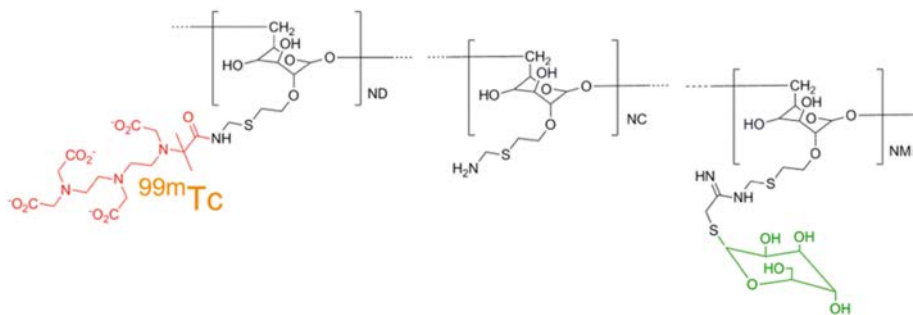
FIG. 4.1. Technetium-99m labelled tilmanocept, ^{99m}Tc DTPA mannosyl dextran, is composed of repeated units of mannose (green) and units of DTPA (red) attached to a 10 kg/mol chain of glucose.
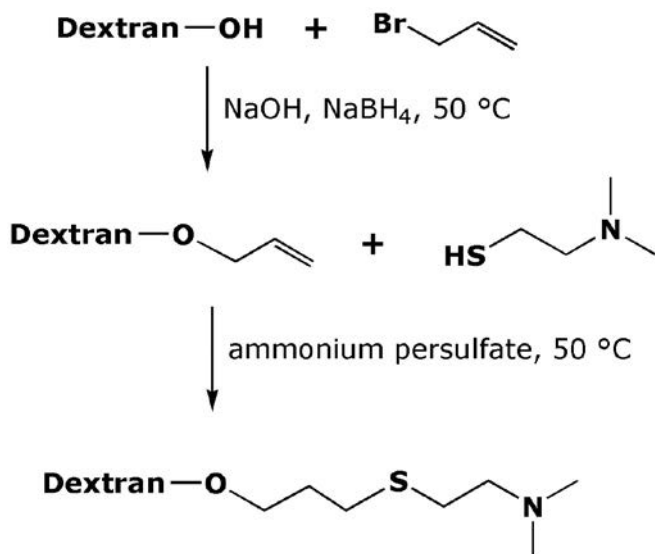

FIG. 4.2. Production of tilmanocept starts with the attachment of aminoterminated leashes, which uses a two step process to prevent cross-linking of the dextran.

mannose to residues on the dextran backbone. The molecule has an average size of 7 nm, which allows for rapid entry into lymphatic channels and rapid injection site clearance [4.20]. Production yields 200 g of tilmanocept. The synthesis begins with the attachment of the aminoterminated leashes, which is a two step process that prevents dextran cross-linking. This is necessary to produce a high density of attachment sites, and consequently, the ability to attach a high number of substrates and chelators or imaging reporters. The high density of receptor
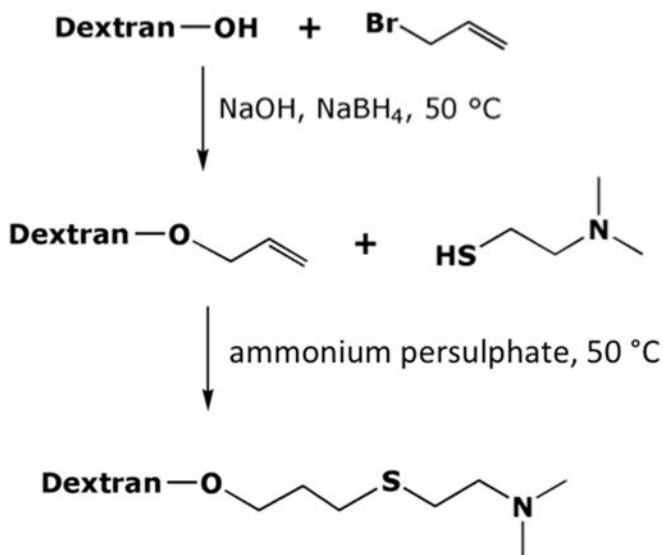
FIG. 4.3. The ratio of starting reactants, 2-imino-2-methoxyethyl-1-thio-D-manno-pyranoside, and the number of amino terminated side chains of the conjugated dextran control the mannose density (average number of mannose groups per dextran) of the product.
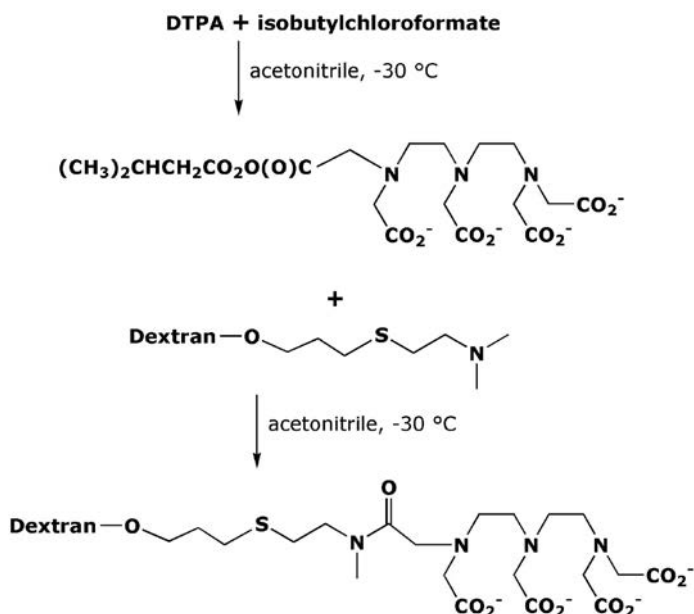

FIG. 4.4. The mixed anhydride method [4.21] was used to attach DTPA. This method prevents cross-linking of the dextran backbone.

substrates enables multivalency, which increases receptor affinity [4.22]. A high density of imaging reporters is a significant consideration during the design of magnetic resonance and CT based contrast agents [4.23, 4.24].

The DTPA side chains enable efficient radiolabelling with [99m]Tc [4.20]. Typical radiolabelling yields were in excess of 98% [4.20], and remain stable at room temperature for at least 20 h (Fig. 4.5). This is in contrast to filtered ^{99m}Tc sulphur colloid, which typically [4.25] loses stability after filtration (Fig. 4.6). The selection of DTPA as the chelator was based on clinical experience with ^{99m}Tc galactosyl neoglycoalbumin [4.26], which is commercially available in Japan as Galactoscint (Nihon Mediphysics, Tokyo). This agent successfully uses DTPA as the chelation system; it exhibited a plasma clearance equivalent to that of ^{131}I albumin [4.27]. A nitrogen sulphur tetradentate chelation system, mercaptoacetyltriglycine (MAG$_3$), which provided similar radiochemical yields and stability [4.28], was explored, but the development was discontinued when it was realized that the FDA would require preclinical toxicology studies with the radiolabelled agent. This is because the chemical structure of the chelation system changes during radiolabelling as the low pH and heat remove the benzoyl protecting group to expose the SH group. Another disadvantage of MAG$_3$ is its inability to chelate +3 cations, which would prevent radiolabelling with ^{111}In, ^{67}Ga or [68]Ga.
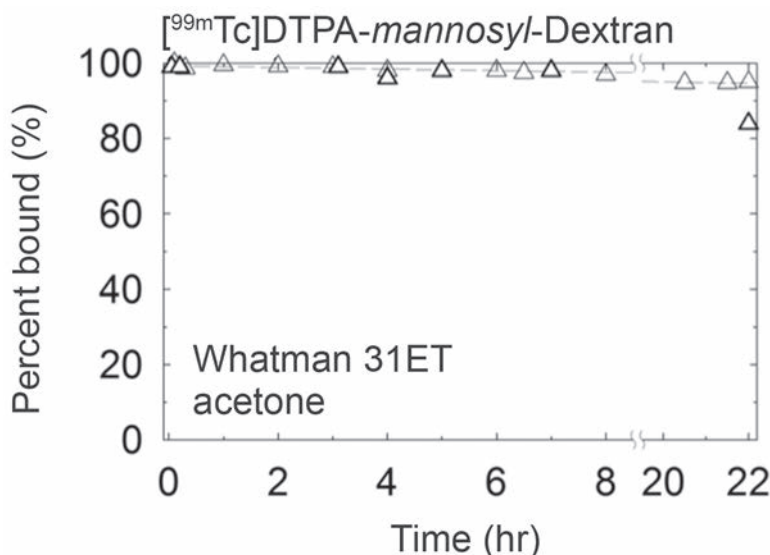

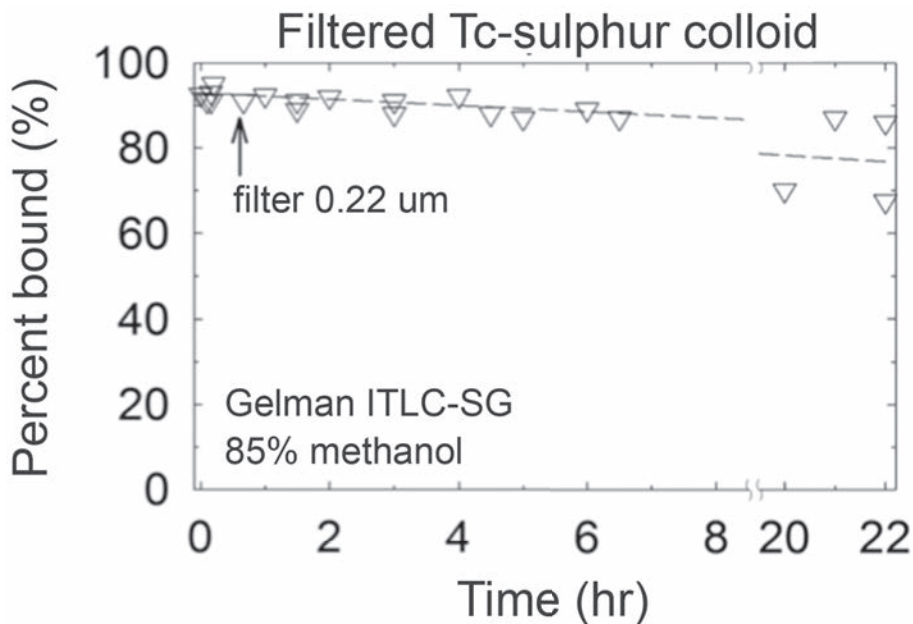FIG. 4.5. Stability of the ^{99m}Tc radiolabel at room temperature.

FIG. 4.6. Filtration of ^{99m}Tc labelled sulphur colloid destabilizes the radiolabel.

The mannose units act as ligands for the mannose binding protein receptor [4.29], which has been designated CD206. This receptor resides at the cell surface macrophages and dendritic cells in high concentrations. Figure 4.7 is a Scatchard plot of ^{99m}Tc tilmanocept binding to J774E cells, which are macrophages that express CD206. The equilibrium dissociation constant K_D was 0.36nM [4.30]. Low K_D values denote high receptor affinity. As a general rule, receptor binding radiopharmaceuticals [4.31] designed for high tissue extraction require dissociation constants in the subnanomolar range. High binding affinity allows for improved retention in sentinel nodes and diminished leakage into higher echelon nodes.

Initially, an SLN agent was constructed with a polylysine backbone [4.32]. The molecule DTPA mannosyl polylysine, consisting of 18 DTPAs, 82 mannosyl groups attached to a chain of 100 lysines, provided receptor specific images of rabbit popliteal and axillary lymph nodes that gave a mean lymph node accumulation of 2.9% of dose 24 h after injection into each foot-pad. A non-specific agent, DTPA polylysine, delivered one tenth of the radioactivity at the same time after injection. Although the polylysine construct demonstrated receptor specific delivery, it was elected to design the agent based on a dextran backbone. This decision was based on three reasons: polylysine is very expensive,
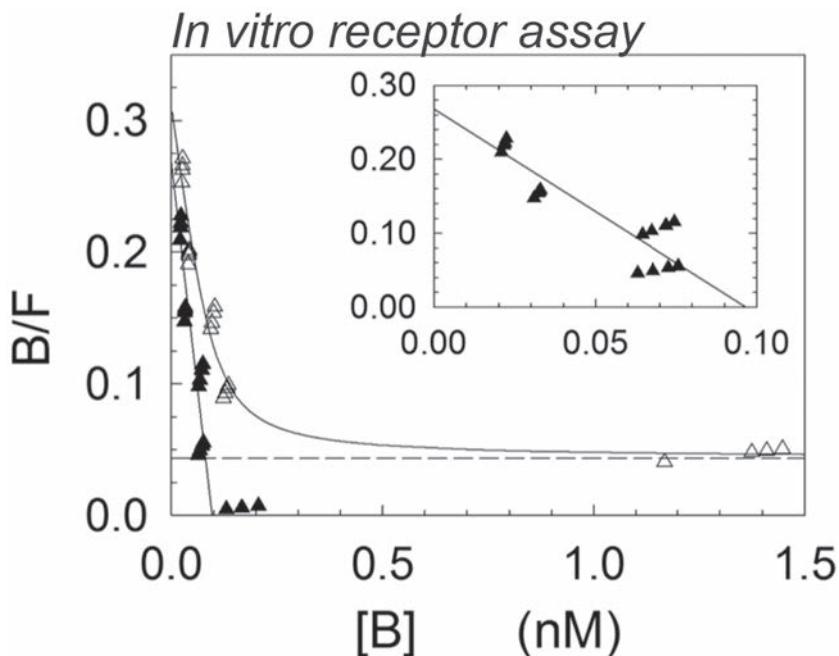
FIG. 4.7. *High density of mannose substrates, 55 per dextran, produced a receptor binding radiopharmaceutical with high binding affinity. The slope of the line within the inset graph provides a measure of the equilibrium dissociation constant K_D (0.36nM).*

it has a very limited human use database and it is relatively hydrophobic. Dextran is inexpensive and has a well established safety record [4.33]. Additionally, clinical grade dextran is available in highly defined molecular sizes, and, most significantly, is very hydrophilic.

4.2.4. Lymphoseek

Lymphoseek (Navidea Biopharmaceuticals, Dublin, OH) is a formulation that contains tilmanocept. The radiolabelling of tilmanocept with ^{99m}Tc employs an 'instant' kit method. The Lymphoseek kit is composed of two vials: one containing a lyophilized drug product, tilmanocept, and one containing a dilutant buffer solution. Lymphoseek contains tilmanocept (0.25 mg, 16 738 g/mole), trehalose dehydrate (20 mg), glycine (0.5 mg), sodium ascorbate (0.5 mg) and stannous chloride (75 µg). The average mannose and DTPA densities of the Lymphoseek preparation are 16.8 mannose units per dextran and 4.4 DTPA units per dextran, respectively. The dilutant buffer solution was 0.2M phosphate buffered saline (PBS). The tilmanocept synthesis, Lymphoseek

product formulation and vial preparation were performed using current good manufacturing practice guidelines and a chemical and manufacturing control package registered with the FDA.

Radiolabelling was conducted via the following steps. A sterile, apyrogenic and oxidant free solution of sodium pertechnetate ^{99m}Tc in injectable isotonic saline was added to the vial containing the lyophilized drug product. Isotonic injectable saline was then added to the vial to produce a 0.5 mL volume. The vial was then gently swirled to produce a clear, colourless solution, and was placed in a lead lined container to stand at room temperature for at least 30 min. The procedure was completed by adding 1.0 mL of PBS from the kit dilutant vial. A patient dose for a single intradermal administration consisted of 0.1 mL of labelled product within a 0.3 mL insulin syringe with a fixed 27 gauge needle. Quality control consisted of instant thin layer chromatography (ITLC) with Whatman 31ET as the stationary phase and dry acetone as the mobile phase. Technetium-99m tilmanocept migrated with the solvent front. During the phase 3 clinical trials, the radiochemical purity typically exceeded 98%. All patients received 3 nmol of tilmanocept. If SLNM was performed on the same day as the injection, the total activity administered was 18.5 MBq. If mapping was performed on the next day, the dose was 37 MBq.

4.3. PRECLINICAL STUDIES

The preclinical studies of tilmanocept were designed to optimize synthesis and purification, evaluate drug pharmacokinetics and establish biodistribution and safety profiles.

4.3.1. Pharmacokinetics

The preclinical studies concluded that tilmanocept possessed three ideal pharmacokinetic properties: rapid clearance from the injection site, appropriate accumulation in the sentinel node and high sentinel node retention. These properties allow for improved SLN visualization secondary to reduced injection site scatter, thus improving the quality of the diagnostic image obtained. Rapid accumulation allows tilmanocept to be effective intraoperatively, while high retention in the sentinel node with reduced washout to higher echelon nodes increases precision and may reduce the number of nodes excised.

4.3.2. Injection site clearance

Injection site clearance studies were performed in rabbits and compared to filtered ^{99m}Tc sulphur colloid. Tilmanocept was injected subdermally into the feet pads of rabbits, with a resultant clearance half-life of 2.21 ± 0.27 h. This was significantly faster than filtered ^{99m}Tc sulphur colloid at both 1 h and 3 h time points, which was confirmed after calculation of the percentage of injected dose (% ID) ($p < 0.05$) [4.20].

This was also true after endoscopic injection of tilmanocept [4.34] into the gastrointestinal tract using a porcine model, again, as compared to filtered ^{99m}Tc sulphur colloid. After endoscopic submucosal injection into either the stomach or colon, tilmanocept revealed clearance half-lives of 3.83 ± 1.18 h and 2.56 ± 1.04 h, respectively. This revealed a statistically significant improvement in injection site clearance ($p = 0.03$) compared with filtered ^{99m}Tc sulphur colloid [4.35].

4.3.3. SLN accumulation

Rapid accumulation in the sentinel node was demonstrated in porcine animal studies, where sentinel node uptake of tilmanocept was not statistically different to uptake of filtered ^{99m}Tc sulphur colloid after injection into either the gastric or colonic submucosa. Tilmanocept exhibited high sentinel node uptake within 10 min of submucosal injection (0.13%–4.5% ID for gastric lymph nodes and 0.54%–2.4% ID for colonic lymph nodes) [4.34]. Rapid accumulation within the sentinel node was also exhibited after peritumoural injection of tilmanocept in porcine prostate cancer models following prostatectomy [4.36].

4.3.4. SLN retention

Tilmanocept exhibited improved and prolonged retention in SLNs compared to filtered ^{99m}Tc sulphur colloid in rabbit studies comparing sentinel nodes to distal nodes. Tilmanocept was injected proximal to the popliteal fossa, and popliteal lymph nodes were compared to distal inguinal lymph nodes to evaluate retention in the sentinel nodes. At both 1 h and 3 h postinjection time points, retention for tilmanocept in the popliteal nodes was higher ($p < 0.05$) than filtered ^{99m}Tc sulphur colloid, representing less leakage of the imaging agent to the distal inguinal nodes. This was further demonstrated in porcine prostatectomy studies where tilmanocept was sustained in the SLN for up to 3 h without washing out to distal nodes [4.35, 4.36].

4.3.5. Biodistribution, toxicity and absorbed radiation dose

Preclinical biodistribution and toxicity studies have shown that tilmanocept possesses an acceptable biodistribution profile and favourable safety profile [4.37, 4.38]. Preclinical safety studies included single dose acute toxicity in rats and rabbits (50× and 500× scaled human dose) and dogs (170×, 780× and 1700×), perivascular irritation studies in rabbits (100×), a repeat dose study in rats and dogs (14 consecutive days at 42×, 85× and 170×), cardiac safety pharmacology studies in dogs (1700× and 3400×), a sensitization study in guinea pigs (56×, 113× and 1130×), a lymphoma mutagenesis study in mice (300×), an in vitro reverse mutation study in bacteria (0.3 nmol/mL, 0.9 nmol/mL, 3 nmol/mL, 9 nmol/mL and 90 nmol/mL) and an in vitro micronucleus study in mice (2.5×, 5× and 10×).

The biological half-life of tilmanocept is 2.21 ± 0.27 h, and the effective dose is half the value of the albumin based nanocolloid, thereby minimizing radiation dose and exposure to the patient as well as to clinical staff [4.39]. No direct toxicity, including anaphylactic reactions or increased mortality, were noted in any of the preclinical animal studies, regardless of dose or route of injection.

4.4. CLINICAL TRIALS

4.4.1. Phase 1 clinical trials

Physician sponsored phase 1 clinical trials, each supported by peer reviewed extramural funding of the University of California, were conducted to establish ^{99m}Tc tilmanocept's clinical safety profile and biodistribution in human subjects. They demonstrated that tilmanocept exhibited faster injection site clearance and equivalent primary SLNs compared to filtered ^{99m}Tc sulphur colloid. After peritumoural injections of 12 breast cancer patients with 1.0 nmol of tilmanocept, a mean injection site clearance half-life of 2.72 ± 1.57 h was measured. This value was significantly shorter than for filtered ^{99m}Tc sulphur colloid, which exhibited a mean clearance half-life of 49.5 ± 38.5 h ($p = 0.0025$) [4.40]. There was no statistical difference (tilmanocept: $0.55\% \pm 16.8\%$ ID versus filtered ^{99m}Tc sulphur colloid: $0.65\% \pm 15.7\%$ ID) in the sentinel node uptake at 3 h postinjection ($p = 0.75$). Twelve additional patients were studied at two additional molar doses (0.2 nmol and 5.0 nmol) [4.37]. No difference in injection site clearance was observed. The mean amounts of ^{99m}Tc tilmanocept in the primary SLN of the 0.2 nmol, 1.0 nmol and 5.0 nmol groups were 0.11 ± 0.20 pmol, 5.5 ± 4.3 pmol and 11.0 ± 8.5 pmol, respectively.

Additional phase 1 trials were performed using a single 0.10 mL intradermal injection. Figure 4.8 depicts the injection site clearance of radioactivity after a single dose intradermal administration of tilmanocept and filtered ^{99m}Tc sulphur colloid in two SLN cases [4.41]. In these cases, tilmanocept exhibited a half-life of 2.62 ± 0.55 h, versus a filtered ^{99m}Tc sulphur colloid half-life of 24.1 ± 17.7 h. The mean SLN uptake of ^{99m}Tc tilmanocept, 1.1 ± 0.5 %IA/g (% of injected activity per gram), was lower than filtered ^{99m}Tc sulphur colloid, 2.5 ± 4.9 %IA/g. These values were higher than the SLN uptake after a peritumoural injection.

A fourth study compared tilmanocept with unfiltered ^{99m}Tc sulphur colloid while specifically using a '2 day' protocol [4.42]. The purpose of this study was to assess tilmanocept's effectiveness with delayed lymphoscintigraphy. Imaging and intraoperative mapping were performed 18–26 h postinjection. Again, tilmanocept exhibited faster injection site clearance and equivalent SLN accumulation, which persisted for longer than 24 h [4.43]. This study demonstrated tilmanocept's high SLN retention. This property extends the potential time period from injection to surgery, permitting 2 day surgical procedures and the ability to image on the same day as injection without the need for additional imaging on the day of surgery.
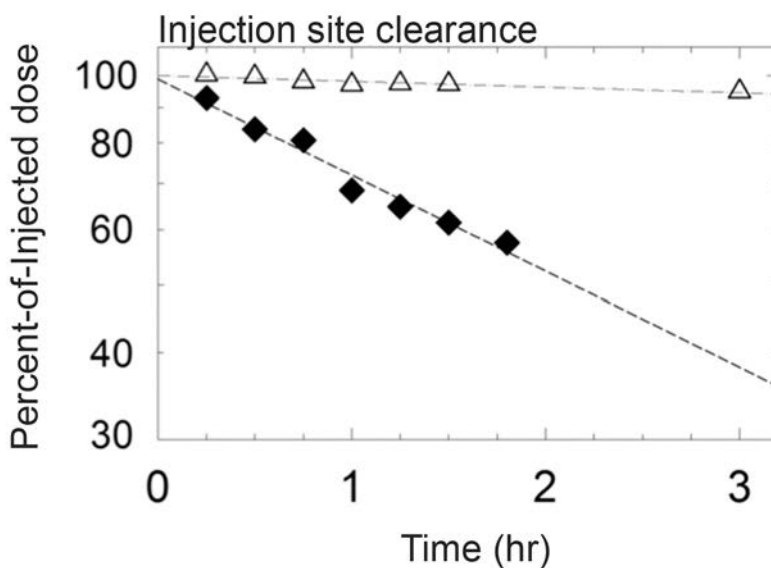

FIG. 4.8. Injection site clearance after a single 0.1 mL intradermal administration; ^{99m}Tc tilmanocept (diamonds) exhibited a half-life of 1.16 ± 0.10 h and filtered ^{99m}Tc sulphur colloid (triangles) exhibited a half-life of 36.7 ± 6.5 h.

Lastly, a preliminary study was conducted to determine the concordance between the number of SLNs detected on early and 'next day' images, and during SLNM. Nine women with unilateral breast cancer and one woman with bilateral breast cancer enrolled in the trial. All patients received ^{99m}Tc tilmanocept (1.0 nmol, 37 MBq) as a single intradermal injection (0.10 mL) the day prior to surgery. Lymphoscintigraphy was performed at 2 h and 15 h, and SLNB was performed between 16 h and 24 h postinjection. Lymphoseek administration the day prior to surgery resulted in the identification of at least one sentinel node in all cases. A total of 19 lymph nodes were identified by lymphoscintigraphy. The concordance between the 2 h and 15 h images was 100% ($\tau = 1.0$, $p = 0.0013$; (τ = Kendall rank correlation coefficient)). In the operating room, 20 sentinel nodes were identified using a gamma detector; the concordance between imaging and SLNM was 93% ($\tau = 0.93$, $p = 0.0020$). Figure 4.9 shows images acquired at 2 h and 14.5 h after an intradermal injection of ^{99m}Tc tilmanocept, demonstrating sustained uptake by a single lymph node. Only one hot lymph node was found at surgery 18.9 h postinjection. Although preliminary, this study highlights the SLN retention of ^{99m}Tc tilmanocept. The small molecular diameter provides rapid SLN uptake, and the high receptor affinity retains the molecules at the SLN for many hours.

An estimated absorbed radiation dose calculated from these preliminary studies concluded that the radiation dose for tilmanocept was 25% of that which would be delivered in an equivalent dose of filtered ^{99m}Tc sulphur colloid [4.37]. Furthermore, the remaining radiation dose after tumour excision in melanoma patients was almost three times higher after filtered ^{99m}Tc sulphur colloid injection
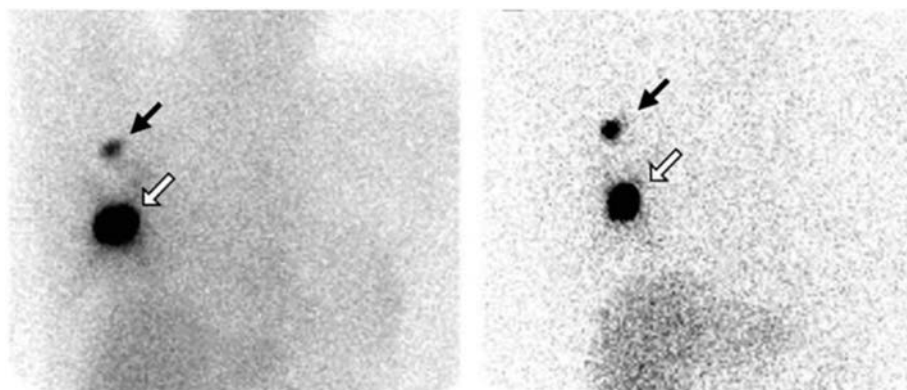

FIG. 4.9. Lymphoscintigraphic images (anterior) acquired at 2 h (left) and 14.5 h (right) postinjection of ^{99m}Tc tilmanocept demonstrated sustained uptake by a single lymph node (black arrow). The injection site is at the open arrow. Only one hot lymph node was found at surgery 18.9 h postinjection.

compared with tilmanocept. No adverse reactions were reported in any patients, and no significant alterations in clinical laboratory tests were noted [4.37, 4.44].

4.4.2. Phase 2 clinical trials

In 2006, after safety standards for tilmanocept were established, Navidea Biopharmaceuticals sponsored a multicentre phase 2 clinical trial [4.45] to evaluate the effectiveness of tilmanocept in breast cancer and melanoma patients in five cancer centres across the USA (MD Anderson Cancer Center, John Wayne Cancer Center, Case Western Reserve University Hospital, University of California, San Francisco, and the University of Louisville). A total of 80 patients were enrolled, consisting of 31 patients with breast cancer and 49 patients with melanoma. They received 50 µg (3 nmol) of tilmanocept, which was injected peritumourally. The primary outcome was to establish and evaluate the applicability of ^{99m}Tc tilmanocept as a radiotracer for SLN identification. Technetium-99m tilmanocept demonstrated an SLN identification rate of 95%, and the SLN identification properties were conserved across tumour types. Concordance between tilmanocept and VBD was assessed: it was 89.5% for breast cancer patients and 97% for melanoma patients. Again, no adverse events related to tilmanocept were reported.

4.4.3. Phase 3 clinical trials

Two multicentre phase 3 clinical trials have been completed [4.46, 4.47]. The first, NEO3-05, was completed in December 2009, and involved a total of 136 breast cancer and melanoma patients, who provided a total of 215 lymph nodes. Fifteen institutions participated. The primary end point of NEO3-05 was concordance of tilmanocept and VBD in the in vivo detection of excised lymph nodes, identified as SLNs, and confirmed by pathology. Tilmanocept revealed a 98% overall concordance rate, which was consistent across tumour types. Reverse concordance was established to determine whether tilmanocept identified lymph nodes that VBD had not identified, and revealed that tilmanocept was able to identify 85 additional lymph nodes that had been missed by VBD; 18% of those missed nodes were found to contain cancer after final pathological evaluation. This analysis translated into a false negative rate for VBD that was three times that of tilmanocept.

A second phase 3 clinical trial, NEO3-09, was completed in 2011. This trial, which used the same entry criteria and end points as NEO3-05, was implemented to extend the safety database. It involved a total of 229 lymph nodes and resulted in a concordance rate of 100%, in that all nodes were identified by both tilmanocept and VBD. Tilmanocept's failed detection rate in this study was 0%,

which confirmed observations from NEO3-05; across the studies, tilmanocept missed no lymph nodes that contained cancer, and facilitated cancer detection in 6 out of a total of 55 patients (10.9%) with node positive disease whose cancer would have been entirely misdiagnosed had VBD been used as a single agent.

No serious tilmanocept related adverse events were reported in the 340 patients who participated in NEO3-05 or NEO3-09, whereas VBD caused anaphylaxis in one patient, which is consistent with reported severe adverse events associated with VBD and/or other radiolabelled colloids.

An additional phase 3 trial, NEO3-06, has completed enrolment. This trial studied 83 patients with head and neck cancer. After SLNM with ^{99m}Tc tilmanocept, a complete lymphadenectomy was performed. The primary end point of the study was to measure the false negative rate. Results from the statistical analysis and reporting of the findings will be available upon completion of full site and data audits planned for later in 2013. An interim evaluation [4.48] based on 19 disease positive patients from three sites revealed a false negative rate of 0%.

4.5. RETROSPECTIVE COMPARATIVE STUDIES

Since the completion of the tilmanocept clinical trials, there have been two studies that addressed tilmanocept's effectiveness compared to other sentinel node imaging agents. Both used meta-analysis of data pooled from the two tilmanocept phase 3 trials, NEO3-05 and NEO3-09, and compared them to meta-analyses of retrospective reviews of the clinical literature.

4.5.1. Comparison to radiocolloids

Results from one of the retrospective reviews revealed a sulphur colloid localization rate of 94.13% and a degree of localization of 1.6 after meta-analysis of the three peer reviewed studies, which, when compared to the tilmanocept data, showed that tilmanocept was superior in both end points measured. It should be noted, however, that no distinction between filtered or unfiltered sulphur colloid was made in this retrospective review.

A second retrospective review compared identical tilmanocept data to a review of the ^{99m}Tc albumin colloid (Nanocoll) literature. Six European trials were used to derive a ^{99m}Tc albumin colloid benchmark to which the tilmanocept end points could be compared. Meta-analysis [4.49] revealed a Nanocoll localization rate of 95% and a degree of localization of 1.67, and similarly concluded that tilmanocept was superior to ^{99m}Tc albumin colloid in both end points evaluated.

4.6. ADDITIONAL IMAGING MODALITIES

4.6.1. Rationale

One of the design requirements of the present study is the ability to chemically attach additional imaging reporters. This can be accomplished using tilmanocept by two independent means. First, the selection of DTPA permits radiolabelling with other +3 cations such as ^{68}Ga or ^{111}In. The first isotope, which is generator produced, would permit PET imaging, and the second isotope would permit imaging at later time points. A second means of adding an additional imaging reporter would be covalent attachment to one of the aminoterminated leashes that were not used to couple DTPA or mannose to the dextran backbone. Approximately five aminoterminated leashes per dextran are available for conjugation. This mechanism provides an opportunity to attach a fluorescent reporter [4.50] for optical imaging. The motivation for the fluorescent imaging reporter would be the ability to combine nuclear and fluorescence imaging. A dual modality agent composed of both fluorescent and nuclear imaging reporters would permit whole body or regional imaging, and the fluorescent reporter would provide images or detection within the surgical field. SLNM is an excellent clinical setting to utilize this opportunity.

4.6.2. PET imaging

Tilmanocept has been radiolabelled with ^{68}Ga [4.51]. Figure 4.10 is a fused PET/CT coronal cross-section of a beagle dog acquired 90 min after a transrectal injection into the prostate. The 1.5 mL dose contained 3.0 nmol of ^{68}Ga tilmanocept (10 MBq). The right common iliac lymph node had a standardized uptake value (SUV) of 54 and the SUV of the left common iliac lymph node was 53. SLNM, conducted 2 h postinjection, detected both lymph nodes; the right common iliac lymph node had a count rate of 1461 counts/min and accumulated 0.18% ID, and the left common iliac had a count rate of 2175 counts/min, which represented 1.66% ID. Two other lymph nodes, the right external iliac and periaortic, were visualized in other cross-sections. Four dogs were studied. There was a high concordance of PET/CT imaging to intraoperative SLNM, with a sensitivity approaching 93% for all nodes when the ex vivo count rates exceeded threefold background.

FIG. 4.10. Coronal fused PET/CT cross-section of a canine pelvis acquired 90 min after a 10 MBq prostate injection of ^{68}Ga tilmanocept. Two lymph nodes (LNs) are visualized (white arrows); the urinary bladder (blue arrow) and injection site (yellow arrow) are also within the field of view.

4.6.3. Fluorescence imaging

A near infrared (IR) cyanine (Cy) dye has been covalently attached to tilmanocept. A series of experiments [4.30] was carried out with ^{99m}Tc labelled Cy7 tilmanocept (Fig. 4.11). The goal was to establish that the attachment of the fluorescent tag did not alter the receptor binding properties of tilmanocept. In vitro binding assays to a macrophage cell line demonstrated that the subnanomolar affinity was maintained and that non-specific binding was not increased. Optical SLN imaging performed in mice (Fig. 4.12) demonstrated dose dependent SLN accumulation, which is a hallmark of in vivo receptor mediated binding [4.52]. These studies formed the motivation for development of a fluorescence imaging version of tilmanocept. Optical imaging will enable a wider dissemination of the SLN concept to hospitals without access to radiopharmaceuticals. This is especially true in developing countries, where hospitals are not equipped to handle radioactivity [4.53].
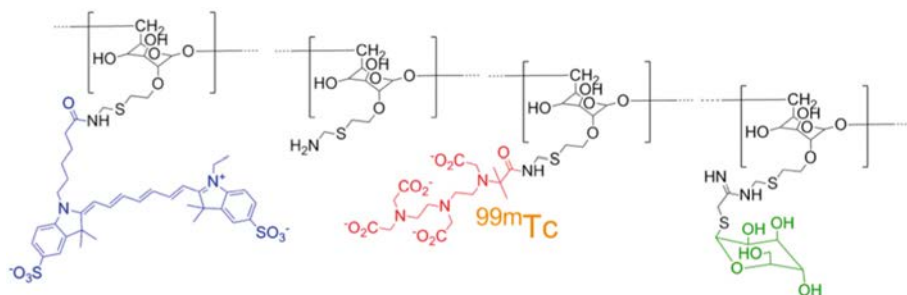
FIG. 4.11. A fluorescent imaging reporter, Cy7 (blue), was covalently attached to tilmanocept via an amino terminated leash. Fluorescence spectra demonstrated an emission peak at 780 nm, which is a 7 nm red shift from unattached Cy7.
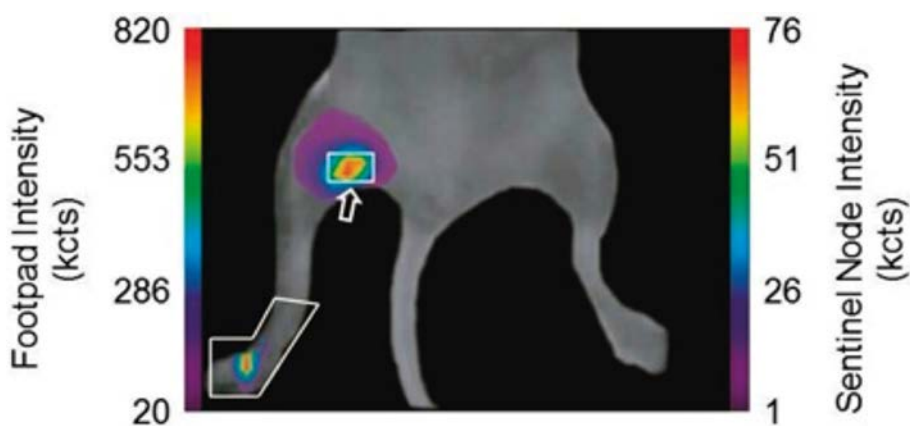
FIG. 4.12. An optical image at 150 min after a 0.11 nmol dose of Cy7 tilmanocept produced an SLN (arrow) with an integrated fluorescence intensity with the region of interest of 780×10^3 counts. The pixel with the highest fluorescence intensity had 64×10^3 counts. A time intensity curve from the SLN demonstrated sustained accumulation from 140×10^3 counts at 15 min to 800×10^3 counts at 100 min.

ACKNOWLEDGEMENTS

REFERENCES TO CHAPTER 4

[4.1]   CABANAS, R.M., An approach for the treatment of penile carcinoma, Cancer. **39** (1977) 491–499.

[4.2]   MORTON, D.L., et al., Technical details of intraoperative lymphatic mapping for early stage melanoma, Arch. Surg. **127** (1992) 392–399.

[4.3]   JATOI, I., HILSENBECK, S.G., CLARK, G.M., OSBORNE, C.K., Significance of axillary lymph node metastasis in primary breast cancer, J. Clin. Oncol. **17** (1999) 2334–2340.

[4.4]   SCHULZE, T., MUCKE, J., MARKWARDT, J., SCHLAG, P.M., BEMBENEK, A., Long-term morbidity of patients with early breast cancer after sentinel lymph node biopsy compared to axillary lymph node dissection, J. Surg. Oncol. **93** (2006) 109–119.

[4.5]   VERONESI, U., et al., Sentinel lymph node biopsy as an indicator for axillary dissection in early breast cancer, Eur. J. Cancer **37** (2001) 454–458.

[4.6]   MARIANI, G., et al., Radioguided sentinel lymph node biopsy in breast cancer surgery, J. Nucl. Med. **42** (2001) 1198–1215.

[4.7]   TANGOKU, A., et al., Current status of sentinel lymph node navigation surgery in breast and gastrointestinal tract, J. Med. Invest. **54** (2007) 1–18.

[4.8]   ROSSI, E.C., IVANOVA, A., BOGGESS, J.F., Robotically assisted fluorescence-guided lymph node mapping with ICG for gynecologic malignancies: a feasibility study, Gynecol. Oncol. **124** (2011) 78–82.

[4.9]   ALEX, J.C., The application of sentinel node radiolocalization to solid tumors of the head and neck: a 10-year experience, Laryngoscope **114** (2004) 2–19.

[4.10] ALBERTINI, J.J., et al., Intraoperative radiolymphoscintigraphy improves sentinel lymph node identification for patients with melanoma, Ann. Surg. **223** (1996) 217–224.

[4.11] LARSON, S.M., NELP, W.B., Radiopharmacology of a simplified technetium-99m-colloid preparation for photoscanning, J. Nucl. Med. **7** (1966) 817–826.

[4.12] GOMMANS, G.M., et al., ^{99m}Tc Nanocoll: a radiopharmaceutical for sentinel node localisation in breast cancer — in vitro and in vivo results, Appl. Radiat. Isot. **67** (2009) 1550–1558.

[4.13] TSOPELAS, C., Particle size analysis of ^{99m}Tc-labeled and unlabeled antimony trisulfide and rhenium sulfide colloids intended for lymphoscintigraphic application, J. Nucl. Med. **42** (2001) 460–466.

[4.14] CLEMENT, O., LUCIANI, A., Imaging the lymphatic system: possibilities and clinical applications, Eur. Radiol. **14** (2004) 1498–1507.

[4.15] ALBO, D., et al., Anaphylactic reactions to isosulfan blue dye during sentinel lymph node biopsy for breast cancer, Am. J. Surg. **182** (2001) 393–398.

[4.16] LAURIE, S.A., KHAN, D.A., GRUCHALLA, R.S., PETERS, G., Anaphylaxis to isosulfan blue, Ann. Allergy Asthma Immunol. **88** (2002) 64–66.

[4.17] EUROPEAN COMMISION, HEALTH AND CONSUMERS DIRECTORATE-GENERAL, "Manufacture of Biological Active Substances and Medicinal Products for Human Use", EU Guidelines for Good Manufacturing Practice for Medicinal Products for Human and Veterinary Use, EudraLex: The Rules Governing Medicinal Products in the European Union, Annex 2, Volume 4, European Commission, Brussels (2012).

[4.18] GE HEALTHCARE S.R.L., Summary of Product Characteristics for Nanocoll Kit for Radiopharmaceutical Preparation, Milan, Italy (2009).

[4.19] CHENG, K.T., et al., "[99mTc]-diethylenetriaminepentaacetic acid-mannosyl-dextran", Molecular Imaging and Contrast Agent Database (MICAD), National Center for Biotechnology Information (US), Bethesda, MD (2011).

[4.20] VERA, D.R., WALLACE, A.M., HOH, C.K., MATTREY, R.F., A synthetic macromolecule for sentinel node detection: [99mTc]DTPA-mannosyl-dextran, J. Nucl. Med. **42** (2001) 951–959.

[4.21] KREJCAREK, G.E., TUCKER, K.L., Covalent attachment of chelating groups to macromolecules, Biochem, Biophys. Res. Commun. **77** (1977) 581–583.

[4.22] VERA, D.R., KROHN, K.A., STADALNIK, R.C., SCHEIBE, P.O., Tc-99m galactosyl-neoglycoalbumin: in vitro characterization of receptor-mediated binding, J. Nucl. Med. **25** (1984) 779–787.

[4.23] SIRLIN, C.B., et al., Gadolinium-DTPA-dextran: a macromolecular MR blood pool contrast agent, Acad. Radiol. **11** (2004) 1361–1369.

[4.24] VERA, D.R., MATTREY, R.F., A molecular CT blood pool contrast agent, Acad. Radiol. **9** (2002) 784–792.

[4.25] HUNG, J.C., et al., Filtered technetium-99m-sulfur colloid evaluated for lymphoscintigraphy, J. Nucl. Med. **36** (1995) 1895–1901.

[4.26] TORIZUKA, K., et al., Phase III multi-center clinical study on [99mTc]-GSA, a new agent for imaging of liver function, Jpn. J. Nucl. Med. **29** (1992) 159–181.

[4.27] SHIRAKAMI, Y., et al., Development of Tc-99m-DTPA-HSA as a new blood pool agent, Jpn. J. Nucl. Med. **24** (1987) 475–478.

[4.28] VERA, D.R., WALLACE, A.M., HOH, C.K., [99mTc]-MAG$_3$-mannosyl-dextran: a receptor-binding radiopharmaceutical for sentinel node detection, Nucl. Med. Biol. **28** (2001) 493–498.

[4.29] KAWASAKI, T., MIZUNO, Y., MASUDA, T., YAMASHINA, I., Mannan-binding protein in lymphoid tissues of rats, J. Biochem. (Tokyo) **88** (1980) 1891–1894.

[4.30] EMERSON, D.A., et al., A receptor-targeted fluorescent radiopharmaceutical for multi-reporter sentinel lymph node imaging, Radiology **265** (2012) 186–193.

[4.31] ECKELMAN, W.C., "Design criteria for targeted molecules: muscarinic cholinergic systems biology", Targeted Molecular Imaging (WELCH, M.J., ECKELMAN, W.C., Eds), Taylor & Francis Group, Boca Raton, FL (2012) 201–215.

[4.32] VERA, D.R., WISNER, E.R., STADALNIK, R.C., Sentinel node imaging via a nonparticulate receptor-binding radiotracer, J. Nucl. Med. **38** (1997) 530–535.

[4.33] DE BELDER, D., "Medical application of dextran and its derivatives", Polysaccharides in Medicinal Applications (DUMITRIU, S., Eds), Marcel Dekker, New York (1996) 505–524.

[4.34] MENDEZ, J., WALLACE, A.M., HOH, C.K., VERA, D.R., Detection of gastric and colonic sentinel nodes via endoscopic administration of Lymphoseek in pigs, J. Nucl. Med. **44** 10 (2003) 1677–1681.

[4.35] ELLNER, S.J., et al., Sentinel lymph node mapping of the colon and stomach using Lymphoseek in a pig model, Ann. Surg. Oncol. **11** (2004) 674–681.

[4.36] SALEM, C.E., WALLACE, A.M., HOH, C.K., VERA, D.R., A preclinical study of prostate sentinel node mapping with Lymphoseek, J. Urol. **175** (2006) 744–748.

[4.37] ELLNER, S.J., et al., Dose-dependent biodistribution of [^{99m}Tc]DTPA-mannosyl-dextran for breast cancer sentinel node mapping, Nucl. Med. Biol. **30** (2003) 805–810.

[4.38] WOEHNL, A., et al., "Molecular imaging of the sentinel lymph node via Lymphoseek", Current Clinical Oncology: From Local Invasion to Metastatic Cancer (LEONG, S.P.L., Eds), Humana Press, New York (2009) 123–133.

[4.39] HOH, C.K., WALLACE, A.M., VERA, D.R., Preclinical studies of [^{99m}Tc] DTPA -mannosyl-dextran, Nucl. Med. Biol. **30** (2003) 457–464.

[4.40] WALLACE, A.M., HOH, C.K., VERA, D.R., DARRAH, D., SCHULTEIS, G., Lymphoseek: a molecular radiopharmaceutical for sentinel node detection, Ann. Surg. Oncol. **10** (2003) 531–538.

[4.41] WALLACE, A.M., HOH, C.K., DARRAH, D.D., SCHULTEIS, G., VERA, D.R., Sentinel lymph node mapping of breast cancer via intradermal administration of Lymphoseek, Nucl. Med. Biol. **34** (2007) 849–853.

[4.42] YEUNG, H., et al., Lymphoscintigraphy and sentinel node localization in breast cancer patients: a comparison between 1-day and 2-day protocols, J. Nucl. Med. **42** (2001) 420–423.

[4.43] WALLACE, A.M., et al., Sentinel lymph node accumulation of Lymphoseek and Tc-99m-sulfur colloid using a "2-day" protocol, Nucl. Med. Biol. **36** (2009) 687–692.

[4.44] WALLACE, A.M., et al., Lymphoseek: a molecular imaging agent for melanoma sentinel lymph node mapping, Ann. Surg. Oncol. **14** (2007) 913–921.

[4.45] LEONG, S.P.L., et al., A phase 2 study of [^{99m}Tc]tilmanocept in the detection of sentinel lymph nodes in melanoma and breast cancer, Ann. Surg. Oncol. **18** (2011) 961–969.

[4.46] WALLACE, A.M., et al., Comparative evaluation of [^{99m}Tc]tilmanocept for sentinel lymph node mapping in breast cancer patients: result of two phase 3 trials, Ann. Surg. Oncol. **20** (2013) 2590–2599.

[4.47] SONDAK, V.K., et al., Combined analysis of phase III trials evaluating [^{99m}Tc] tilmanocept and vital blue dye for identification of sentinel lymph nodes in clinically node-negative cutaneous melanoma, Ann. Surg. Oncol. **20** (2013) 680–688.

[4.48] MARCINOW, A.M., et al., Use of a novel receptor-targeted (CD206) radiotracer, ^{99m}Tc-tilmanocept, and SPECT/CT for sentinel lymph node detection in oral cavity squamous cell carcinoma: initial institutional report in an ongoing phase 3 study, JAMA Otolaryngolog. Head Neck Surg. **139** (2013) 895–902.

[4.49] TOKIN, C.A., et al., The efficacy of tilmanocept in sentinel lymph node mapping and identification in breast cancer patients: a comparative review and meta-analysis of the ^{99m}Tc-labeled nanocolloid human serum albumin standard of care, Clin. Exp. Metastasis **29** (2012) 681–686.

[4.50] VERA, D.R., et al., Cy5.5-DTPA-galactosyl-dextran: a fluorescent probe for in vivo measurement of receptor biochemistry, Nucl. Med. Biol. **32** (2005) 687–693.

[4.51] STROUP, S.P., et al., Preoperative sentinel lymph node mapping of the prostate using PET/CT fusion imaging and Ga-68-labeled tilmanocept in a dog model, Clin. Exp. Metastasis **29** (2012) 673–680.

[4.52] VERA, D.R., KROHN, K.A., STADALNIK, R.C., SCHEIBE, P.O., [Tc-99m] galactosyl-neoglycoalbumin: in vivo characterization of receptor-mediated binding to hepatocytes, Radiology **151** (1984) 191–196.

[4.53] KESHTGAR, M.R.S., et al., Implementing sentinel lymph node biopsy programmes in developing countries: challenges and opportunities, World J. Surg. **35** (2011) 1159–1168.

Chapter 5

A NEW CLASS OF ^{99m}Tc(I) AGENTS FOR SLND: CHEMICAL DESIGN AND SYNTHESIS

M. MORAIS, J.D.G. CORREIA, I. SANTOS
Unidade de Ciências Químicas e Radiofarmacêuticas, ITN,
Instituto Superior Técnico,
Universidade Técnica de Lisboa,
Sacavém, Portugal

M. PELECANOU, I. PIRMETTIS
Institute of Biosciences & Applications

M. PAPADOPOULOS
Institute of Nuclear & Radiological Sciences & Technology, Energy & Safety,

Demokritos National Center for Scientific Research,
Athens, Greece

5.1. SUMMARY

The unique features of the organometallic technetium and rhenium tricarbonyl moiety have earned considerable attention in the design of novel specific radiopharmaceuticals in recent years. As part of the CRP focused on the Development of ^{99m}Tc Radiopharmaceuticals for Sentinel Node Detection and Cancer Diagnosis, the design of mannosylated dextran derivatives loaded with pyrazolyl (pz) diamine and cysteine chelating units for coordination to the organometallic core *fac*-[M(CO)$_3$]$^+$ (M = Re, ^{99m}Tc) are reported in this chapter. The corresponding rhenium derivatives were prepared as congeners of the ^{99m}Tc(CO)$_3$ mannosylated dextran and used as non-radioactive alternatives for large scale synthesis and structural characterization.

5.2. INTRODUCTION

Technetium-99m is the most widely used radioisotope in nuclear medicine, with an estimated 40 million annual radiodiagnostic procedures carried out worldwide [5.1]. The preferential use of ^{99m}Tc based radiopharmaceuticals

reflects the almost ideal nuclear properties of the isotope, as well as their low cost and on-site availability from commercial ^{99}Mo/^{99m}Tc generators. Technetium-99m emits a 140 keV γ ray with 89% abundance, which is close to optimal for imaging using commercial gamma cameras. The 6 h half-life is sufficiently long for preparation of the radiopharmaceutical in situ and for in vivo accumulation in the target tissue, yet short enough to minimize radiation dose to the patient. Moreover, this radioisotope presents a wide range of oxidation states, from −I (d^8) to + VII (d^0), which enables diverse coordination chemistry and the preparation of a wide variety of complexes with different biological properties [5.2, 5.3].

Because ^{99m}Tc complexes are always obtained in very low concentrations (10^{-10}M−10^{-7}M), their structural characterization is performed indirectly by synthesizing analogous complexes with the relatively stable ^{99}Tc isomer (half-life: 2.14 × 10^5 years, β$^-$ decay) or with the non-radioactive VIIB congener rhenium (Re). The rich coordination chemistry of Tc and Re led to the design of complexes with improved biological properties towards target specific SPECT imaging (^{99m}Tc) or therapy ($^{186/188}$Re). The higher oxidation states (+V, +IV and +III) have been extensively explored for the development of ^{99m}Tc radiopharmaceuticals, with the most studied cores being [Tc=O]$^{3+}$, [O=Tc=O]$^+$ and [Tc≡N]$^{2+}$ at the +V oxidation state. Presently, most of the perfusion and target specific ^{99m}Tc radiopharmaceuticals in routine clinical use have the [Tc=O]$^{3+}$ core [5.2–5.5]. Recently, the lower oxidation state +I received considerable attention when Alberto and co-workers developed a convenient and fully water based methodology to prepare the organometallic precursors *fac*-[M(CO)$_3$(H$_2$O)$_3$]$^+$ directly from permetallated salts [MO$_4$]$^-$(M=Tc,Re) [5.6–5.9]. Initially, *fac*-[^{99m}Tc(CO)$_3$(H$_2$O)$_3$]$^+$ was synthesized by direct reduction of Na[^{99m}TcO$_4$], with sodium borohydride in aqueous solution in the presence of carbon monoxide. After this first important achievement, an even more attractive method was developed, which involved the use of boranocarbonate, K$_2$[H$_3$BCO$_2$], to produce CO in situ, and, simultaneously, to reduce Tc(VII) to Tc(I). Currently, the synthesis of the precursor is carried out using a kit formulation (IsoLink, Covidien, formerly Mallinckrodt Medical BV).

The tricarbonyl moiety offers a great number of advantages for the design of novel radiopharmaceuticals. The compact nature of the core *fac*-[M(CO)$_3$]$^+$ with an almost spherical shape renders a tight octahedral coordination sphere with the appropriate ligand system, preventing further ligand attack or reoxidation. The low spin d^6 electronic configuration of the metal centre is, in general, associated with complexes of high thermodynamic stability and kinetic inertness, which are key issues for in vivo applications. Moreover, the low MW tricarbonyl moiety allows the labelling of relevant biomolecules in high yield and with high specific activity.

All three water molecules in the precursor *fac*-[^{99m}Tc(CO)$_3$(H$_2$O)$_3$]$^+$ are very labile and can be replaced by mono, bi or tridentate chelating ligands to form stable complexes. Among these, the complexes stabilized by tridentate ligands display the highest stability, both in vivo and in vitro. Histidine, pyridine, pyrazole, thioimidazole and cysteine derivatives, together with pure aliphatic or mixed aromatic aliphatic triamines stabilize the organometallic core quite efficiently, allowing the preparation of complexes with different biological properties. Among these, pz diamine and cysteine derivatives have been explored as efficient tridentate N, N, N and S, N, O donor atom ligands, respectively, for stabilization of the *fac*-[M(CO)$_3$]$^+$ moiety. The coordination mode of these model chelators has been well established by X ray structural analysis (Fig. 5.1) and by nuclear magnetic resonance (NMR) spectroscopy [5.10−5.13].

Derivatization of such ligands gives bifunctional chelators that allow the conjugation and labelling of a wide range of biologically active peptides and small molecules. The relevant biological properties of some of those ^{99m}Tc(CO)$_3$ labelled biomolecules in adequate animal models [5.14−5.23], as well as the well defined coordination capability of pz diamine and cysteine derivatives towards the *fac*-[M(CO)$_3$]$^+$ moiety, prompted the conjugation of these bifunctional
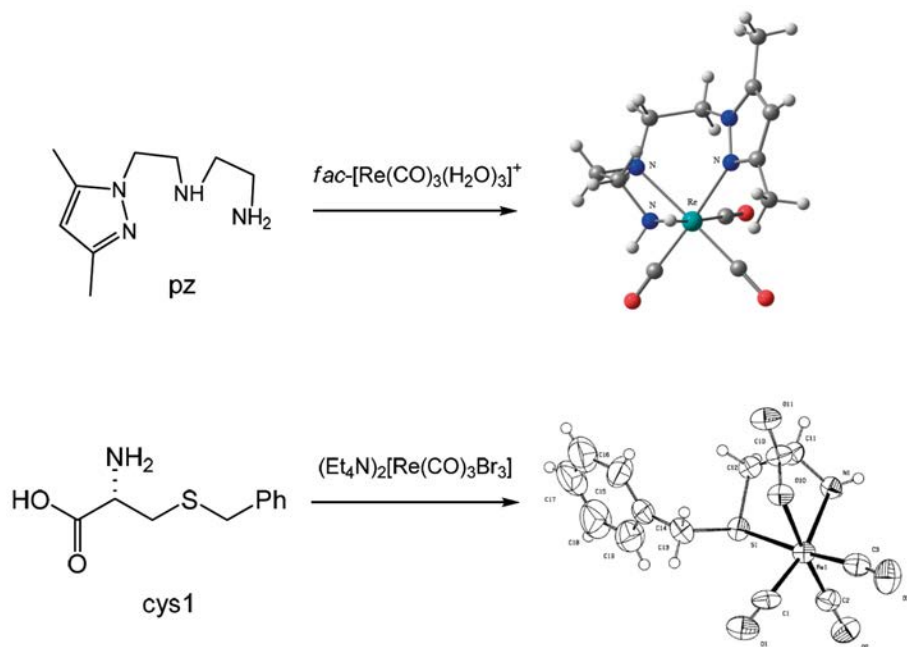

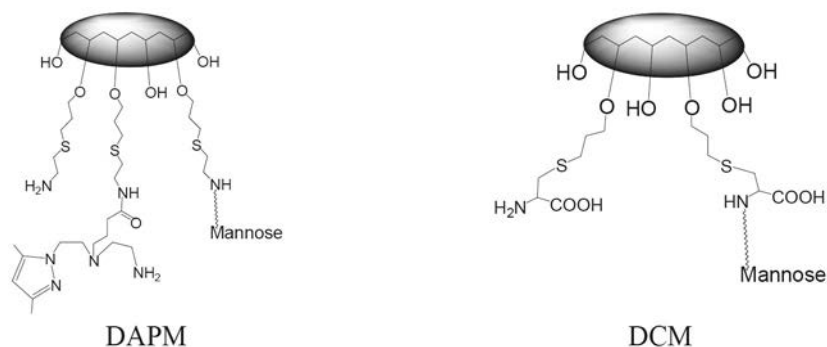FIG. 5.1. *Molecular structures of Re(CO)$_3$ complexes stabilized by pz diamine and cysteine derivatives.*

FIG. 5.2. Schematic representation of mannosylated dextran with pz diamine (DAPM) and cysteine units (DCM) as chelators for the fac-[M(CO)$_3$]$^+$ moiety (M = Re, ^{99m}Tc).

chelators to polymeric nanoparticles such as mannosylated dextran for SLND (Fig. 5.2).

5.3. RESULTS

The synthesis of mannosylated dextran containing the pz diamine (dextran aminepyrazolyl diamine mannose; DAPM) or cysteine chelators (dextran propyl-S-cysteine mannose with MW = 20 000 g/mol; DCM20) was performed by following a stepwise procedure (Figs 5.3 and 5.4) [5.24, 5.25]. The preparation of DAPM involved the attachment of amino terminal leashes to the hydroxyl units of dextran by addition of cysteamine to allyl dextran (**1**) to yield dextran amine (**2**), followed by conjugation of the activated chelator (pz(Boc)COOsucc) to the free amines. Mannosylation of most of the remaining amino groups in the final step afforded DAPM (Fig. 5.3).

Depending on the molar ratio pz(Boc)COOsucc/**2**, the synthetic pathway allowed the preparation of three mannosylated derivatives that contain 1 (DAPM1), 4 (DAPM4) or 8 (DAPM8) pz units per mole of dextran. In the case of the cysteine containing dextran derivative DCM20, there are only two major synthetic steps starting from the allyl dextran derivative (**1**). The direct incorporation of the amino acid into the dextran backbone reduced the overall synthetic steps. Indeed, there is no need to synthesize, activate and conjugate the bifunctional chelating agent to dextran (Fig. 5.4).

FIG. 5.3. Synthesis of mannosylated dextran derivatives containing 1 (DAPM1), 4 (DAPM4) or 8 (DAPM8) pz units/mol dextran, respectively: (i) BrC_3H_5, NaOH (2.5M), H_2O; (ii) $NH_2(CH_2)_2SH$, $(NH_4)_2S_2O_8$, dimethylsulphoxide; (iii) pz(Boc)COOsucc, borate buffer 0.1M, pH9; (iv) IME mannose, borate buffer 0.1M, pH9; (v) trifluoroacetic acid (TFA)/H_2O.

FIG. 5.4. Synthesis of DCM20: (i) BrC_3H_5, NaOH (2.5M), H_2O; (ii) L-cysteine, $(NH_4)_2S_2O_8$, H_2O, nitrogen; (iii) 2-imino-2-methoxethyl-1-thio-β-D-mannoside, borate buffer (0.01M, pH9).

Moreover, the incorporation of cysteine into the dextran backbone provides an amino group for conjugation to mannose, whereas the remaining non-mannosylated cysteine groups serve as S, N, O chelators for stabilization of the fac-[^{99m}Tc(CO)$_3$]$^+$ core.

All compounds were characterized using NMR spectroscopy. The mannose and the chelator loading in the polymer backbone were determined based on the ^{1}H NMR data. For the DAPM derivatives, the total numbers of mannose, pz units and free amines per mole of dextran were calculated based on the intensity ratios of the peaks corresponding to the mannose anomeric proton (δ, 5.22), 3,5-Me$_2$pz (δ, 2.08) and protons adjacent to free amines (δ, 2.74, H^e), respectively, which are easily assigned in the ^{1}H NMR spectra. As an illustrative example, Fig. 5.5 presents the ^{1}H NMR spectrum obtained for DAPM4, with assignment of the most relevant peaks.

In an analogous way, the mannose and cysteine loading in DCM20 was determined based on the relative intensity of the characteristic peaks of each functionality (Fig. 5.6).

Colorimetric assays (sulphuric acid phenol assay and trinitrobenzene sulphonate assay) corroborate the NMR results for glucose and amine content per mole of dextran.
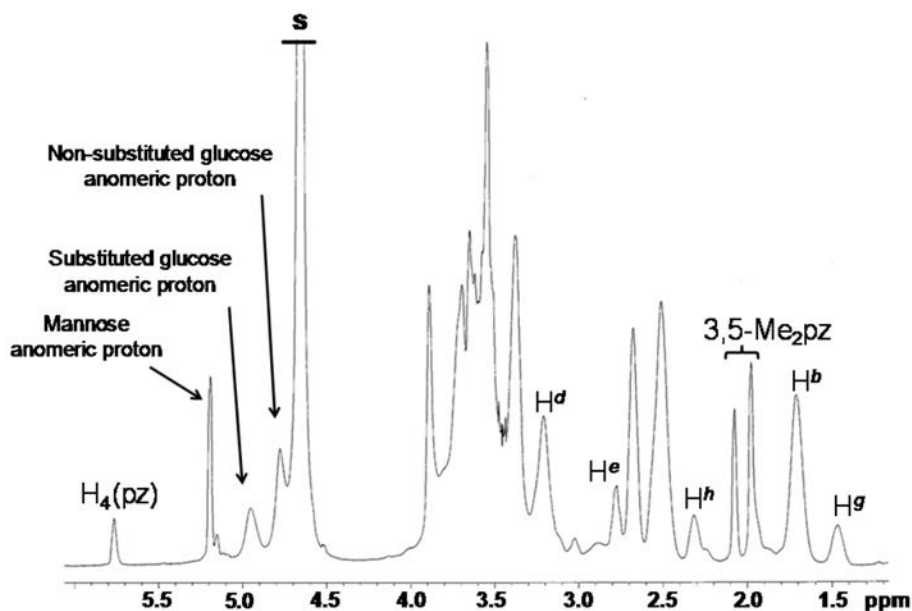

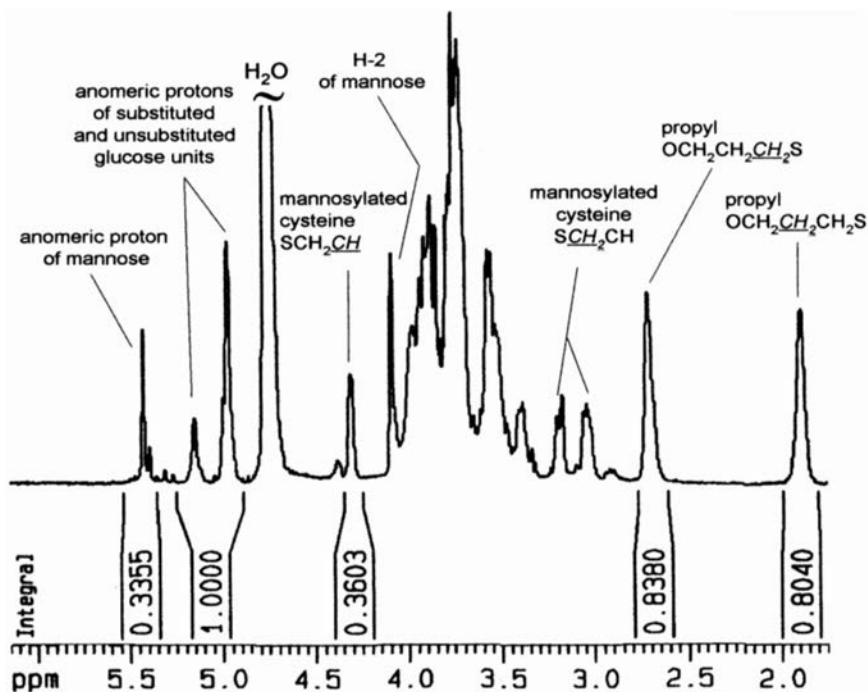FIG. 5.5. ^{1}H NMR spectrum of DAPM4 in D$_2$O at 25°C.

FIG. 5.6. *^1H NMR spectrum (range δ_H, 6.15–1.75) of DCM20 in D_2O at 25°C.*

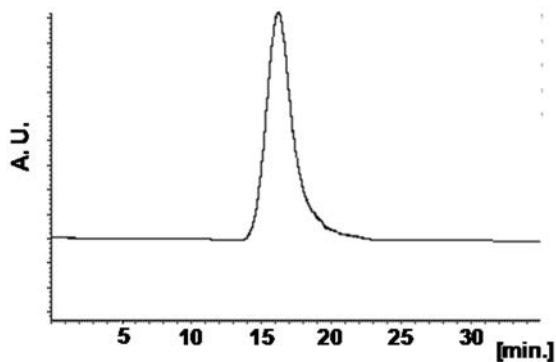FIG. 5.7. *SEC-HPLC trace of DAPM4 (wavelength λ = 200 nm; retention time t_R = 15.8 min).*

The purity of all the polymeric compounds was checked by analytical size exclusion high performance liquid chromatography (SEC-HPLC). As an example, Fig. 5.7 depicts a typical SEC-HPLC trace, showing the formation of a single major product (>98%) assigned to DAPM4.

The rhenium containing mannosylated dextran derivatives were prepared by reaction of the precursors *fac*-[Re(CO)$_3$(H$_2$O)]Br or [NEt$_4$] *fac*-[ReBr$_3$(CO)$_3$] with DAPM4, DAPM8 or DCM20. The resulting metallated compounds are surrogates of the ^{99m}Tc(CO)$_3$ mannosylated dextran derivatives, and were used as a non-radioactive alternative for large scale synthesis and structural characterization.

The synthesis of the rhenium polymeric compounds containing the pz diamine chelator was monitored by reversed phase high performance liquid chromatography (RP-HPLC) and ^{1}H NMR spectroscopy. As an example, Fig. 5.8 shows the RP-HPLC traces and ^{1}H NMR spectra for the reaction mixture at 1 h and 16 h, after appropriate work-up of the collected samples.
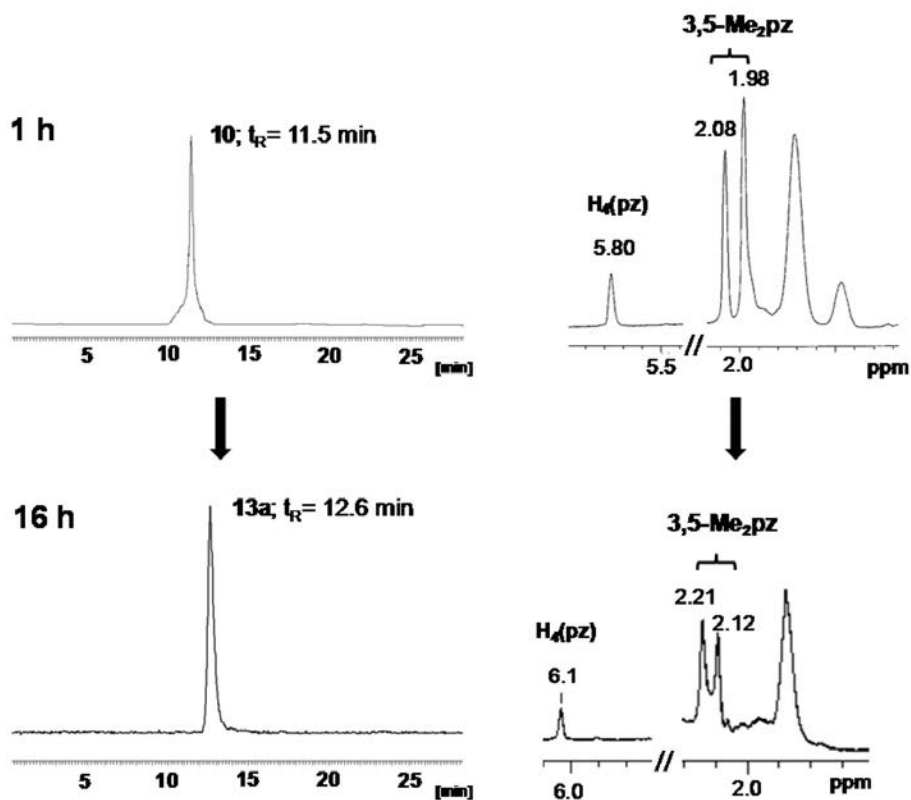

FIG. 5.8. RP-HPLC (254 nm) and ^{1}H NMR data of the reaction mixture at 1 h and 16 h (25°C).

After 16 h of reaction, the ^{1}H NMR spectra showed the disappearance of the singlet (δ, 5.80) corresponding to H(4) of the free pz diamine chelator, and the appearance of a new singlet (δ, 6.10). At this time point, the reaction was complete because only one species was detected by RP-HPLC, and the chemical shifts of the resonances owing to H(4) and 3,5-Me$_2$ groups of the pz ring in Re(CO)$_3$ DAPM4 and Re(CO)$_3$ DAPM8 compare well with other results described in the literature for Re analogues [5.21−5.23]. The ^{13}C NMR spectra for the same compounds allowed identification of the resonances owing to the carbonyl groups of the *fac*-[Re(CO)$_3$]$^+$ (δ, 195.2−193). Two intense absorption bands (2027 cm^{-1} and 1998 cm^{-1}) in the IR spectra also confirmed the presence of the organometallic core (data not shown).

Metallation of DCM20 was achieved after 5 h. In the NMR spectra, changes are evident in the chemical shifts of protons attached to the coordinating S atom of cysteine (i.e. the βCH$_2$ of cysteine and the OCH$_2$CH$_2$CH$_2$S of the propylene chain). In addition, the βCH$_2$ protons of cysteine broaden and become barely visible, hiding in the baseline, and becoming visible only when the temperature of the sample is raised. This broadening provides a solid sign for the coordination of the S atom of cysteine to the Re(CO)$_3^+$ core (Fig. 5.9) [5.11, 5.12].
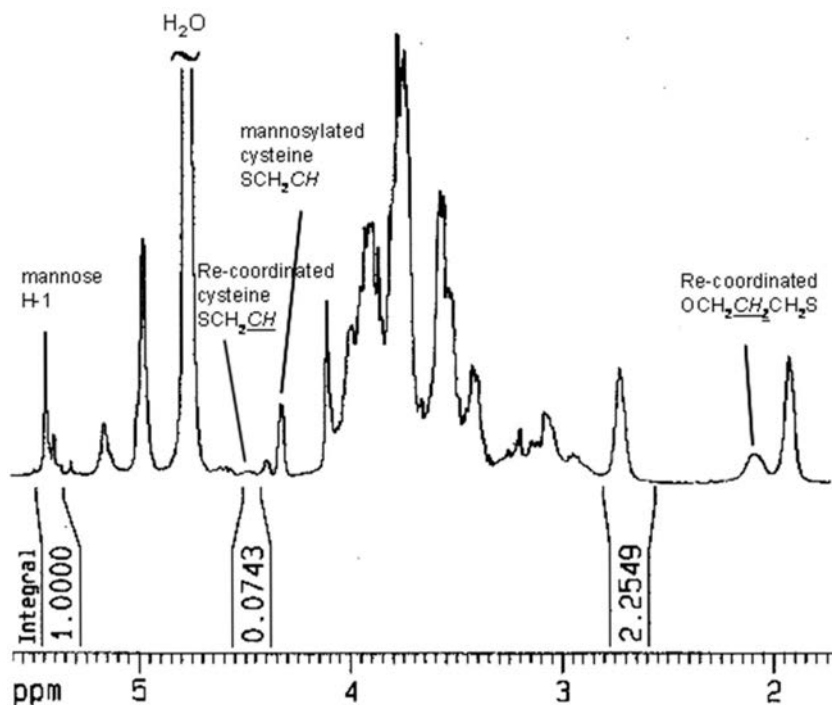

FIG. 5.9. ^{1}H spectrum (range δ_H, 5.60–1.70) of Re(CO)$_3$ DCM20 in D$_2$O at 25°C.

Moreover, the IR spectra of Re(CO)$_3$ DCM20 show strong bands at 2019 cm^{-1} and 1895 cm^{-1}, which are attributed to the ν(C≡O) stretching modes, denoting the presence of the *fac*-[Re(CO)$_3$]$^+$ core. Furthermore, in the ^{13}C NMR spectra of Re(CO)$_3$ DCM20, three peaks attributed to the carbonyl groups of the *fac*-[Re(CO)$_3$]$^+$ moiety can be clearly seen in the range δ_C 198–195, which is in agreement with other S, N, O complexes in the literature [5.11, 5.12]. The purity of all metallated compounds was checked by SEC-HPLC and RP-HPLC.

The detailed structural characterization of the rhenium congeners allowed characterization of the ^{99m}Tc radioactive nanocompounds. As an example, Fig. 5.10 displays the RP-HPLC traces obtained for ^{99m}Tc(CO)$_3$ DAPM4 (γ detection) and Re(CO)$_3$ DAPM4 (ultraviolet (UV) detection). Similar results were obtained for all compounds in this study.

DLS and zeta potential measurements allowed physical characterization (size and charge, respectively) of the mannosylated dextran derivatives, as well as the metallated analogues. The final compositions of all the dextran derivatives, their physical parameters and the calculated MWs for each compound are summarized in Table 5.1.

The DLS data show that mannosylated dextran containing pz diamine or cysteine units, as well as the rhenium compounds, present similar particle sizes. Moreover, the hydrodynamic diameter of the nanopolymers increases with the polymer backbone functionalization, from dextran (4.3 nm) to final
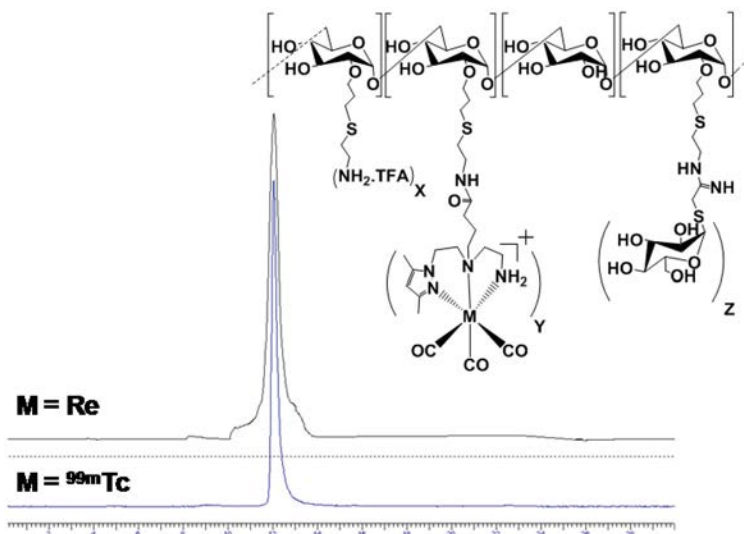

FIG. 5.10. *RP-HPLC traces of M(CO)$_3$ DAPM4 (M = Re, UV/VIS detection; M = ^{99m}Tc, γ detection).*

104

TABLE 5.1. GROUP DENSITY, HYDRODYNAMIC DIAMETER, ZETA POTENTIAL AND CALCULATED MWs OF DEXTRAN, DAPM4, DAPM8, DCM20, Re(CO)$_3$ DAPM4, Re(CO)$_3$ DAPM8 AND ReCO$_3$ DCM20*

Compound	Group density (units/mol dextran)				Diameter* (nm)	Zeta potential* (mV)	MW (calculated) (g/mol)
	Amine	pz	Mannose	Cysteine			
Dextran	—	—	—	—	4.3 ± 0.4	−9.9 ± 0.5	10 000
DAPM4	13	4	13	—	7.0 ± 0.3	6.6 ± 0.3	18 820
DAPM8	9	8	13	—	7.0 ± 0.7	7.3 ± 0.6	20 132
DCM20	—	—	24	6	6.5 ± 0.5	−6.3 ± 0.1	22 270
Re(CO)$_3$ DAPM4	13	4	13	—	8.4 ± 0.5	7.1 ± 0.7	19 904
Re(CO)$_3$ DAPM8	9	8	13	—	8.7 ± 0.3	7.1 ± 0.1	22 300
ReCO$_3$ DCM20	—	—	24	6	8.3 ± 0.5	−6.3 ± 0.1	23 083

Note: —, no data available.

* Results are expressed as mean ± standard deviation.

polymeric compounds (6.5–7 nm). This trend is also observed upon metallation because the particle size of the derivatives containing pz diamine or cysteine increased to 8.7 nm or 8.3 nm, respectively. On the other hand, zeta potential measurements indicated a negative charge for dextran (−9.9 ± 0.5 mV). Dextran functionalization with amines and pz diamine units led to compounds DAPM4 (6.6 ± 0.3 mV) and DAPM8 (7.3 ± 0.6 mV) with positive surface charges. On the contrary, DCM2O displayed a negative surface charge (−6.3 ± 0.1 mV). Coordination of *fac*-[Re(CO)$_3$]$^+$ moiety to the previous compounds produced no effects on their surface charges.

REFERENCES TO CHAPTER 5

[5.1] WORLD NUCLEAR ASSOCIATION, Radioisotopes in Medicine (2014), http://www.world-nuclear.org/info/inf55.html

[5.2] ARANO, Y., Recent advances in ^{99m}Tc radiopharmaceuticals, Ann. Nucl. Med. **16** (2002) 79–93.

[5.3] BANERJEE, S.R., et al., New directions in the coordination chemistry of ^{99m}Tc: a reflection on technetium core structures and a strategy for new chelate design, Nucl. Med. Biol. **32** (2005) 1–20.

[5.4] LIU, S., The role of coordination chemistry in the development of target-specific radiopharmaceuticals, Chem. Soc. Rev. **33** (2004) 445–461.

[5.5] LIU, S., Bifunctional coupling agents for radiolabeling of biomolecules and target-specific delivery of metallic radionuclides, Adv. Drug Deliv. Rev. **60** (2008) 1347–1370.

[5.6] ALBERTO, R., et al., Metal carbonyl syntheses XXII. Low pressure carbonylation of $[MOCl_4]^-$ and $[MO_4]$: the technetium(I) and rhenium(I) complexes $[NEt_4]_2[MCl_3(CO)_3]$, J. Organomet. Chem. **493** (1995) 119–127.

[5.7] ALBERTO, R., SCHIBLI, R., EGLI, A., SCHUBIGER, A.P., A novel organometallic aqua complex of technetium for the labeling of biomolecules: synthesis of *fac*-$[^{99m}Tc(H_2O)_3(CO)_3]^+$ from $[^{99m}TcO_4]$ in aqueous solution and its reaction with a bifunctional ligand, J. Am. Chem. Soc. **120** (1998) 7987–7988.

[5.8] ALBERTO, R., SCHIBLI, R., WAIBEL, R., ABRAM, U., SCHUBIGER, A.P., Basic aqueous chemistry of $[M(OH_2)_3(CO)_3]^+$ (M = Re, Tc) directed towards radiopharmaceutical application, Coord. Chem. Rev. **190–192** (1999) 901–919.

[5.9] ALBERTO, R., ORTNER, K., WHEATLEY, N., SCHIBLI, R., SCHUBIGER, A.P., Synthesis and properties of boranocarbonate: a convenient in situ CO source for the aqueous preparation of $[^{99m}Tc(OH)_2(CO)_3]^+$, J. Am. Chem. Soc. **123** (2001) 3135–3136.

[5.10] ALVES, S., PAULO, A., CORREIA, J.D.G., DOMINGOS, A., SANTOS, I., Coordination capabilities of pyrazolyl containing ligands towards the *fac*-$[Re(CO)_3]^+$ moiety, J. Chem. Soc. Dalton Trans. **24** (2002) 4714–4719.

[5.11] STAVEREN, D., et al., S-functionalized cysteine: powerful ligands for the labelling of bioactive molecules with triaquatricarbonyltechnetium-99m(1+) ($[^{99m}Tc(OH_2)_3(CO)_3]^+$), Helv. Chim. Acta **88** (2005) 447–460.

[5.12] HE, H., et al., $Re(CO)_3$ complexes synthesized via an improved preparation of aqueous *fac*-$[Re(CO)_3(H_2O)_3]^+$ as an aid in assessing ^{99m}Tc imaging agents. Structural characterization and solution behavior of complexes with thioether-bearing amino acids as tridentate ligands, Inorg. Chem. **44** (2005) 5437–5446.

[5.13] HE, H., LIPOWSKA, M., CHRISTOFOROU, A.M., MARZILLI, L.G., TAYLOR, A.T., Initial evaluation of new ^{99m}Tc(CO)$_3$ renal imaging agents having carboxyl-rich thioether ligands and chemical characterization of $Re(CO)_3$ analogues, Nucl. Med. Biol. **34** (2007) 709–716.

[5.14] ALVES, S., et al., Pyrazolyl derivatives as bifunctional chelators for labeling tumor-seeking peptides with the *fac*-$[M(CO)_3]^+$ moiety (M = ^{99m}Tc, Re), Bioconjug. Chem. **16** (2005) 438–449.

[5.15] ALVES, S., et al., Pyrazolyl conjugates of bombesin: a new tridentate ligand framework for the stabilization of fac-[M(CO)$_3$]$^+$ moiety, Nucl. Med. Biol. **33** (2006) 625–634.

[5.16] ALVES, S., et al., In vitro and in vivo evaluation of a novel ^{99m}Tc(CO)$_3$-pyrazolyl conjugate of cyclo-(Arg-Gly-Asp-D-Tyr-Lys), Bioconjug. Chem. **18** (2007) 530–537.

[5.17] PALMA, E., et al., A new biphosphonate-containing ^{99m}Tc(I) tricarbonyl complex potentially useful as a boneseeking agent: synthesis and biological evaluation, J. Biol. Inorg. Chem. **12** (2007) 667–679.

[5.18] VITOR, R.F., et al., Pyrazolyl–diamine ligands that bear anthracenyl moieties and their rhenium(I) tricarbonyl complexes: synthesis, characterisation and DNA-binding properties, ChemBioChem. **9** (2008) 131–142.

[5.19] MORAIS, M., RAPOSINHO, P.D., OLIVEIRA, M.C., CORREIA, J.D.G., SANTOS, I., Evaluation of novel (99m)Tc(I)-labeled homobivalent α-melanocyte-stimulating hormone analogs for melanocortin-1 receptor targeting, J. Biol. Inorg. Chem. **17** (2012) 491–505.

[5.20] CHOI, K.-H., HONG, Y.-D., CHOI, O.-J., CHOI, S.-J., Synthesis and physical evaluation of ^{99m}Tc(CO)$_3$-labeled cysteine–arylpiperazines for a neuroreceptor(5-HT$_{1A}$) imaging, Bull. Korean Chem. Soc. **27** (2006) 1689–1692.

[5.21] ALBERTO, R., PAK, J.K., STAVEREN, D., MUNDWILER, S., BENNY, P., Mono-, bi-, or tridentate ligands? The labeling of peptides with ^{99m}Tc-carbonyls, Biopolymers **76** (2004) 324–333.

[5.22] KARAGIORGOU, O., et al., (S)-(2-(2'-pyridyl)ethyl)cysteamine and (S)-(2-(2'-pyridyl)ethyl)-D,L-homocysteine as ligands for the "fac-[M(CO)$_3$]$^+$" (M = Re, ^{99m}Tc) core, Inorg. Chem. Comm. **44** (2005) 4118–4120.

[5.23] PARK, S.H., JANG, B.S., PARK, K.B., Synthesis and biological characterization of 99^{m}Tc(I) tricarbonyl cysteine complex, a potential diagnostic for assessment of renal function, J. Lab. Compd. Radiopharm. **48** (2005) 63–73.

[5.24] MORAIS, M., et al., Mannosylated dextran derivatives labeled with *fac*-[M(CO)$_3$]$^+$ (M = ^{99m}Tc, Re) for specific targeting of sentinel lymph node, Mol. Pharm. **8** (2011) 609–620.

[5.25] PIRMETTIS, I., et al., New ^{99m}Tc(CO)$_3$ mannosylated dextran bearing S-derivatized cysteine chelator for sentinel lymph node detection, Mol. Pharm. **9** (2012) 1681–1692.

Chapter 6

A NEW CLASS OF ^{99m}Tc(I) AGENTS FOR SLND: LABELLING AND QUALITY CONTROL

M. MORAIS, J.D.G. CORREIA, I. SANTOS
Unidade de Ciências Químicas e Radiofarmacêuticas, ITN,
Instituto Superior Técnico,
Universidade Técnica de Lisboa,
Sacavém, Portugal

M. PELECANOU, I. PIRMETTIS
Institute of Biosciences & Applications

M. PAPADOPOULOS
Institute of Nuclear & Radiological Sciences & Technology, Energy & Safety,

Demokritos National Center for Scientific Research,
Athens, Greece

6.1. SUMMARY

In an attempt to prepare a new class of tracers for SLND, the radiolabelling of mannosylated dextran derivatives containing the tridentate pz diamine and cysteine chelators for stabilization of the organometallic core fac-$[^{99m}Tc(CO)_3]^+$ are reported. This chapter demonstrates the optimization of the labelling conditions to achieve high radiochemical purity and specific activity. These results are of paramount importance for the biological properties of the compounds, namely their mannose receptor targeting properties.

6.2. INTRODUCTION

The successful introduction of a stable, water soluble Tc(I) organometallic precursor by Alberto et al. opened a new avenue in radiopharmaceutical sciences, mainly when a fully aqueous based preparation of the precursor fac-$[^{99m}Tc(CO)_3(H_2O)_3]^+$ by direct reduction of Na$[^{99m}TcO_4]$ with sodium borohydride in the presence of carbon monoxide was reported [6.1, 6.2]. The potential of this preparation was enhanced by a remarkable and innovative

procedure that used potassium boranocarbonate, $K_2[H_3BCO_2]$, to reduce Tc(VII) to Tc(I) and simultaneously generate CO in situ [6.2]. Currently, the synthesis of the precursor can be carried out using a kit formulation (IsoLink, Covidien, formerly Mallinckrodt Medical BV).

Using the tricarbonyl core, a wide variety of new complexes with relevant biological properties have been designed and evaluated in the past few years [6.3−6.14].

The easy availability of this Tc(I) precursor has contributed towards significant progress in radiopharmaceutical chemistry, with the major advantages including: (a) applicability to a wide range of biologically relevant molecules, (b) high thermodynamic and kinetic stability of the resultant ^{99m}Tc complexes, (c) high specific activity of the labelled biomolecules, often without any purification step, (d) relatively low MW of the metal moiety and (e) easy fine tuning of the pharmacokinetics of the final complexes owing to the wide range of bifunctional chelators available for the metal core.

In this chapter, the labelling of mannosylated dextran derivatives (DAPM1, DAPM4, DAPM8 and DCM20) containing the tridentate pz diamine and cysteine chelators with the organometallic moiety *fac*-[^{99m}Tc(CO$_3$)]$^+$ is described. Chromatographic characterization of the resulting radiolabelled dextran derivatives, as well as the assessment of their stability in vitro, is also reported.

6.3.   RESULTS

6.3.1.   **Radiolabelling with [^{99m}Tc(CO)$_3$]$^+$**

The mannosylated dextran derivatives bearing the pz diamine (DAPM1, DAPM4 and DAPM8) or S-derivatized cysteine (DCM20) chelating units have been labelled with the *fac*-[^{99m}Tc(CO)$_3$]$^+$ moiety under different experimental conditions [6.15, 6.16]. The dextran derivatives DAPM1, DAPM4 and DAPM8 (final concentration: 2.5×10^{-5}M−5×10^{-5}M) reacted with the precursor *fac*-[^{99m}Tc(CO)$_3$(H$_2$O)$_3$]$^+$ in a N$_2$ flushed capped vial at 100°C for 30 min, yielding quantitatively ^{99m}Tc(CO)$_3$ labelled mannosylated dextran derivatives of the type ^{99m}Tc(CO)$_3$ L (L = DAPM1, DAPM4 and DAPM8) (Fig. 6.1) [6.15]. The dextran derivative DCM20 (final concentration: 2.2×10^{-6}M) reacted with the precursor *fac*-[^{99m}Tc(CO)$_3$(H$_2$O)$_3$]$^+$ in a capped vial at 75°C for 25 min, yielding quantitatively the ^{99m}Tc(CO)$_3$ labelled mannosylated dextran derivative ^{99m}Tc(CO)$_3$ DCM20 (Fig 6.2) [6.16]. The tricarbonyl precursor *fac*-[^{99m}Tc(CO)$_3$(OH$_2$)$_3$]$^+$ was prepared using a kit formulation (IsoLink). Briefly, addition of freshly eluted Na[^{99m}TcO$_4$] solution (1.5−2.0 mL) to an IsoLink kit, followed by heating for 30 min at 100°C, afforded the radioactive
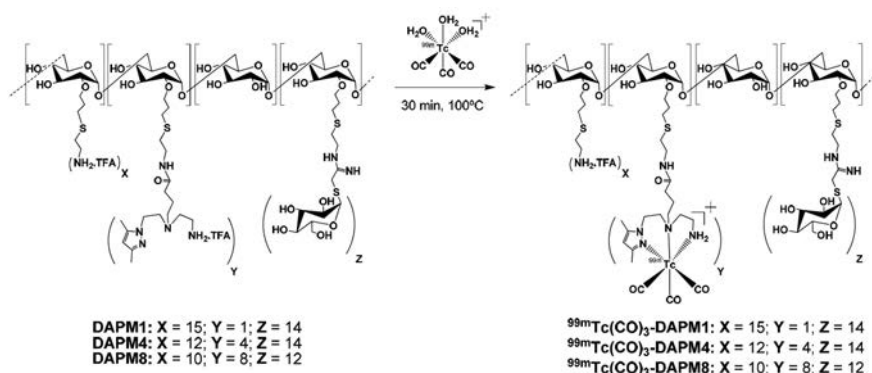
FIG. 6.1. Synthesis of $^{99m}Tc(CO)_3$ DAPM1, $^{99m}Tc(CO)_3$ DAPM4 and $^{99m}Tc(CO)_3$ DAPM8.
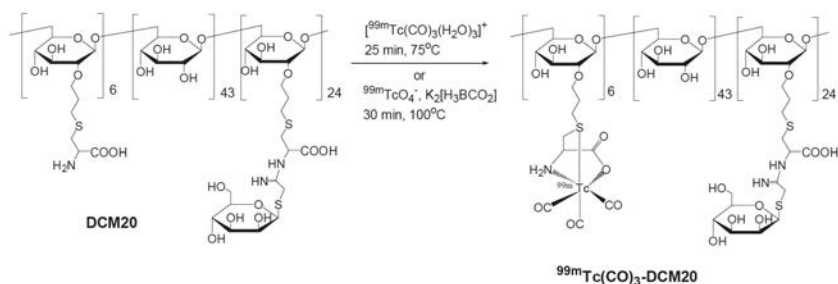
FIG. 6.2. Synthesis of $^{99m}Tc(CO)_3$ DCM20.

synthon fac-$[^{99m}Tc(CO)_3(OH_2)_3]^+$. The reaction vial was cooled and the solution neutralized with 1M HCl (160–170 µL) to destroy the remaining boranocarbonate. The product was controlled by RP-HPLC.

DCM20 was also quantitatively labelled at low ligand concentration (final concentration: 1.5×10^{-6}M) through an efficient one pot reaction, by dissolving the compound (50 µg) in a Na[$^{99m}TcO_4$] solution (1.5 mL) and transferring the resulting solution into the IsoLink kit. The vial was then kept at 100°C for 30 min [6.16].

6.3.2. Quality control

The radiochemical control of all radiolabelled mannosylated dextran derivatives of the type $^{99m}Tc(CO)_3$ − L (L = DAPM1, DAPM4, DAPM8, and DCM20) was performed by ITLC, RP-HPLC and SEC-HPLC [6.15, 6.16].

6.3.2.1. ITLC

Analysis was performed using PALL Life Sciences (product 61886) or Gelman Sciences Inc. (product 51432) strips and three different eluent systems (A, B, C):

— *System A*: Methyl ethyl ketone. The $[^{99m}TcO_4]^-$ migrates with the solvent front ($R_f = 1$; $R_f =$ retention factor), whereas *fac*-$[^{99m}Tc(CO)_3(H_2O)_3]^+$, radioactive nanoconjugates and colloidal species stay at the origin ($R_f = 0$).

— *System B*: 5% HCl 6N/CH_3OH. *fac*-$[^{99m}Tc(CO)_3(H_2O)_3]^+$ and $[^{99m}TcO_4]^-$ migrate with the solvent front ($R_f = 1$), whereas radioactive nanoconjugates and colloidal species stay at the origin ($R_f = 0$).

— *System C*: $C_5H_5N/CH_3COOH/H_2O$ (3:5:1). Colloidal species stay at the origin ($R_f = 0$), whereas *fac*-$[^{99m}Tc(CO)_3(H_2O)_3]^+$, $[^{99m}TcO_4]^-$ and radioactive nanoconjugates migrate with the solvent front ($R_f = 1$).

Radioactivity detection was performed on a radiochromatographer (Berthold LB 2723) equipped with a 20 mm diameter NaI(Tl) scintillation crystal.

6.3.2.2. HPLC

Technetium-99m$(CO)_3$ DAPM1, $^{99m}Tc(CO)_3$ DAPM4 and $^{99m}Tc(CO)_3$ DAPM8: HPLC analysis was performed on Perkin Elmer equipment coupled to a gamma detector (Berthold Lb 509) and a UV/VIS detector (Shimadzu SPD-10 AV or Perkin Elmer Lc 290). Analysis was carried out either by RP-HPLC or by SEC-HPLC. RP-HPLC: Supelco Discovery Bio Wide Pore C18 25 cm × 4.6 mm, 5 μm analytical column; flow, 1 mL/min; eluents, A, trifluoroacetic acid (TFA) 0.1% in H_2O; B, TFA 0.1% in CH_3CN. SEC-HPLC: Shodex OHpack SB-803 HQ analytical column; flow, 0.5 mL/min; eluent, ammonium acetate 0.5M. Resolution of the column was calculated to be 0.76 ± 0.29 min. The wavelengths for UV detection were 220 nm and 254 nm for RP-HPLC and SEC-HPLC, respectively.

Technetium-99m DCM20: HPLC analysis was performed by two systems. System I: A Waters 600 chromatography system was coupled to a Waters 991 photodiode array detector and a GABI gamma detector (Raytest). HPLC solvents consisted of water containing 0.1% TFA (solvent A) and methanol containing 0.1% TFA (solvent B). For the radiochemical analysis, a Nucleosil C18 reversed phase column (10 μm, 250 × 4 mm) was used. The HPLC system started with 100% of A from 0 min to 1 min followed by a linear gradient to 30% A (70% B) in 9 min; this composition was held for another 10 min. The flow rate

was 1 mL/min. System II: A Waters 600E chromatography system was coupled to a Waters 486 UV detector and a GABI gamma detector (Raytest) (γ trace for ^{99m}Tc). Separations were achieved on a size exclusion column (Shodex SB-803HQ) (8 mm × 300 mm) eluted with water at a flow rate of 1 L/min.

All radioactive probes were obtained with high radiochemical purity and specific activity, as illustrated by RP-HPLC radiochromatograms of ^{99m}Tc(CO)$_3$ DAPM4 and ^{99m}Tc (CO)$_3$_DCM20 (Fig. 6.3).

6.3.3. Stability

The in vitro stabilities of ^{99m}Tc(CO)$_3$ DAPM1, ^{99m}Tc(CO)$_3$ DAPM4, ^{99m}Tc(CO)$_3$ DAPM8 and ^{99m}Tc (CO)$_3$_ DCM20 towards transchelation were studied in the presence of a large excess of cysteine or histidine in PBS (~24 h at 37°C). These amino acids have been selected because they are present in several proteins in vivo and contain a set of donor atoms with high affinity for Tc(I). Table 6.1 summarizes the radiochemical purities of the radiolabelled dextran derivatives at different time points.

The results in Table 6.1 show that, despite being obtained in almost quantitative yield, ^{99m}Tc(CO)$_3$ DAPM1 displays relatively low stability in the presence of cysteine and histidine. On the contrary, ^{99m}Tc(CO)$_3$ DAPM4, ^{99m}Tc(CO)$_3$ DAPM8 and ^{99m}Tc(CO)$_3$ DCM20 are highly stable under the test conditions, presenting, in both cases, high radiochemical purity (≥90%), even after long incubation times. Therefore, ^{99m}Tc(CO)$_3$ DAPM4, ^{99m}Tc(CO)$_3$ DAPM8 and ^{99m}Tc(CO)$_3$ DCM20 were selected as the most promising radioactive compounds to pursue animal studies.
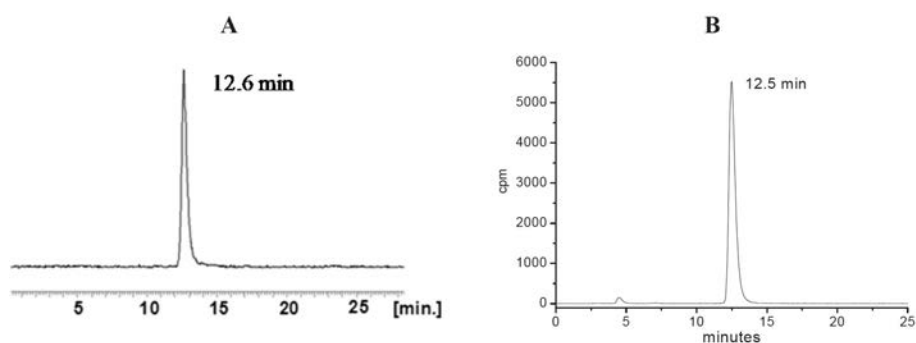

FIG. 6.3. RP-HPLC radiochromatograms of (A) ^{99m}Tc(CO)$_3$ DAPM4 and (B) ^{99m}Tc (CO)$_3$_DCM20. cpm: counts per minute.

TABLE 6.1. IN VITRO STABILITIES OF RADIOLABELLED MANNOSYLATED DEXTRAN DERIVATIVES $^{99m}Tc(CO)_3$ L (L = DAPM1, DAPM4, DAPM8, DCM20) IN THE PRESENCE OF CYSTEINE AND HISTIDINE AT DIFFERENT TIME POINTS

Compound	Activity bound to dextran (%)						
	Cysteine				Histidine		
	0 h	2 h	4 h	6 h	2 h	4 h	6 h
$^{99m}Tc(CO)_3$ DAPM1	98	85	75	ND	89	85	ND
$^{99m}Tc(CO)_3$ DAPM4	98	96	94	90	99	98	97
$^{99m}Tc(CO)_3$ DAPM8	98	95	94	90	99	98	97
$^{99m}Tc (CO)_3$ DCM20	98	95	94	90	98	96	97

Note: ND: not determined.

ACKNOWLEDGEMENTS

REFERENCES TO CHAPTER 6

[6.1] ALBERTO, R., et al., A novel organometallic aqua complex of technetium for the labeling of biomolecules: synthesis of *fac*-$[^{99m}Tc(H_2O)_3(CO)_3]^+$ from $[^{99m}TcO_4]^-$ in aqueous solution and its reaction with a bifunctional ligand, J. Am. Chem. Soc. 120 (1998) 7987–7988.

[6.2] Alberto, R., Ortner, K., Wheatley, N., Schibli, R., Schubiger, A.P., Synthesis and properties of boranocarbonate: a convenient in situ CO source for the aqueous preparation of $[^{99m}Tc(OH)_2(CO)_3]^+$, J. Am. Chem. Soc. 123 (2001) 3135–3136.

[6.3] Alberto, R., Schibli, R., Waibel, R., Abram, U., Schubiger, A.P., Basic aqueous chemistry of $[M(OH_2)_3(CO)_3]^+$ (M = Re, Tc) directed towards radiopharmaceutical application, Coord. Chem. Ver. 190–192 (1999) 901–919.

[6.4] SANTOS, I., PAULO, A., CORREIA, J.D.G., Rhenium and technetium complexes anchored by phosphines and scorpionates for radiopharmaceutical applications, Top. Curr. Chem. 252 (2005) 45–84.

[6.5] ALBERTO, R., The particular role of radiopharmacy within bioorganometallic chemistry, J. Organomet. Chem. 692 (2007) 1179–1186.

[6.6] GARCIA, R., PAULO, A., SANTOS, I., Rhenium and technetium complexes with anionic or neutral scorpionates: an overview of their relevance in biomedical applications, Inorg. Chim. Acta 362 (2009) 4315–4327.

[6.7] Alberto, R., The chemistry of technetium-water complexes within the manganese triad: challenges and perspectives, Eur. J. Inorg. Chem. 2009 (2009) 21–31.

[6.8] Alberto, R., Organometallic radiopharmaceuticals, Top. Organomet. Chem. 32 (2010) 219–246.

[6.9] LIPOWSKA, M., et al., First evaluation of a ^{99m}Tc-tricarbonyl complex, ^{99m}Tc(CO)$_3$(LAN), as a new renal radiopharmaceutical in humans, J. Nucl. Med. 47 (2006) 1032–1040.

[6.10] LIU, S., Ether and crown ether-containing cationic ^{99m}Tc complexes useful as radiopharmaceuticals for heart imaging, Dalton Trans. 2007 (2007) 1183–1193.

[6.11] LIU, Z.L., et al., Kinetic characterization of a novel cationic ^{99m}Tc(I)-tricarbonyl complex, ^{99m}Tc-15C5-PNP, for myocardial perfusion imaging, J. Nucl. Card. 17 (2010) 858–867.

[6.12] MARIA, L., et al., Tris(pyrazolyl)methane ^{99m}Tc tricarbonyl complexes for myocardial imaging, Dalton Trans. 2009 (2009) 603–606.

[6.13] GOETHALS, L.R., et al., Rapid hepatic clearance of ^{99m}Tc-TMEOP: a new candidate for myocardial perfusion imaging, Cont. Med. Mol. Imag. 6 (2011) 178–188.

[6.14] MORAIS, M., RAPOSINHO, P.D., CORREIA, J.D.G., SANTOS, I., Technical University of Lisbon, Portugal, unpublished data.

[6.15] Morais, M., et al., Mannosylated dextran derivatives labeled with *fac*-[M(CO)$_3$]$^+$ (M = ^{99m}Tc, Re) for specific targeting of sentinel lymph node, Mol. Pharm. 8 (2011) 609–620.

[6.16] Pirmettis, I., et al., New ^{99m}Tc(CO)$_3$ mannosylated dextran bearing S-derivatized cysteine chelator for sentinel lymph node detection, Mol. Pharm. 9 (2012) 1681–1692.

Chapter 7

4 + 1 Tc(III) COMPLEXES IN THE DESIGN AND DEVELOPMENT OF ^{99m}Tc LABELLED DEXTRAN MANNOSE DERIVATIVES AS POTENTIAL RADIOPHARMACEUTICALS FOR SLND

A. REY

Cátedra de Radioquímica, Facultad de Química,
Universidad de la República,
Montevideo, Uruguay

H.-J. PIETZSCH
Helmholtz-Zentrum,
Dresden-Rossendorf,
Germany

7.1. SUMMARY

With the objective to develop a potential ^{99m}Tc radiopharmaceutical for SLND, it was decided to focus on the formation of 4 + 1 Tc(III) complexes. This system is based on an oxofree core with the metal at a low oxidation state, and provides a non-polar building block that is stable against ligand exchange in vivo. DC25 and DCM30 were derivatized to incorporate the isocyanide necessary to coordinate ^{99m}Tc. The Tc complexes were formed by simultaneous coordination of the tetradentate and tripodal ligand 2,2', 2'' nitrilotris ethanethiol and isocyanide dextrans as the coligand. Labelling was achieved by substitution using ^{99m}Tc ethylenediaminetetraacetic acid (EDTA) as the precursor. Radiochemical purity, determined by SEC-HPLC and thin layer chromatography (TLC), was above 90%. The biodistribution of the derivative containing mannose as the pharmacophore (DCM30-iso) in Wistar rats showed a high uptake in popliteal lymph nodes and a very low uptake in external lumbar nodes and other organs. This result was corroborated by dynamic and static imaging. The same derivative without mannose (DC25-iso), on the other hand, showed negligible uptake in all lymph nodes. Results suggest that uptake in lymph nodes can be attributed to mannose. With the objective to assess the influence of the labelling method on the biological behaviour of labelled dextran mannose derivatives, the biodistribution of ^{99m}Tc DCM30 was also studied under the same conditions. A high uptake in the first lymph node (popliteal) was observed at all time points, while the activity in

the second node (external lumbar) was significantly lower. However, the uptake in popliteal lymph nodes was significantly lower compared to ^{99m}Tc DCM30-iso at 15 min and 30 min postinjection. The uptake in other organs was negligible, except for in the blood and liver, which demonstrated low uptakes.

7.2. INTRODUCTION

The 4 + 1 Tc(III) complexes are a class of Tc complexes bearing the Tc(III) core proposed by Pietzsch et al. [7.1] as a new non-polar Tc chelate system for the design of neutral and lipophilic complexes. Figure 7.1 depicts the general structure of this type of complex.

Formed by combination of a tetradentate tripodal 2-[bis-(2-mercapto-ethyl)-amino]-ethanethiol (NS_3) ligand and a monodentate coligand (isocyanide or tertiary phosphine), these complexes have the advantage of high versatility in conjugating biomolecules because both monodentate and tetradentate ligands are, at least in principle, able to bear functional groups, although the introduction of the biomolecule in the tetradentate ligand might generate a chiral carbon [7.2]. The donors can also be varied, but phosphines have the problem of sometimes being rather bulky cosubstituents [7.3].
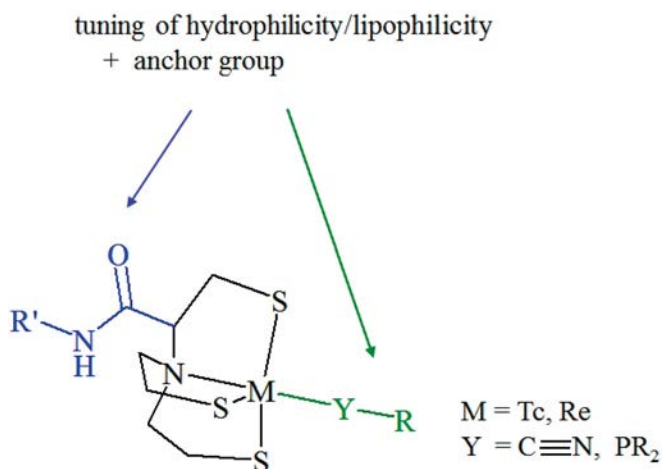
FIG. 7.1. General structure of 4 + 1 Tc(III) complexes.

A very important feature of these complexes is that the metal is well shielded by the 4 + 1 donor atom arrangement, thus avoiding interference with biological activity [7.4–7.6]. Furthermore, complexes are very stable, both in labelling milieu and in human plasma. In vitro challenge experiments with glutathione clearly indicated that no transchelation reactions occur. There were also no indications for in vivo reoxidation of Tc(III) to Tc(V) species or pertechnetate [7.7, 7.8].

The tripodal molecule 2,2', 2"-nitrilotris(ethanethiol) is the most widely used NS$_3$ tetradentate ligand. Derivatization of this ligand to introduce hydrophilic groups such as hydroxy groups, carboxyl groups or carbohydrates increases the hydrophilicity of the overall complex and is useful for fine tuning pharmacokinetics [7.9−7.11]. Figure 7.2 depicts the application of this concept to the development of a [99mTc] labelled arginylglycylaspartic acid (RGD) peptide for imaging tumoural neoangiogenesis [7.12].

This labelling concept has also been applied to the development of [99mTc] dextran mannose derivatives as potential radiopharmaceuticals for SLND. For this purpose, a dextran derivative bearing mannose as the active moiety and an isocyanopropyl group as the monodentate ligand for Tc(III) complexation were necessary. Figure 7.3 depicts the structure.
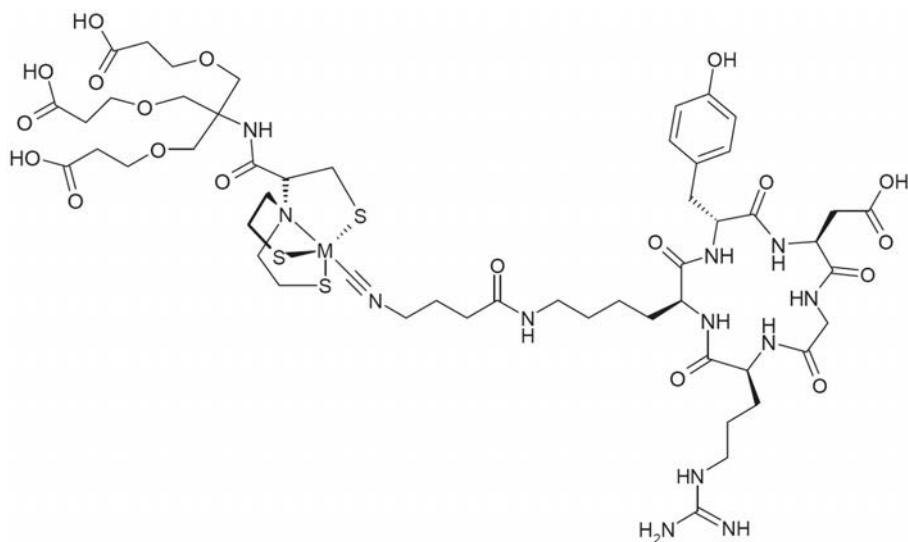
FIG. 7.2. RGD peptide labelled by means of 4 + 1 Tc(III) complexes.
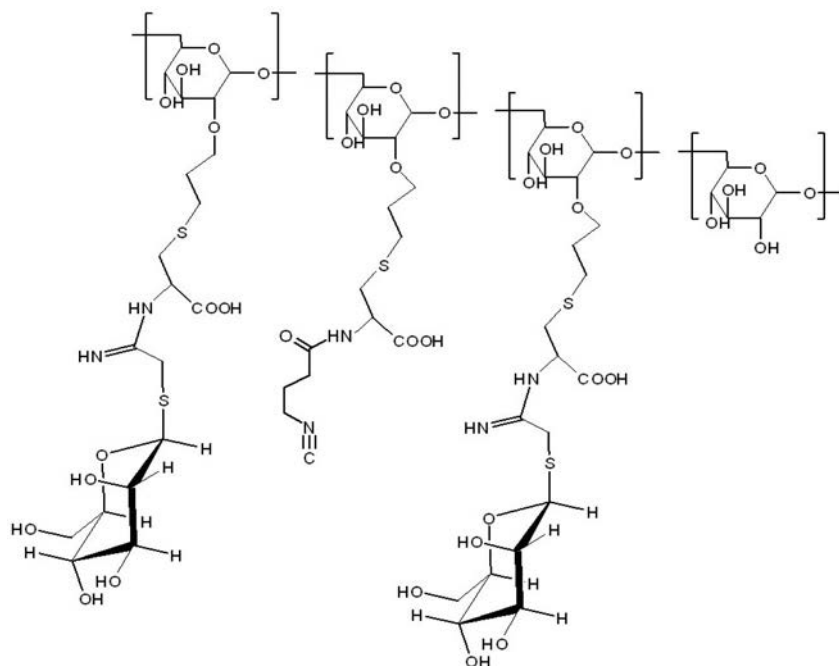
FIG. 7.3. Structure of a dextran derivative bearing an isocyanide moiety as the monodentate ligand for Tc(III) complexation.
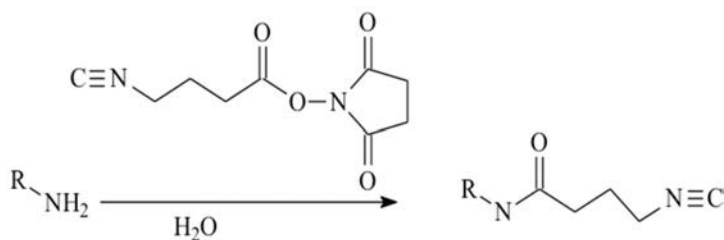
FIG. 7.4. Conjugation of isocyanide moiety to the biomolecule though an amino group.

The amino group of cysteine was used as the point for attaching both the mannose and the electron donor group. Introduction of the latter is achieved by reaction of the amine groups of the cysteine with 4-isocyano-butyric acid 2,5-dioxo-pyrrolidin-1-yl ester, as shown in Fig. 7.4.

The procedure can be performed as a batch, and kept for at least 2 weeks at 5°C−10°C. Derivatization in small quantities prior to each labelling procedure was also performed. On average, dextran derivative bears 45 cysteine branches:

1 cysteine is derivatized with the isocyanopropyl group, 36 cysteine branches are mannosylated and 8 remain free.

7.3.   MATERIALS AND METHODS

7.3.1.   General

All laboratory chemicals were reagent grade and used without further purification. Solvents for chromatographic analysis were HPLC grade. Technetium-99m NaTcO$_4$ was obtained from a commercial generator. The dextran derivative containing S-derivatized cysteine (DC25, MW ~ 23 kg/mol) and the mannosylated dextran derivative containing S-derivatized cysteine (DCM30) were provided by I. Pirmettis (Institute of Nuclear & Radiological Sciences & Technology, Energy & Safety, Demokritos National Centre for Scientific Research, Greece). Radiochemical purity was checked by TLC in silica gel using water as the mobile phase and by SEC-HPLC on a Superdex Peptide 10/300 GL column eluted with 50mM, pH7.0 PBS and 0.15M NaCl, at 0.5 mL/min flow rate. Radioactivity was detected with a homemade γ ray NaI(Tl) detector. NMR spectra were recorded in D$_2$O at 25°C on a Bruker 500 MHz Avance DRX spectrometer using 2,2,3,3-tetradeutero-3-trimethylsilyl-propionic acid sodium salt as the internal reference. Assignment of the spectra was based on a series of ^{1}H–^{1}H and ^{1}H–^{13}C correlation experiments. The 2,2', 2"-nitrilotris(ethanethiol) was prepared by reaction of tris(2-chloroethyl)amine hydrochloride with potassium thioacetate, followed by reduction with LiAlH$_4$. The final product was precipitated as oxalate salt and used as such in further reactions [7.2]. The coupling agent 4-isocyanobutyric acid 2,5-dioxopyrrolidin-1-yl ester was synthesized according to previously published methods [7.1, 7.8, 7.11].

7.3.2.   Synthesis of dextran derivative with isocyanopropyl arms

7.3.2.1. Dextran cysteine derivative with isocyanide arms (DC25-iso)

The dextran cysteine derivative DC25 (30 mg, 0.1 µmol) and triethylamine (100 µL) were dissolved in water (1 mL) in a vessel protected from light. N-hydroxysuccinimidyl 4-(isocyano)butanoate (12.3 mg, 58 µmol) was added. The reaction was stirred at room temperature until the reagent was completely consumed. The solution was evaporated in vacuo, and the white solid was washed with methanol and diethyl ether. The yield was 73% [7.13].

7.3.2.2. Dextran cysteine mannose derivative with isocyanide arms (DCM30-iso)

The dextran cysteine mannose derivative DCM30 (12 mg, 0.3 µmol) and triethylamine (100 µL) were dissolved in water (1 mL) in a vessel protected from light. N-hydroxysuccinimidyl 4-(isocyano)butanoate (4.5 mg, 21 µmol) was added. The reaction was stirred at room temperature until the reagent was completely consumed. The solution was evaporated in vacuo, and the white solid was washed with methanol and diethyl ether. The yield was 75% [7.13].

7.3.3. Radiolabelling and control of radiochemical purity

As shown in Fig. 7.5, labelling was performed by a two step substitution procedure using ^{99m}Tc EDTA/mannitol as the precursor. This precursor was obtained by direct reduction of pertechnetate using stannous chloride as the reducing agent, as follows. Technetium-99m [TcO$_4$] Na (300−1000 MBq, 1 mL) was added to a vial containing EDTA sodium salt (5 mg), mannitol (5 mg) and stannous chloride dihydrate (0.08 mg), and the mixture was incubated at room temperature for 5 min. The radiochemical purity was checked by TLC on silica gel using acetone and water as the mobile phases. The radiochemical purity was higher than 90%.
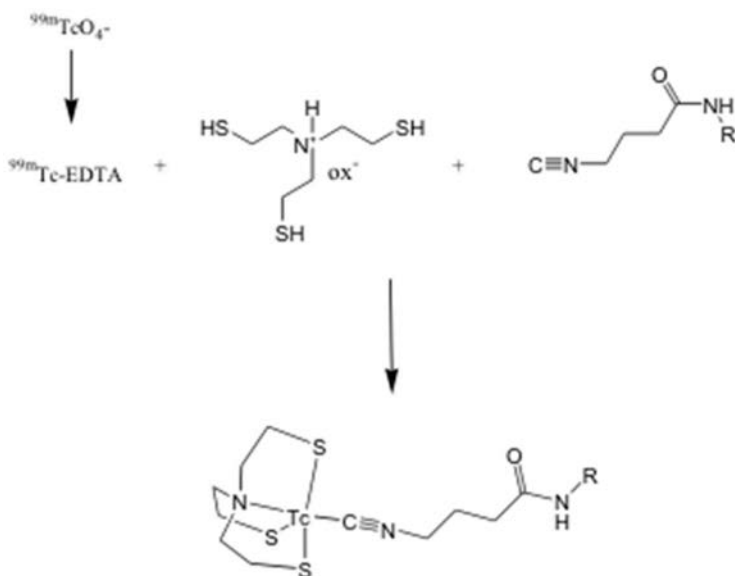

FIG. 7.5. Labelling procedure.

Substitution was achieved by the simultaneous action of the dextran derivative and the tetradentate NS_3 coligand 2,2', 2''-nitrilotris(ethanethiol).

The experimental procedure used for substitution was as follows. A solution of derivatized dextran mannose derivative in saline solution (800 μg in 250−500 μL) and 2,2',2''-nitrilotris(ethanethiol) oxalate (1 mg) was mixed with ^{99m}Tc EDTA and incubated at 70°C for 30 min. The in vitro stability of the ^{99m}Tc labelled compounds incubated at 37°C for up to 4 h postlabelling was evaluated using SEC-HPLC.

The radiochemical purity could be assessed by a single TLC run using water as the mobile phase because the labelled dextran remained at the origin, while ^{99m}Tc EDTA and ^{99m}TcO$_4^-$ migrated with the solvent front.

To confirm that coordination of the dextran derivative with ^{99m}Tc took place through the isonitrile, the labelling procedure was also performed using a derivative without the isocyanide group. The radiochemical purity was assessed using TLC and HPLC.

7.3.4. Biological evaluation

7.3.4.1. Biodistribution studies

Experimental animal studies were approved by the Ethics Committee of the Faculty of Chemistry at the University of the Republic, Uruguay. Normal Wistar rats (female, 250–300 g, three animals per group) were anaesthetized with sodium thiopental (50 mg/kg) administered in the peritoneal cavity. Then, ^{99m}Tc DCM30-iso derivatives (50 μL, 0.37 MBq, 0.2 nmol) were injected subcutaneously in the rear foot-pad, and 10 min before sacrifice, a volume of 0.05 mL of patent blue was also injected for visual identification of lymph nodes. Animals were sacrificed at different time intervals postinjection (15 min, 30 min, 60 min, 180 min and 24 h). Popliteal and external lumbar lymph nodes, as well organs and samples of blood and muscle, were collected, weighed and assayed for radioactivity. The injected foot was also removed for determination of activity remaining at the injection site. To establish if lymph node uptake can be attributed to the presence of the mannose moiety, biodistribution of labelled ^{99m}Tc DC25-iso was also performed under the same conditions. Popliteal extraction (E) was calculated according to:

$$E\ (\%) = \frac{\%ID_{POPLITEAL} - \%ID_{INGUINAL}}{\%ID_{POPLITEAL}} \times 100 \qquad (7.1)$$

7.3.4.2. Imaging studies

Imaging studies were performed in normal Wistar rats (female, 250–300 g). After peritoneal anaesthesia with sodium thiopental, animals were injected in the rear foot-pad with ^{99m}Tc labelled dextran derivatives DCM30-iso and DC25-iso (0.05 mL, 100 MBq, 2 nmol). Imaging was performed using a rectangular field (53.8 cm × 39.9 cm) gamma/camera (Sophy Camera DSX) equipped with a low energy, high resolution, parallel hole collimator. Static images were obtained at 15 min, 30 min, 45 min and 60 min postinjection.

7.4. RESULTS AND DISCUSSION

7.4.1. Synthesis and characterization of dextran derivatives with isocyano propyl arms

Dextran isocyanide derivatives DC25-iso and DCM30-iso were synthesized in high yields from their respective dextran precursors (~75% yields). Detailed NMR experiments allowed for complete assignment of signals to their respective nuclei. Two dimensional ^{1}H–^{1}H (correlation spectroscopy and nuclear Overhauser effect spectroscopy) and ^{1}H–^{13}C correlation techniques were able to confirm the expected structure.

7.4.2. Radiochemical purity and stability of ^{99m}Tc dextran derivatives

Mannosylated and non-mannosylated dextran isocyanide derivatives (DCM30-iso and DC25-iso, respectively) gave the 4 + 1 complex with the NS$_3$ ligand at a high yield (~90%). Figure 7.6 depicts a typical chromatographic profile of the precursor (^{99m}Tc EDTA) and of the final product, clearly demonstrating that substitution was complete and that ^{99m}Tc labelled dextran was obtained as the only reaction product.

When dextran derivative without the isocyanide group was used in the 4 + 1 labelling process, both chromatographic methods showed that the final product was ^{99m}Tc EDTA, indicating that the isocyanide group is crucial for achieving an adequate labelling yield. The radiochemical purity remained over 90% for 4 h, demonstrating that no decomposition occurred within the studied period.
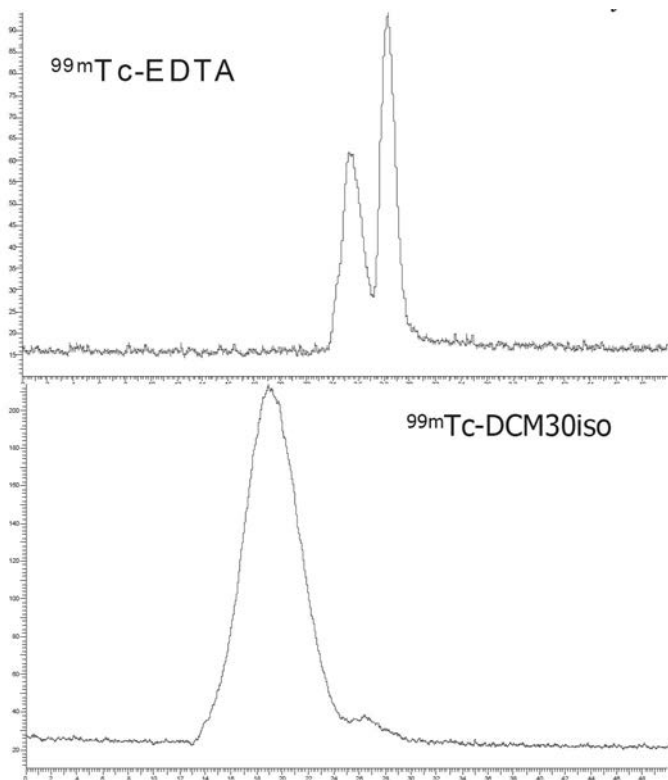
FIG 7.6. Determination of radiochemical purity of ^{99m}Tc labelled dextran mannose derivative using SEC-HPLC.

7.4.3. Biological evaluation

7.4.3.1. Biodistribution studies

Table 7.1 summarizes the results obtained at different time points between 15 min and 24 h after subcutaneous administration in the right foot-pad of Wistar rats of ^{99m}Tc DCM30-iso. Table 7.2 shows the results obtained after administration of the non-mannosylated isocyanide dextran derivative analogue (^{99m}Tc DC25-iso).

TABLE 7.1. BIODISTRIBUTION OF ^{99m}Tc DCM30-ISO IN RATS AFTER SUBCUTANEOUS ADMINISTRATION*

Organs	% ID/organ					
	15 min	30 min	60 min	180 min	24 h
Blood	3.9 ± 1.6	2.38 ± 0.94	2.26 ± 0.67	8.51 ± 0.71	0.64 ± 0.11
Liver	2.8 ± 1.9	4.33 ± 0.66	5.17 ± 0.30	11.26 ± 0.76	6.28 ± 0.41
Lungs	0.09 ± 0.09	0.07 ± 0.01	0.07 ± 0.01	0.39 ± 0.18	0.05 ± 0.01
Spleen	0.10 ± 0.09	0.05 ± 0.02	0.08 ± 0.02	0.049 ± 0.25	0.11 ± 0.01
Kidneys	0.38 ± 0.36	0.34 ± 0.12	0.22 ± 0.05	1.072 ± 0.092	0.70 ± 0.18
Thyroid	0.03 ± 0.03	0.01 ± 0.01	0.010 ± 0.005	0.014 ± 0.013	0.010 ± 0.005
Muscle	0.40 ± 0.40	1.13 ± 0.57	0.84 ± 0.39	1.70 ± 0.75	0.46 ± 0.14
Stomach	0.14 ± 0.10	0.08 ± 0.02	0.20 ± 0.11	0.244 ± 0.036	0.18 ± 0.15
Intestine	0.40 ± 0.29	0.87 ± 0.18	0.98 ± 0.20	6.5 ± 1.3	1.36 ± 0.02
Bladder + urine	0.20 ± 0.27	1.30 ± 0.70	3.18 ± 1.24	15.9 ± 8.3	49.4 ± 9.4
Popliteal lymph node	9.4 ± 1.2	5.90 ± 0.82	3.55 ± 1.40	5.42 ± 0.88	7.0 ± 1.0

TABLE 7.1. BIODISTRIBUTION OF ^{99m}Tc DCM30-ISO IN RATS AFTER SUBCUTANEOUS ADMINISTRATION* (cont.)

Organs	% ID/organ				
	15 min	30 min	60 min	180 min	24 h
External lumbar lymph node	1.18 ± 0.52	1.33 ± 0.91	1.42 ± 0.99	0.79 ± 0.54	3.40 ± 0.43
Popliteal extraction	87.8 ± 4.0	78.6 ± 12.6	76.4 ± 12.3	86.3 ± 7.8	51.3 ± 0.80
Injected foot	78.0 ± 6.4	77.1 ± 2.6	79.8 ± 3.0	45.7 ± 3.1	19.8 ± 1.5

* Results are expressed as % ID per organ and whole blood (mean ± standard deviation on three animals per time point).

TABLE 7.2. BIODISTRIBUTION OF ^{99m}Tc DC25-ISO IN RATS AFTER SUBCUTANEOUS ADMINISTRATION*

Organs	% ID/organ			
	15 min	30 min	60 min	24 h
Blood	9.0 ± 2.5	5.8 ± 1.6	5.7 ± 0.4	0.54 ± 0.10
Liver	10.4 ± 1.8	11.0 ± 2.0	10.8 ± 0.3	1.62 ± 0.51
Lungs	0.53 ± 0.12	0.27 ± 0.08	0.30 ± 0.02	0.04 ± 0.01
Spleen	0.12 ± 0.02	0.06 ± 0.02	0.08 ± 0.01	0.04 ± 0.02
Kidneys	4.8 ± 2.4	2.9 ± 0.02	4.6 ± 0.9	8.5 ± 1.8
Thyroid	0.054 ± 0.004	0.03 ± 0.02	0.05 ± 0.02	0.010 ± 0.005
Muscle	8.9 ± 1.4	6.0 ± 1.2	4.7 ± 0.2	0.40 ± 0.08
Stomach	0.47 ± 0.06	0.25 ± 0.01	0.50 ± 0.21	0.52 ± 0.14
Intestine	5.7 ± 2.5	8.1 ± 1.3	14.4 ± 0.9	2.28 ± 0.20
Bladder + urine	3.4 ± 1.7	15.3 ± 2.8	25.6 ± 2.9	76.8 ± 6.5
Popliteal lymph node	0.25 ± 0.04	0.20 ± 0.12	0.20 ± 0.07	0.55 ± 0.07
External lumbar lymph node	0.06 ± 0.03	0.11 ± 0.06	0.10 ± 0.04	0.25 ± 0.02
Injected foot	41.1 ± 5.4	25.8 ± 6.3	15.6 ± 1.2	2.23 ± 0.37

* Results are expressed as % ID per organ and whole blood (mean ± standard deviation on three animals per time point)

Lymph node uptake of ^{99m}Tc DCM30-iso (dextran with mannose pending arms) was much higher than that of the corresponding dextran conjugate without mannose (^{99m}Tc DC25-iso). These findings support the hypothesis that radioactivity localization in lymph nodes has occurred by a receptor mediated mechanism to macrophages present in these organs.

7.4.3.2. Imaging studies

Dynamic images up to 30 min after subcutaneous administration of ^{99m}Tc DCM30-iso and ^{99m}Tc DC25-iso in rats are shown in Fig. 7.7.

Biodistribution profiles of both compounds are consistent with the results obtained by dissection. Lymph nodes are clearly visible for ^{99m}Tc DCM30-iso. Liver and bladder can also be visualized. On the other hand, the uptake in lymph nodes is significantly lower for ^{99m}Tc DC25-iso. In this case, liver and bladder are the organs that show a higher uptake.

Static images acquired 30 min postadministration confirm the above findings, as shown in Fig. 7.8.

7.5. CONCLUSIONS

With the aim of developing new radiopharmaceuticals for SLND, evaluation and biological evaluation of mannosylated and non-mannosylated isocyanide dextran derivatives labelled with Tc(III) in a 4+1 linking arrangement have been studied. Labelling with high yields and radiochemical purities was achieved with both derivatives. Biodistribution results demonstrated high uptakes in the first lymph node and low uptakes in the following node, as well as low activities in the rest of the body when mannose moieties were present. On the other hand, lack of mannose resulted in negligible uptakes in all lymph nodes. Imaging experiments corroborated the biodistribution data. These results are promising, and further biological evaluation is required to confirm the findings.
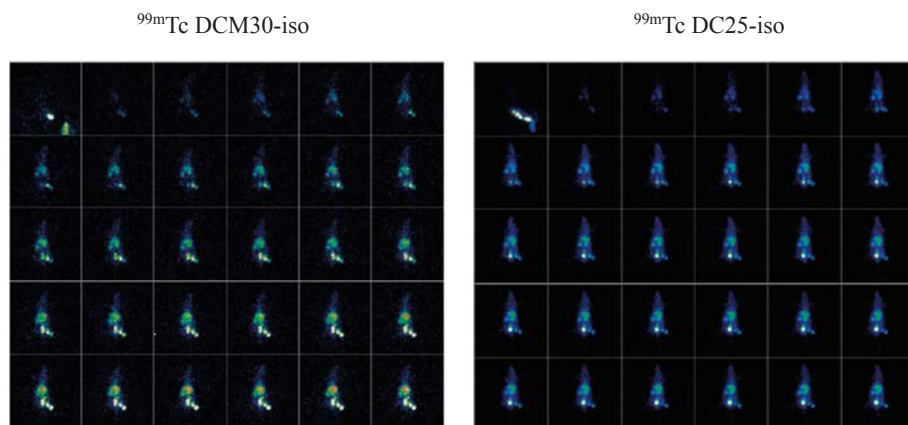
^{99m}Tc DCM30-iso $\qquad$ ^{99m}Tc DC25-iso

FIG. 7.7. Dynamic acquisitions (0–30 min) after subcutaneous administration of ^{99m}Tc DCM30-iso (left) and ^{99m}Tc DC25-iso (right) in rats.
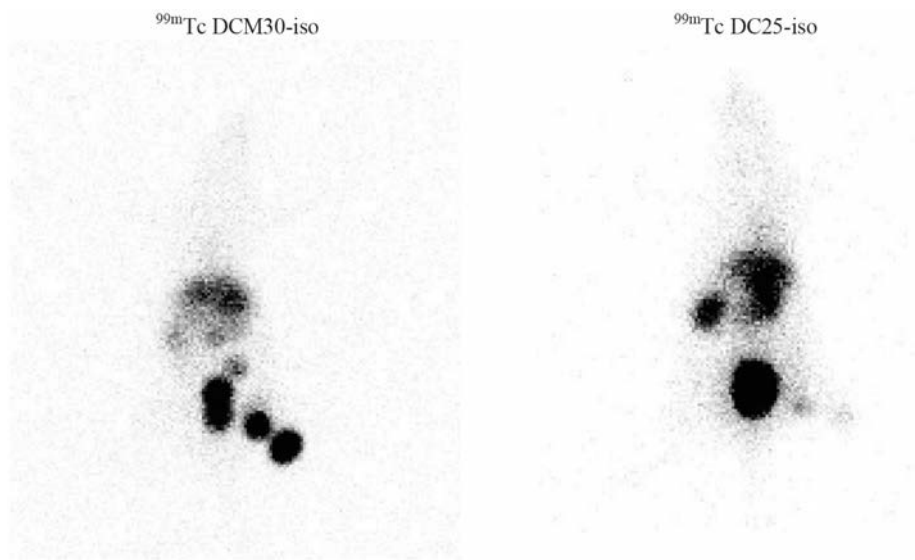
FIG. 7.8. Static acquisitions (30 min) after subcutaneous administration of ^{99m}*Tc DCM30-iso (left) and* ^{99m}*Tc DC25-iso (right).*

REFERENCES TO CHAPTER 7

[7.1]   PIETZSCH, H.-J., et al., Mixed-ligand technetium(III) complexes with tetradendate/monodendate NS3/isocyanide coordination: a new nonpolar technetium chelate system for the design of neutral and lipophilic complexes stable in vivo, Bioconjug. Chem. **12** (2001) 538–544.

[7.2]   SPIES, H., GLASER, M., Synthesis and reactions of trigonal-bipyramidal rhenium and technetium complexes with a tripodal, tetradentate NS3 ligand, Inorg. Chim. Acta **240** (1995) 465–478.

[7.3]   ALBERTO, R., "Technetium", Comprehensive Coordination Chemistry II (McCLEVERTY, J.A., MEER, T.S., Eds), Vol. 5, Elsevier Science, Amsterdam (2003) 127–271.

[7.4]   DREWS, A., et al., Synthesis and biological evaluation of technetium(III) mixed-ligand complexes with high affinity for the cerebral 5-HT1A receptor and the alpha1-adrenergic receptor, Nucl. Med. Biol. **29** (2002) 389–398.

[7.5]   WALTHER, M., et al., Synthesis and biological evaluation of a new type of (99m) technetium-labeled fatty acid for myocardial metabolism imaging, Bioconjug. Chem. **18** (2007) 216–230.

[7.6]   KÜNSTLER, J.U., et al., Organometallic ^{99m}Tc(III) '4 + 1' bombesin(7-14) conjugates: synthesis, radiolabeling, and in vitro/in vivo studies, Bioconjug. Chem. **18** (2007) 1651–1661.

[7.7] SCHILLER, E., et al., Mixed-ligand rhenium-188 complexes with tetradentate/ monodentate NS3/P ('4 + 1') coordination: relation of structure with antioxidation stability, Bioconjug. Chem. **16** (2005) 634–643.

[7.8] SEIFERT, S., et al., Novel procedures for preparing Tc-99m(III) complexes with tetradentate/monodentate coordination of varying lipophilicity and adaptation to Re-188 analogues, Bioconjug. Chem. **15** (2004) 856–863.

[7.9] KÜNSTLER, J.U., et al., Novel ^{99m}Tc '4 + 1' peptide conjugates: tuning the biodistribution by variation of coligands, Eur. J. Med. Chem. **45** (2010) 3645–3655.

[7.10] KÜNSTLER, J.U., et al., Efficient preparation of ^{99m}Tc(III) '4 + 1' mixed-ligand complexes for peptide labeling with high specific activity, Appl. Radiat. Isot. **68** (2010) 1728–1733.

[7.11] KÜNSTLER, J.U., et al., Impact of functionalized coligands on the pharmacokinetics of ^{99m}Tc(III) '4 + 1' mixed-ligand complexes conjugated to bombesin, J. Inorg. Biochem. **105** (2011) 1383–1390.

[7.12] GIGLIO, J., et al., "Design and evaluation of potential ^{99m}Tc-radiopharmaceuticals based on the Tc-carbonyl, 4 + 1 mixed-ligand chelate system and Tc-nitrido approaches", Labelling of Small Biomolecules Using Novel Technetium-99m Cores, Technical Reports Series No. 459, IAEA, Vienna (2007) 261–285.

[7.13] GIGLIO, J., et al., Design and development of (^{99m})Tc-'4 + 1'-labeled dextran-mannose derivatives as potential radiopharmaceuticals for sentinel lymph node detection, Cancer Biother. Radiopharm. **28** (2013) 541–551.

Chapter 8

BIOLOGICAL EVALUATION OF
LOW VALENCE ^{99m}Tc DEXTRAN DERIVATIVES
FOR SLND: RESULTS OF A MULTILABORATORY STUDY

R. PASQUALINI
CIS bio international/IBA, Saclay, RP Innovative,
Clamart, France

8.1. SUMMARY

SLNB allows accurate staging of regional lymph node basins by surgical removal and histological examination of those lymph nodes that receive direct lymph drainage from the tumour site. This technique has become the standard of care in breast cancer and melanoma, and is increasingly being applied to other solid cancers with high metastatic potential in lymph nodes. The SLNM can be performed using blue dyes, radiotracers or both. Radiopharmaceuticals based on ^{99m}Tc colloids (either inorganic or of albumin origin) are the currently used radiotracers, although a newly approved dextran based, receptor targeted agent, ^{99m}Tc tilmanocept, is expected to be gradually adopted by the nuclear medicine community.

Recognizing the importance of the receptor targeted approach for SLNM, the IAEA initiated a CRP in 2007 to evaluate the ability of newer low valence ^{99m}Tc dextran derivatives to selectively localize in the SLN. This chapter is based on work carried out at participating institutions in several Member States.

Low MW dextran (12 kg/mol and 20 kg/mol), to which mannose residues were added for specificity to mannose receptors expressed by SLN macrophages, was derivatized to incorporate either cysteine/cysteamine or pz moiety for facilitating radiolabelling with a Tc(I) carbonyl core. Isocyanide groups were also added to mannosylated dextran for the formation of 4 + 1 Tc(III) complexes.

The new dextran derivatives (20 kg/mol and 30 kg/mol MW) were quantitatively labelled with ^{99m}Tc (>90% radiochemical purity). Both Tc(I) and Tc(III) complexes were inert to ligand exchange with cysteine and histidine, and remained stable after 6 h at room temperature.

The biological properties of the radiolabelled dextran derivatives were tested in vivo (gamma imaging) and ex vivo (biodistribution) after intradermal/ subcutaneous administration to mice, rats and rabbits. Approved ^{99m}Tc labelled colloids (rhenium sulphide, sulphur colloids and calcium phytate) were used

to standardize the protocol for identifying the sentinel node and the secondary nodes in animals. Animal experiments have shown rapid and high accumulation in the popliteal lymph node that remained almost stable for a long period of time. Uptake in the SLN was similar to that displayed by ^{99m}Tc tilmanocept, showing a saturable receptor mediate mechanism.

Ranking the ^{99m}Tc dextran derivatives according to their biological properties led to [^{99m}Tc(CO)$_3$ DCM20] and [^{99m}Tc(CO)$_3$ DAPM8] being selected as the most promising agents for potential use in humans.

8.2. INTRODUCTION

The SLN is the hypothetical first lymph node, or group of nodes, that receives lymph collected from a primary tumour mass. If cancerous dissemination occurs, it is postulated that the SLN will trap any metastasizing cells leaving the tumour. If the SLN is negative for tumour metastasis, the presence of cancerous cells in all other lymph nodes in the same lymphatic chain is highly improbable [8.1–8.5].

This technique has become the standard of care in breast cancer [8.6, 8.7] and melanoma [8.8, 8.9], and is increasingly being applied to other solid cancers with high metastatic potential in lymph nodes, such as oral and oropharyngeal squamous cell carcinoma [8.10]. SLNM can be performed using a dye (patent blue or isosulphan blue), using radiotracers or both. Radiopharmaceuticals based on ^{99m}Tc colloids (either inorganic or of albumin origin) are the currently used radiotracers [8.11]. Despite their long standing use, large variations exist in the nature and size of ^{99m}Tc labelled colloids currently used for the detection of SLNs [8.2, 8.12]. Studies in the USA were initiated with sulphur colloid, which is a radiopharmaceutical that was initially approved for liver and spleen scintigraphy [8.13]. This radiocolloid (filtered or unfiltered) is still used. In Europe, albumin colloids and a preformed rhenium sulphide colloid have been approved for SLND. Of the two, albumin colloid is the most frequently used tracer in Europe. Technetium-99m labelled antimony trisulphide is the colloid of choice in Australia, whereas ^{99m}Tc calcium phytate is the tracer used in Japan.

Ideally, an SLN imaging agent would rapidly clear from the injection site to allow easy detection of nodes that are located close to the injection site. Residence of activity in the SLN should be selective and long enough to allow different protocols for detection (external acquisition or radioguided surgery). The radiotracer should be obtained with high specific activity to avoid saturation of the phagocytic process, with consequent leakage of radioactivity to the higher echelon nodes of the region. Finally, its preparation should be easy to perform, and the administered product should be safe. Radiocolloids hardly match all the

above mentioned requirements. In particular, clearance from the injection site may be slow, especially for large sized colloids. On the other hand, colloids based on HSA, although displaying the appropriate size range, may raise potential concerns about the quality of the donated blood, which has to be monitored for viral contamination. Some of these drawbacks have been overcame by the introduction, by Vera et al., of a totally synthetic ^{99m}Tc DTPA mannosyl dextran derivative that accumulates in the lymphatic tissues of rats and rabbits by binding to mannose receptors present on the surface of macrophage cells [8.14]. The compound consists of a dextran backbone with an average MW of 9500 g/mol, to which mannose glycosides and DTPA moiety are attached through cysteamine arms. The final amino, mannose and DTPA densities were 23, 55 and 8 moles per dextran, respectively. The MW of the dextran derivative was approximately 36 000 g/mol. This receptor based agent has shown excellent results in animals [8.14], and has been investigated in a multicentre, open label, comparative study against VBD for the detection of SLNs in melanoma and breast tumours [8.15]. The clinical study demonstrated the concordance of in vivo detection rates of this new agent and VBD in lymph nodes. The compound, named ^{99m}Tc labelled tilmanocept, was approved by the FDA in March 2013 for use in patients with breast cancer or melanoma who are undergoing surgery to remove tumour draining lymph nodes. The drug, marketed under the name of Lymphoseek, has been approved by the European Medicines Agency (an extensive discussion of this new tracer is given by Vera et al. in Chapter 4).

Recognizing the importance of the receptor targeted approach for SLNM, the IAEA initiated a CRP in 2007 aimed at synthesizing newer low valence ^{99m}Tc dextran derivatives and evaluating their potentiality in mapping SLNs in rodents. This chapter is based on the biological work carried out at institutions participating in the CRP Development of ^{99m}Tc Radiopharmaceuticals for Sentinel Node Detection and Cancer Diagnosis (see the list of contributors to drafting and review at the end of this publication).

In an effort to explore new mannosylated dextran derivatives that could produce a superior ^{99m}Tc labelled SLNM agent, it was decided to investigate the potential of the fac-$[^{99m}Tc(CO)_3]^+$ core and the $[^{99m}Tc(NS_3)]$ fragment for ^{99m}Tc labelling. The former core has recently attracted growing interest, particularly after Alberto et al. reported an aqueous preparation of the $[^{99m}Tc(CO)_3(H_2O)_3]^+$ precursor [8.16] and the availability of the IsoLink boronocarbonate kit by Mallinckrodt Medical BV [8.17]. As a tridentate ligand is required for the replacement of the aquo ligands and the formation of a stable complex with a ^{99m}Tc tricarbonyl core, mannosylated dextran molecules were equipped with S-derivatized cysteine arms (providing the S, N, O set of ligating atoms) [8.18–8.20] or with S-derivatized pz diamine arms (providing the N, N, N set of ligating atoms) [8.21, 8.22]. Isocyanide groups were also appended to

mannosylated dextran for ligation of the [^{99m}Tc(NS$_3$)] fragment in the so called 4 + 1 mixed ligand arrangement [8.23–8.26]. The chemical structures of dextran derivatives evaluated in this study are reported in Fig. 8.1.

Laboratory code: DC15
MW of starting dextran ~ 12 kg/mol
MW of dextran derivative ~ 17 kg/mol
^{99m}Tc core: [^{99m}Tc(CO)$_3$)]$^+$

Dextran propyl-S-cysteine

Laboratory code: DCM20
MW of starting dextran ~ 12 kg/mol
MW of dextran derivative ~ 22 kg/mol
^{99m}Tc core: [^{99m}Tc(CO)$_3$)]$^+$

Dextran propyl-S-cysteine mannose

X = 15; Y = 1; Z = 14
Laboratory code: DAPM1
MW of starting dextran ~ 10 kg/mol
MW of dextran derivative ~ 16 kg/mol
X = 12; Y = 4; Z = 14
Laboratory code: DAPM4
MW of starting dextran ~ 10 kg/mol
MW of dextran derivative ~ 17 kg/mol
X = 10; Y = 8; Z = 12
Laboratory code: DAPM8
MW of starting dextran ~ 10 kg/mol
MW of dextran derivative ~ 17 kg/mol
^{99m}Tc core: [^{99m}Tc(CO)$_3$)]$^+$
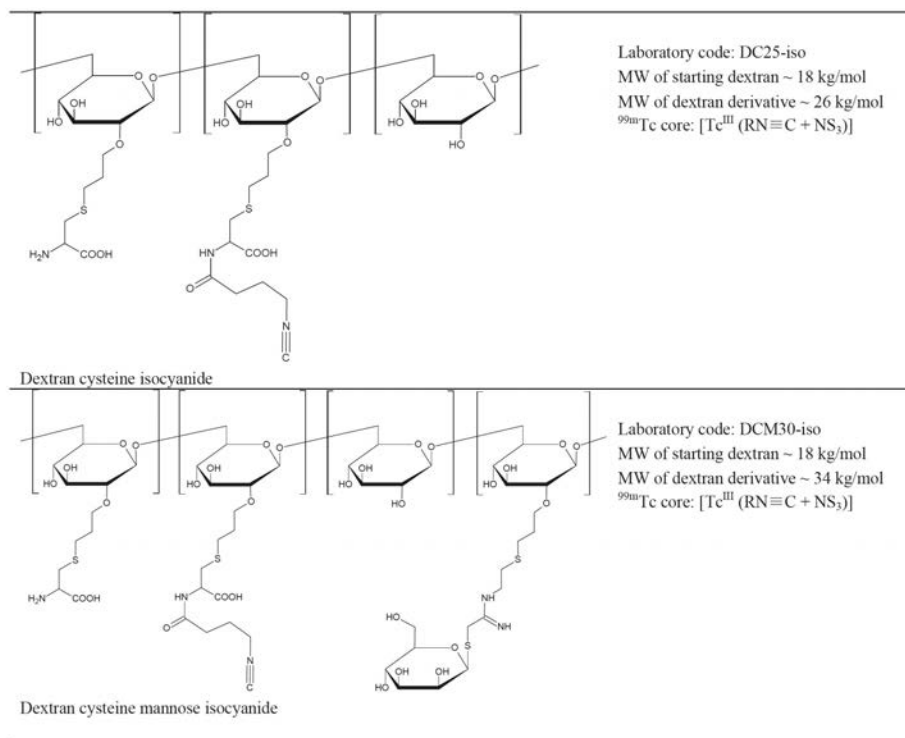
Dextran amine pz diamine mannose

FIG. 8.1. Chemical structure of dextran derivatives under study.

8.3. MATERIALS AND METHODS

8.3.1. Synthesis of dextran derivatives

Detailed synthesis of the different dextran derivatives is discussed in Chapter 5. Briefly, dextran bearing S-derivatized cysteine chelator (DC15) and mannosylated dextran (DCM20) were obtained through a two and three step synthesis, respectively. Dextran (MW = 11 800 g/mol) was reacted with allyl bromide to yield allyl dextran with about 40% coupling. Addition of cysteine to allyl dextran in the presence of ammonium persulphate resulted in the S-derivatized cysteine, compound DC15. The mannosylated product DCM20 was obtained in good yield after in situ hydrolysis and activation of cyanomethyl 2,3,4,6-tetra-*O*-acetyl-1-thio-β-D-mannoside (CNM thiomannose) and coupling to DC15. All intermediates, as well as the final products, were purified by ultrafiltration using a membrane with an MW cut-off of 3000 g/mol, then lyophilized [8.27].

Mannosylated dextran bearing pz diamine chelators (DAPM1–4–8) were obtained using a synthetic strategy similar to that used for the preparation of DC15/DCM20 compounds. Dextran (MW = 9500–10 500 g/mol) was reacted with allyl bromide to yield allyl dextran with about 50% coupling. The addition of aminoethanthiol and ammonium persulphate resulted in the S-derivatized amine. This intermediate was reacted in dry CH_2Cl_2 with the carboxylic acid of the Boc protected pz diamine chelator using N,N'-dicyclohexylcarbodiimide and N-hydroxysuccinimide as activators. CNM thiomannose was deacetylated with sodium methoxide. After the removal of methanol, the CNM mannose was reacted with dextran bearing the Boc protected pz diamine arms. The protecting group was removed with TFA/H_2O, giving the final conjugates, as TFA salt, in quantitative yields. All intermediates and the final product were purified by dialysis, then lyophilized [8.28].

Mannosylated dextran derivatives bearing isocyanide groups for ligation with [99m]Tc(III) (DCM-iso) were prepared following a four step synthesis. Dextran (MW = 18 000 g/mol) was reacted with allyl bromide to yield allyl dextran (40% of the glucose units were allylated). Addition of cysteine to allyl dextran in the presence of ammonium persulphate resulted in the S-derivatized cysteine, compound DC25. Mannose residues were introduced by reacting DC25 with CNM thiomannose as previously described (DCM30). The isocyanide group was introduced by reacting DCM30 with 4-isocyano-butyric acid 2,5-dioxo-pyrrolidin-1-yl ester under basic conditions. All intermediates, as well as the final products, were purified by ultrafiltration using a membrane with a MW cut-off of 3000 g/mol [8.29]. The procedure can be performed as a batch and kept for at least 2 weeks at 5°C–10°C, or performed in small quantities prior to each labelling procedure.

Proton and ^{13}C NMR spectroscopy (300–500 MHz) was used to establish the chemical identity of intermediates and final products. Colorimetric tests were used to determine the density of amine residues per mole of dextran (2,4,6-trinitrobenzene sulphonic acid assay) and to obtain the number of sugar units per dextran molecule (sulphuric acid/phenol colorimetric assay).

8.3.2. Physical characterization of dextran derivatives

The hydrodynamic diameters of DCM and DAPM derivatives and the starting dextran were determined by DLS using a ZetaSizer Nano ZS-90 from Malvern Instruments (UK). Measurements were carried out at 25°C with a 173° scattering angle. All the compounds were dissolved in saline (2 mL), resulting in different concentrations because different quantities of compounds were used for labelling (50 µg DCM20, 400 µg DAPM).

8.3.3. Radiolabelling

Technetium-99m, as ^{99m}Tc [TcO$_4$] Na, was obtained from commercial generators available in each Member State.

8.3.3.1. Dextran derivative formulation for ^{99m}Tc labelling

DC15/DCM20: 1 mL of 0.22 µm Millipore filtered aqueous solutions of DC15 or DCM20 (50 µg/mL or 400 µg/mL) was dispensed in 10 mL penicillin vials and lyophilized at −4°C for 24 h. At the end of the lyophilization cycle, the vials were stoppered and sealed under vacuum.

DAPM$_{1-4-8}$: Vials containing DAPM derivatives (50–500 µg) were prepared either extemporaneously, by dispensing the appropriate volume of a water solution, or by lyophilization of aqueous solutions of the derivatives.

DC25-iso/DCM30-iso: Vials containing DC25-iso or DCM30-iso (500 µg) were prepared extemporaneously before labelling.

Dextran derivatives were labelled either with a $[^{99m}Tc(CO)_3]^+$ core (dextran propyl-S-cysteine/DCM/DPAM derivatives) or with a $[^{99m}Tc(NS_3)]$ fragment (DC25-iso/DCM30-iso derivatives). Common labelling and quality control procedures were established to obtain comparable results within laboratories.

8.3.3.2. Labelling with $[^{99m}Tc(CO)_3]^+$ core: formation of $[^{99m}Tc(CO)_3(H_2O)_3]^+$ precursor

Radiolabelling with $[^{99m}Tc(CO)_3]^+$ core was performed by a two step procedure using $[^{99m}Tc(CO)_3(H_2O)_3]^+$ as a precursor. The precursor was obtained using the IsoLink kit (Mallinckrodt Medical BV) or by a homemade kit (10 mL vial containing 4.0 mg Na$_2$CO$_3$, 5.5 mg NaBH$_4$, 15–20 mg Na/K tartrate and 1 atm. carbon monoxide headspace volume). Typically, 1 mL of $^{99m}TcO_4$ (37–1850 MBq/mL, 1–50 mCi/mL) was added to the IsoLink vial and heated for 25 min at 100°C in a water bath. The solution was cooled, and the pH was adjusted to 7–8.5 with the addition of 0.1M HCl or PBS/HCl solution.

8.3.3.3. Labelling with $[^{99m}Tc(CO)_3]^+$ core: formation of $[^{99m}Tc(CO)_3$ DC15/DCM20] and $[^{99m}Tc(CO)_3$ DAPM]

Typically, the vials containing solid dextran derivatives were reconstituted with 200 µL of saline and flushed with nitrogen before radiolabelling. Approximately 500 µL of the pH adjusted $[^{99m}Tc(CO)_3(H_2O)_3]^+$ intermediate was added to the individual vials. DC15 and DC25 were labelled at 70°C–80°C

for 25–30 min, whereas labelling of DAPM derivatives occurred at 100°C for 30 min.

8.3.3.4. Labelling with $[^{99m}Tc(NS_3)]$ fragment: formation of ^{99m}Tc EDTA precursor

The ^{99m}Tc EDTA precursor was prepared by adding $^{99m}TcO_4^-$ (300 MBq, 1 mL) to a vial containing 5 mg EDTA, 5 mg mannitol and 0.08 mg SnCl$_2$. Formation of the precursor took place in 5 min at room temperature.

8.3.3.5. Labelling with $[^{99m}Tc(NS_3)]$ fragment: formation of $[^{99m}Tc(DC25\text{-}iso + NS_3)]$ and $[^{99m}Tc(DCM30\text{-}iso + NS_3)]$

A solution of DC25-iso or DCM30-iso in saline (800 µg in 250–500 µL) and NS$_3$ (1 mg) was mixed with ^{99m}Tc EDTA and incubated at 70°C for 30 min.

8.3.4. Control of radiochemical purity

8.3.4.1. Radiochemical purity of $[^{99m}Tc(CO)_3 DC15/DCM20]$ and $[^{99m}Tc(CO)_3 DAPM]$

Correct formation of the $[^{99m}Tc(CO)_3(H_2O)_3]^+$ precursor, as well as the radiochemical purity of the final products, was ascertained using a reversed phase C18 column. The chromatographic conditions varied slightly from one laboratory to another. The following is an example of the analytical conditions for determination of the radiochemical purity. Solvents consisted of water containing 0.1% TFA (solvent A) and methanol containing 0.1% TFA (solvent B). The column was a Nucleosil C18 reversed phase column (10 µm, 250 mm × 4 mm). Separation started with 100% of A from 0 min to 1 min, followed by a linear gradient to 30% A (70% B) in 9 min; this composition was held for another 10 min. The flow rate was 1 mL/min. Peak elution was monitored using an appropriate radioactivity detector. Radioactive preparations were also tested by SEC-HPLC (e.g. Shodex SB-803HQ, 8 mm × 300 mm) eluted with water at a flow rate of 1 mL/min. In this system, retention times were as follows: $^{99m}TcO_4^-$, $t_R = 3.5$ min; fac-$[^{99m}Tc(OH_2)_3(CO)_3]^+$ precursor, $t_R = 5.0$ min; ^{99m}Tc dextrans, $t_R = 11$–13 min.

For a rapid evaluation of radiochemical purity, samples were also analysed by ITLC using methanol:HCl (99:1) as the mobile phase, or paper chromatography (Whatman 1) using acetone as the mobile phase.

The radiochemical stability of the [^{99m}Tc(CO)$_3$] dextran derivatives in the final preparation was evaluated at room temperature. The chemical inertness of the complexes was also investigated by challenging each ^{99m}Tc complex with a large molar excess (1:100) of cysteine or histidine solutions in 1×10^{-3}M PBS at pH7.4. The samples were incubated at 37°C and analysed by RP-HPLC.

8.3.4.2. *Radiochemical purity of [^{99m}Tc EDTA] precursor*

Correct formation of the [^{99m}Tc EDTA] precursor was checked by TLC in silica gel using acetone and water as the mobile phase.

8.3.4.3. *Radiochemical purity of [^{99m}Tc (DC25-iso + NS$_3$)] and [^{99m}Tc (DCM30-iso + NS$_3$)]*

Radiochemical purity was checked by TLC in silica gel using water as the mobile phase and by molecular exclusion HPLC on a Superdex Peptide 10/300 GL column, using 50mM PBS, pH7.0, in 0.15M NaCl at 0.5 mL/min flow rate.

8.3.5. Determination of partition coefficient of some ^{99m}Tc(CO)$_3$ dextran derivatives

The octanol water partition coefficient was determined at room temperature for the following labelled dextran derivatives: [^{99m}Tc(CO)$_3$ DC15], [^{99m}Tc(CO)$_3$ DCM20] and [^{99m}Tc(CO)$_3$ DAPM1].

8.3.6. Biological evaluation

Experimental animal studies were approved by each respective local ethics committee. Commercially approved ^{99m}Tc labelled colloids (rhenium sulphide, sulphur colloids or calcium phytate) were used to standardize the protocol for identifying the sentinel node and the secondary nodes in animals.

8.3.6.1. *Biodistribution studies*

Biodistribution studies were performed in female (Wistar or Sprague Dawley) rats. Some participating institutions were also able to perform biodistribution studies in mice and in rabbits.

Rats weighing 200–250 g were used in experiments. Each animal was first anaesthetized with a mixture of xylazine/ketamine (or acepromazine/ketamine) administered in the peritoneal cavity. Then, approximately 50 µL of

the ^{99m}Tc labelled preparation (~1.8 MBq) was injected subcutaneously in the foot-pad region (in some experiments, the intradermal route was used). This was followed by gentle massage of the area of injection for up to 2 min with a strip of gauze (animals were rejected if more than 1% of the administered activity was recovered in the gauze). The animals (at least three per time point) were then kept for the respective incubation periods (60 min and 180–240 min) under normal conditions, with water provided ad libitum. A volume of 50 µL of 1% patent blue solution was injected into the same site approximately 10 min before sacrifice for visual detection of lymph nodes. The popliteal and inguinal lymph nodes, injection site and tissue and organs of interest were removed and weighed before radioactivity measurement. Results were expressed as a percentage of the administered activity found in sampled tissues and organs. The popliteal lymph node extraction (E) was calculated as:

$$E(\%) = \frac{\%ID_{POPLITEAL} - \%ID_{INGUINAL}}{\%ID_{POPLITEAL}} \times 100 \tag{8.1}$$

A similar protocol was followed for experiments in male BALB/c mice (20 ± 2 g). In these animals, a smaller volume (5–25 µL) and a reduced activity (90–180 kBq) were used.

In rabbits, intramuscular injection of 0.2 mL of ketamine was used as anaesthesia. An activity of 111 MBq in 0.2 mL dextran derivative was injected intradermally in both rear foot-pads. After injection, both foot-pads were massaged for 3 min. At 50 min postinjection, 0.1 mL of a vital dye (patent blue V) was injected intradermally in both foot-pads. Surgical dissection was started 10 min later to measure the uptake in popliteal and iliac nodes.

The influence of administered mass and volume on tracer localization was also studied in rats and mice.

8.3.6.2. Gamma camera imaging

Anaesthetized animals (rats/rabbits) were horizontally placed under the collimator of a gamma camera, equipped with a low energy, high resolution collimator, using a 256 × 256 matrix size, zoom 2 (1 min/frame) for dynamic studies and a 512 × 512 matrix size, zoom 2 for static studies. For optimal image resolution, the distance between the collimator and animal was about 10 cm. SPECT/CT images were also obtained in rats and mice for some selected compounds.

8.4. RESULTS

8.4.1. Synthesis and characterization of dextran derivatives

All dextran derivatives depicted in Fig. 8.1 were synthesized in high yields (~90% yields per synthetic step). Detailed NMR experiments allowed for the complete assignment of signals to their respective nuclei. Two dimensional ^{1}H–^{1}H (correlation spectroscopy and nuclear Overhauser effect spectroscopy) and ^{1}H–^{13}C (heteronuclear single quantum coherence spectroscopy and heteronuclear multiple bond) correlation techniques were able to confirm the expected structure as depicted in Fig. 8.1. Detailed information on the characterization of dextran derivatives are reported in Chapter 5.

8.4.2. Physical characterization of dextran derivatives

The size distribution measurements revealed the formation of aggregates as early as 30 min after preparation, increasing the size of particles from 7–10 nm to 230–310 nm and even 700 nm. That was the case for all preparations. In the case of DCM20, a rapid switch to 314 nm and a small number of aggregates of sizes greater than 5000 nm (240 nm after sonication) were observed. In the case of DAPM, the initial distribution showed particles and aggregates of size 11 nm (close to the expected value, corresponding with analyses after synthesis), 84 nm and 277 nm, which was switched in time (24 h) to 266 nm. Even aggregates of sizes greater than 5000 nm were formed (but only with 1.3% intensity).

8.4.3. Radiochemical purity and stability of ^{99m}Tc dextran derivatives

8.4.3.1. Complexes [$^{99m}Tc(CO)_3$ DC15/DCM20]

The mannosylated compound DCM20, as well as its non-mannosylated derivative DC15, were successfully labelled with $^{99m}Tc(CO)_3$ core (95% radiochemical yields), even at low ligand concentration (1.5×10^{-6}M) using the *fac*-[$^{99m}Tc(OH_2)_3(CO)_3$]$^+$ precursor. Figure 8.2 shows radioactive profiles of DCM20 preparations, as well as the precursor *fac*-[$^{99m}Tc(OH_2)_3(CO)_3$]$^+$ and pertechnetate obtained using RP-HPLC.
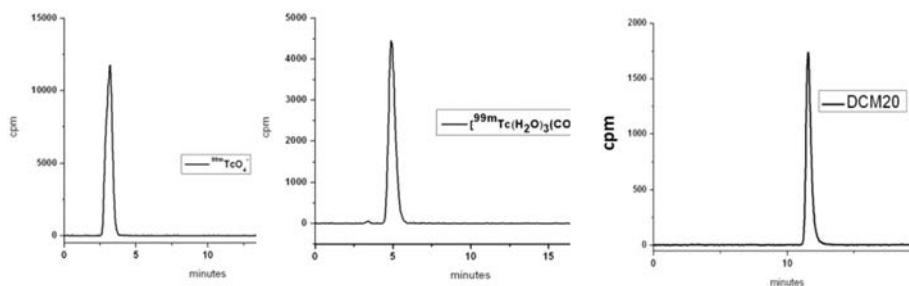
FIG. 8.2. RP-HPLC profiles of $^{99m}TcO_4^-$ (left), fac-$[^{99m}Tc(OH_2)_3(CO)_3]^+$ (middle) and $^{99m}Tc(CO)_3(DCM20)$ (right). cpm: counts per minute.

The $[^{99m}Tc(CO)_3\ DC15]$ and $[^{99m}Tc(CO)_3\ DCM20]$ complexes showed high inertness towards histidine challenge (<3% of the total radioactivity was transchelated after 6 h incubation).

8.4.3.2. Complexes $[^{99m}Tc(CO)_3\ DAPM]$

The mannosylated dextran pz diamine derivatives, DAPM1–4, were successfully labelled with $^{99m}Tc(CO)_3$ core (radiochemical yield of 98% at the time of labelling). However, up to 25% of the radioactivity bound to the DAPM derivative bearing only one pz diamine group underwent transchelation after histidine and cysteine challenges. No appreciable ^{99m}Tc activity was lost from DAPM4 and DAPM8 complexes after 6 h of chemical challenge.

8.4.3.3. Complexes $[^{99m}Tc\ (DC25\text{-}iso + NS_3)]$ and $[^{99m}Tc\ (DCM30\text{-}iso + NS_3)]$

The isocyanide derivatives of dextran and mannosylated dextran gave the 4 + 1 complex with the NS_3 ligand with high yield (~90%).
Typical SEC-HPLC profiles of $^{99m}Tc\ [EDTA]$ and $[^{99m}Tc\ (DCM30\text{-}iso + NS_3)]$ are shown in Fig. 8.3, clearly demonstrating that substitution was complete and that ^{99m}Tc labelled dextran was obtained as the only product of the reaction.
The stability of the labelled dextran for at least 4 h was also established by both previously described chromatographic methods.

8.4.4. Octanol water partition coefficients

The octanol water partition coefficients, obtained at room temperature, of some selected $^{99m}Tc(CO)_3$ dextran derivatives are reported in Table 8.1.
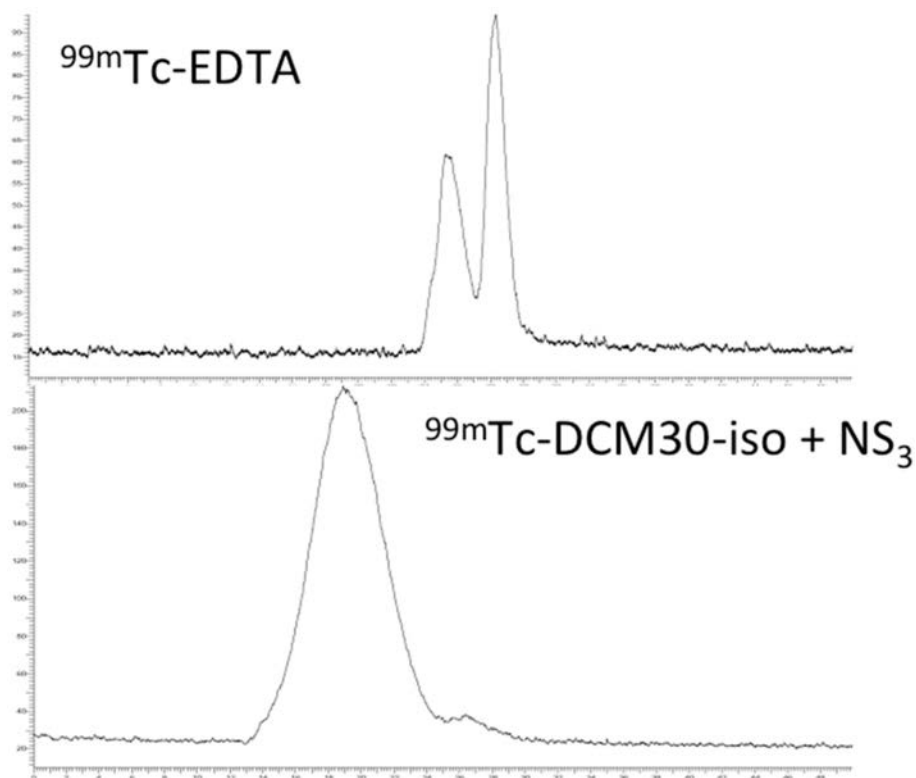
FIG. 8.3. SEC-HPLC profiles of ^{99m}Tc [EDTA] (top) and [^{99m}Tc (DCM30-iso + NS$_3$)] (bottom).

TABLE 8.1. OCTANOL WATER PARTITION COEFFICIENTS OF $^{99m}Tc(CO)_3$ DEXTRAN DERIVATIVES

Ligand	Octanol water	Log P
DC15	0.003	−2.495
DCM20	0.007	−2.133
DAPM1	0.060	−1.225

All products were highly hydrophilic, with values of log P (P = octanol/water partition coefficient) in the negative range.

8.4.5. Biodistribution studies

The results of biodistribution studies in mice, rats and rabbits on ^{99m}Tc dextran derivatives synthesized for the purposes of this study are presented in Table 8.2.

TABLE 8.2. BIODISTRIBUTION OF ^{99m}Tc(CO)$_3$ DEXTRAN DERIVATIVES IN MICE AT 1 H AND 4 H AFTER INTRADERMAL ADMINISTRATION*

Organ	DC15 2 µg/25 µL	DCM20 2 µg/25 µL	DAPM4 2.3 µg/25 µL
Liver 1 h p.i.	13.41 ± 0.63	23.34 ± 3.50	2.97 ± 0.40
Liver 4 h p.i.	2.94 ± 0.36	21.60 ± 3.29	3.76 ± 0.43
Spleen 1 h p.i.	0.90 ± 0.05	13.82 ± 3.62	1.03 ± 0.11
Spleen 4 h p.i.	0.91 ± 0.21	15.41 ± 3.48	1.52 ± 0.53
Blood 1 h p.i.	1.29 ± 0.12	2.93 ± 0.44	0.87 ± 0.14
Blood 4 h p.i.	0.68 ± 0.11	1.27 ± 0.07	0.76 ± 0.06
IS 1 h p.i.	3.13 ± 0.92	30.68 ± 8.33	68.28 ± 11.00
IS 4 h p.i	1.77 ± 0.21	36.09 ± 3.09	67.30 ± 1.45
SLN 1 h p.i.	0.24 ± 0.02	3.18 ± 0.18	4.77 ± 1.01
SLN 4 h p.i.	0.13 ± 0.01	3.47 ± 1.02	4.12 ± 1.14
2LN 1 h p.i.	0.07 ± 0.01	2.16 ± 0.41	1.40 ± 0.49
2LN 4 h p.i.	0.08 ± 0.01	2.07 ± 0.47	1.19 ± 0.36
PE 1 h p.i.	70.8	32.1	70.6
PE 4 h p.i.	70.8	32.1	70.6

Note: IS: injection site; PE: popliteal extraction; p.i.: postinjection; SLN: sentinel lymph node; 2LN: second lymph node.

* Results are expressed as % ID per gram of organ and blood, except for the radioactivity found in lymph nodes and remaining at the injection site, for which the recoveries are expressed as % ID (mean ± standard deviation are calculated on five animals per time point).

8.4.5.1. Biodistribution in mice

Table 8.2 summarizes the results obtained 1 h and 4 h after intradermal administration in the right foot-pad of BALB/c mice of 2 µg/50 µL of ^{99m}Tc(CO)$_3$ dextran derivatives.

The SLN uptake of ^{99m}Tc[(CO)$_3$ DCM20] (dextran with mannose pending arms) was much higher than that of the corresponding dextran conjugate without mannose ([^{99m}Tc(CO)$_3$ DC15]). These findings support the hypothesis that radioactivity localization in lymph nodes has occurred by a receptor mediated mechanism to macrophages present in these organs.

8.4.5.2. Biodistribution in rats

Table 8.3 summarizes the results obtained 1 h and 3 h after subcutaneous administration in the right foot-pad of Wistar rats of ^{99m}Tc(CO)$_3$ dextran derivatives.

TABLE 8.3. BIODISTRIBUTION OF ^{99m}Tc(CO)$_3$ DEXTRAN DERIVATIVES IN RATS AT 1 h AND 3 h AFTER SUBCUTANEOUS ADMINISTRATION*

Organ	DCM20 ~4 µg/50 µL	DAPM1 ~50 µg/50 µL	DAPM4 50 µg/50 µL	DAPM8 50 µg/50 µL
Liver 1 h p.i.	0.97 ± 0.05	1.01 ± 0.07	4.80 ± 1.03	5.44 ± 1.06
Liver 3 h p.i.	1.16 ± 0.12	1.66 ± 0.13	6.49 ± 0.09	6.84 ± 0.01
Spleen 1 h p.i.	0.03 ± 0.00	0.02 ± 0.01	0.32 ± 0.10	0.25 ± 0.11
Spleen 3 h p.i.	0.07 ± 0.04	0.09 ± 0.01	0.31 ± 0.04	0.45 ± 0.04
Blood 1 h p.i.	0.64 ± 0.13	0.02 ± 0.03	0.91 ± 0.02	1.72 ± 0.81
Blood 3 h p.i.	0.73 ± 0.48	0.10 ± 0.02	0.96 ± 0.37	1.55 ± 0.65
IS 1 h p.i.	43.53 ± 2.50	92.58 ± 0.94	83.85 ± 1.37	81.58 ± 0.35
IS 3 h p.i.	48.51 ± 5.41	79.48 ± 4.27	79.50 ± 5.02	81.13 ± 0.01
SLN 1 h p.i.	4.40 ± 0.01	4.91 ± 0.06	6.71 ± 2.35	7.53 ± 069

TABLE 8.3. BIODISTRIBUTION OF $^{99m}Tc(CO)_3$ DEXTRAN DERIVATIVES IN RATS AT 1 h AND 3 h AFTER SUBCUTANEOUS ADMINISTRATION* (cont.)

Organ	DCM20 ~4 µg/50 µL	DAPM1 ~50 µg/50 µL	DAPM4 50 µg/50 µL	DAPM8 50 µg/50 µL
SLN 3 h p.i.	0.02 ± 0.01	4.45 ± 0.86	5.98 ± 1.68	5.21 ± 0.78
2LN 1 h p.i.	0.05 ± 0.08	0.39 ± 0.08	2.59 ± 1.06	0.41 ± 0.15
2LN 3 h p.i.	0.08 ± 0.01	0.42 ± 0.06	1.41 ± 0.50	0.59 ± 0.14
PE 1 h p.i.	99.6 ± 0.2	92.6 ± 0.9	61.8 ± 2.4	94.5 ± 2.5
PE 3 h p.i.	98.0 ± 3.1	79.5 ± 4.3	76.7 ± 1.7	87.8 ± 3.8

Note: IS: injection site; PE: popliteal extraction; SLN: sentinel lymph node; 2LN: second lymph node.

* Results are expressed as % ID per whole organ and for total blood (mean ± standard deviation are calculated on four animals per time point).

Table 8.4 summarizes the results obtained 1 h and 3 h after subcutaneous administration in the right foot-pad of Wistar rats of $[^{99m}Tc$ (DCM30-iso + NS$_3$)] and $[^{99m}Tc$ (DC25-iso + NS$_3$)] derivatives.

The SLN uptake of $[^{99m}Tc$ (DCM30-iso + NS$_3$)] (dextran with mannose pending arms) was significantly higher than that of the corresponding dextran conjugate without mannose ($[^{99m}Tc$ (DC25-iso + NS$_3$)]). Again, these findings are in favour of the hypothesis of radioactivity localization by a receptor mediated mechanism to macrophages present in the lymph nodes.

8.4.5.3. Biodistribution in rabbits

A planar gamma camera study of rabbits showed that only popliteal nodes were clearly imaged, whereas signals from iliac lymph nodes (second echelon lymph nodes) were overlapped by radioactivity accumulated in the bladder. Therefore, to obtain information about the biodistribution patterns of these new ^{99m}Tc dextran derivatives in rabbits, ex vivo experiments were carried out.

TABLE 8.4. BIODISTRIBUTION OF [^{99m}Tc (DCM30-ISO + NS$_3$)] AND [^{99m}Tc (DC25-ISO + NS$_3$)] IN RATS 1 h AND 3 h AFTER SUBCUATNEOUS ADMINISTRATION*

Organ	DCM30-iso ~25 μg/50 μL	DC25-iso ~25 μg/50 μL
Liver 1 h p.i.	5.17 ± 0.30	10.80 ± 0.30
Liver 3 h p.i.	11.26 ± 0.76	NP
Spleen 1 h p.i.	0.08 ± 0.02	0.02 ± 0.01
Spleen 3 h p.i.	0.05 ± 0.25	NP
Blood 1 h p.i.	2.26 ± 0.67	0.08 ± 0.01
Blood 3 h p.i.	8.51 ± 0.71	NP
IS 1 h p.i.	79.80 ± 3.00	15.6 ± 1.2
IS 3 h p.i.	45.70 ± 3.10	NP
SLN 1 h p.i.	3.55 ± 1.40	0.20 ± 0.07
SLN 3 h p.i.	5.42 ± 0.88	NP
2LN 1 h p.i.	1.42 ± 0.99	0.10 ± 0.04
2LN 3 h p.i.	0.79 ± 0.54	NP
PE 1 h p.i.	60.0 ± 1.3	50.0 ± 0.1
PE 3 h p.i.	85.4 ± 0.7	NP

Note: IS: injection site; NP: not performed; PE: popliteal extraction; p.i.: postinjection; SLN: sentinel lymph node; 2LN: second lymph node.

* Results are expressed as % ID per whole organ and total blood (mean ± standard deviation are calculated on three animals per time point).

Table 8.5 summarizes the results obtained 1 h after subcutaneous administration in the right foot-pad of rabbits of some ^{99m}Tc(CO)$_3$ dextran derivatives.

TABLE 8.5. BIODISTRIBUTION OF SOME ^{99m}Tc(CO)$_3$ DEXTRAN DERIVATIVES IN RABBITS AT 1 h AFTER SUBCUTANEOUS ADMINISTRATION*

Organ	DCM20 ~60 µg/0.2 mL	DAPM4 ~60 µg/0.2 mL	DAPM8 ~60 µg/0.2 mL
Liver 1 h p.i.	0.75 ± 0.01	2.11 ± 0.03	1.50 ± 0.12
Spleen 1 h p.i.	0.44 ± 0.14	0.49 ± 0.14	0.40 ± 0.14
Blood 1 h p.i.	0.45 ± 0.01	0.19 ± 0.01	0.48 ± 0.01
IS 1 h p.i.	36.44 ± 2.12	42.88 ± 3.99	41.98 ± 2.79
SLN 1 h p.i.	4.11 ± 1.90	5.56 ± 1.55	6.79 ± 1.89
2LN 1 h p.i.	0.27 ± 0.06	0.78 ± 0.03	0.34± 0.07
PE 1 h p.i.	91.9 ± 0.1	85.8 ± 2.2	94.8 ± 1.76

Note: IS: injection site; PE: popliteal extraction; SLN: sentinel lymph node; 2LN: second lymph node.

* Results are expressed as % ID per gram, except for the radioactivity found in lymph nodes and at the injection site, for which the recoveries are expressed as % ID (mean ± standard deviation are calculated on three animals per time point).

8.4.5.4. *Effect of the mass of administered tracer on biodistribution*

To investigate whether uptake of mannosylated dextran derivatives is a saturable process, the influence of the mass of administered tracer on SLN uptake was explored. Experiments were performed in mice and rats. Table 8.6 shows the results of a study in which the effect of the amount of [^{99m}Tc(CO)$_3$ DCM20] on biodistribution was tested.

The results on [^{99m}Tc(CO)$_3$ DCM20] showed that the biological behaviour of this complex is very sensitive to the injected dosage. When the injected mass in mice decreased from 2 µg to 0.005 µg, the uptake of SLN doubled, and the uptake in the second lymph node decreased by a factor of four (but it should be

TABLE 8.6. BIODISTRIBUTION OF [^{99m}Tc(CO)$_3$ DCM20] IN MICE AND RATS AT 1 h AFTER INTRADERMAL ADMINISTRATION*

Organ	2 µg/25 µL mice	0.005 µg/5 µL mice	0.05 µg/30 µL rats	0.05 µg/5 µL rats
Blood (whole)	2.93 ± 0.44	1.09 ± 0.13	3.98 ± 0.11	1.07 ± 0.14
IS	30.68 ± 8.33	76.65 ± 4.14	55.02 ± 2.16	49.10 ± 2.64
SLN	3.18 ± 0.18	6.37 ± 0.86	17.76 ± 1.89	32.10 ± 8.21
2LN	2.16 ± 0.41	0.54 ± 0.09	0.70 ± 0.19	0.74 ± 0.13
PE	32.1 ± 0.2	91.5 ± 0.8	96.1 ± 1.9	97.7 ± 8.1

Note: IS: injection site; PE: popliteal extraction; SLN: sentinel lymph node; 2LN: second lymph node.

* Results are expressed as % ID (mean ± standard deviation are calculated on four to five animals per time point).

noted that the injected volume also decreased from 25 µL to 5 µL). This induced a sharp increase of popliteal extraction from 30%–40% to 90%. In this study, the SLN uptake in rats was very high, and the activity remaining at the injection site 1 h after the application of the tracer was relatively low.

8.4.6. Gamma camera imaging

Examples of dynamic acquisitions in rats after subcutaneous administration of 9–18 MBq of ^{99m}Tc dextran derivatives in 0.1 mL are shown in Figs 8.4 and 8.5. The images of the earliest acquisitions (0–1 min) are in the upper left corners, whereas the latest acquisitions (14–15 min) are in the lower right corners of Figs 8.4 and 8.5.

Figure 8.5 shows anterior views of the animals positioned upside down. The injection site (hottest spot), SLN, bladder, kidneys and liver are easily discernible on the images.

The radioactivity pattern of ^{99m}Tc dextran derivatives under study was also clearly delineated after static acquisition, as shown in Fig. 8.6 for three different compounds administered to rats.
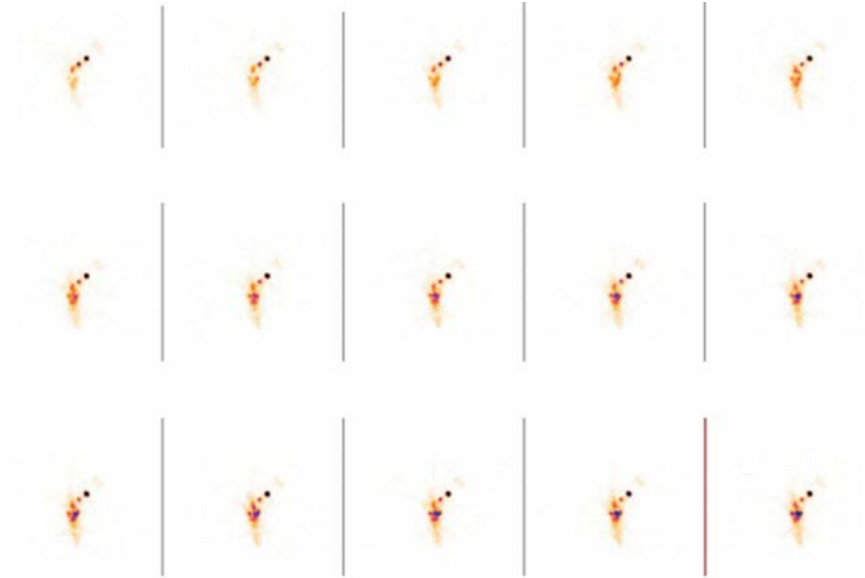
FIG. 8.4. Dynamic acquisitions (0–15 min) after intradermal administration of [$^{99m}Tc(CO)_3DCM20$].

FIG. 8.5. Dynamic acquisitions (0–15 min) after intradermal administration of [$^{99m}Tc(CO)_3DAPM8$].
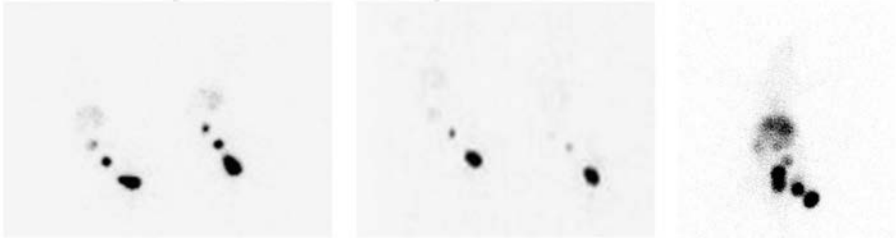
FIG. 8.6. Static acquisitions in rats 30 min postinjection of 0.5 µg of [^{99m}Tc(CO)$_3$ DCM20] (left), [^{99m}Tc(CO)$_3$ DAPM8] (middle) and [^{99m}Tc (DCM30-iso + NS$_3$)] (right).
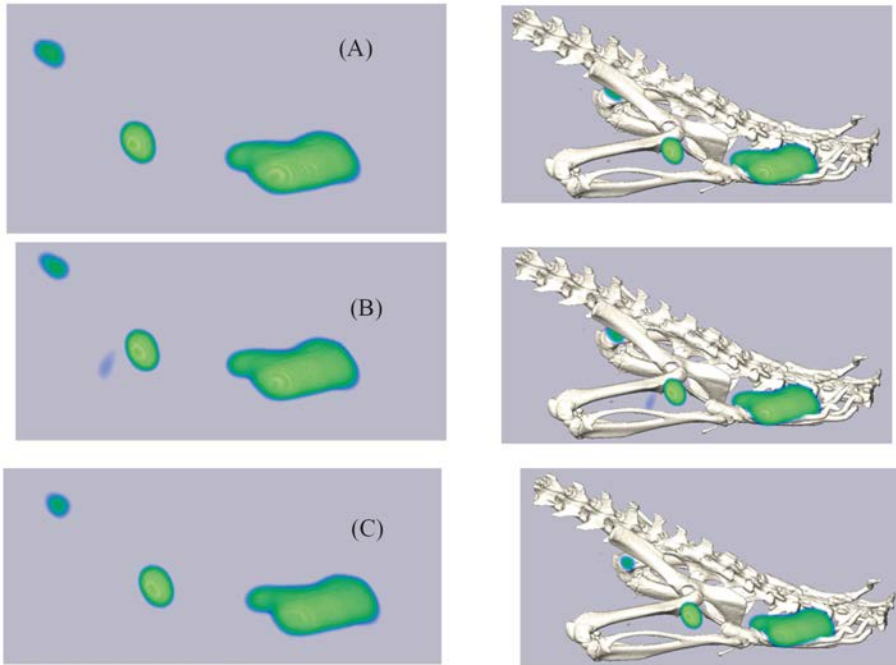
FIG. 8.7. SPECT (left) and SPECT/CT fusion (right) images of rats receiving [^{99m}Tc(CO)$_3$ DCM20] from foot-pads subcutaneously. The images were taken at: (A) 30 min, (B) 1 h (B) and (C) 3 h postinjection.

The ability of these tracers to visualize SLNs was also demonstrated by SPECT images. Figure 8.7 shows the images obtained in rats after subcutaneous administration of [^{99m}Tc(CO)$_3$ DCM20] in the rear foot-pad. The radioactivity levels at the popliteal lymph node were found to be significantly higher than those in the inguinal lymph node (the second lymph node in this animal

mode), although high radioactivity levels were also detected at the injection site. The SPECT images remained almost unchanged from 15 min to 180 min postinjection, indicating that this agent satisfied another important criterion: sustained accumulation in the SLN.

8.5. DISCUSSION

The dextran derivatives under study have been successfully synthesized and thoroughly characterized using chemical and NMR techniques. The synthetic pathways used are robust and flexible enough to allow the preparation of derivatives in which the number of grafted chelator and mannosylated arms can be adjusted predictably and accurately. The chemical structure of the synthesized compounds is in agreement with the hydrodynamic diameter determined by DLS in saline. In freshly prepared samples, DCM and DAPM show hydrodynamic sizes ranging from 7 nm to 10 nm. These values are similar to those found for DTPA mannosyl dextran (7.1 ± 0.9 nm) [8.14] and MAG_3 mannosyl dextran (5.5 ± 2.4 nm) [8.30], and have been confirmed in two recently published articles dealing with DCM [8.27] and DAPM [8.28]. In this work, size distribution measurements revealed the formation of aggregates as early as 30 min after preparation, increasing the sizes of particles from 7–10 nm to 230–310 nm and even 700 nm. These findings, not reported in the two articles cited above, need to be confirmed by additional experiments.

The mannosylated dextran derivatives, as well as their non-mannosylated analogues, were successfully labelled with a ^{99m}Tc carbonyl core and ^{99m}Tc(NS$_3$) fragments in high radiochemical yields. Of particular interest are dextran derivatives bearing cysteine arms (providing the S, N, O set of ligating atoms to bind to a ^{99m}Tc carbonyl core) that may be labelled, even at a very low ligand concentration (1.5 × 10^{-6}M) [8.27]. Mannosylated dextran bearing cysteine arms are stable compounds that can be stored in the form of lyophilized powder for long periods of time. In contrast, owing to the propensity of isocyanide groups to polymerize, mannosylated dextran bearing isocyanide arms are less stable compounds and should be prepared shortly before the radiolabelling process. The ^{99m}Tc labelled dextran derivatives are inert complexes, as demonstrated by the results obtained after challenging tests with cysteine and histidine, and may undergo high dilutions without significant degradation.

Biological evaluation in mice, rats and rabbits has shown rapid and high accumulation in the popliteal lymph node (the SLN in our animal model) that remained almost stable for long periods of time. Uptake characteristics are similar to those displayed by ^{99m}Tc tilmanocept [8.31]. The results of this work have clearly confirmed that, as for ^{99m}Tc tilmanocept, uptake in lymph nodes is

154

the result of a receptor mediated mechanism. Indeed, the uptake by lymph nodes of mannosylated dextran derivatives, either labelled with a ^{99m}Tc carbonyl core or with a Tc(NS$_3$) fragment, was much higher than that of the corresponding dextran derivative without mannose. Additionally, experiments in mice and rats were able to demonstrate that the biological behaviour of ^{99m}Tc mannosylated dextran complexes was very sensitive to injected mass. It is likely that this characteristic has contributed to induce some degree of heterogeneity that has been observed between results obtained in different laboratories.

Results from biodistribution can be used to classify the tracers under study. There may be different criteria for establishing a rank order of imaging tracers on the basis of their best biological properties. For SLNM agents, it was decided to assign a rank on the basis of qualitative scores driven by the assessment of the following properties:

— Extent of uptake in the SLN (at 30 min postinjection);
— First to second lymph node ratio;
— Residence of radioactivity in the first lymph node;
— Activity remaining at the injection site;
— Activity in organs (liver/kidneys) and blood.

The activity remaining at the site of injection was considered to have less impact on the overall quality of the tracer than the 'specificity' for the first lymph node. Thus, this characteristic was not used as a primary selection criterion (activity remaining at the site of injection is of little or no concern for SLND in melanoma, and is not a big issue in the case of breast tumours). Potential for kit pharmaceutical development was not included in the ranking score. Because the biological results obtained during this multilaboratory project were obtained using different animal models and following slightly different protocols, experimental data could not be simply mixed together to increase the statistical power of the decision tree process. However, although with several limitations, the biodistribution results allowed selection of [[99m]Tc(CO)$_3$ DCM20] and [[99m]Tc(CO)$_3$ DAPM8] as the most promising agents for potential use in humans.

8.6. CONCLUSIONS

Results in mice, rats and rabbits showed that low valence ^{99m}Tc mannosylated dextran derivatives are rapidly localized in SLNs following a saturable receptor mediate mechanism. These radioconjugates, in particular [[99m]Tc(CO)$_3$ DCM20] and [[99m]Tc(CO)$_3$ DAPM8], retained a high binding capacity to SLNs. Imaging in rats and rabbits revealed a rapid uptake into SLNs. In addition to the uptake

in SLNs, the clearance from the injection site was also found to be inversely related to the mass of the administered compound. Further evaluation in a well controlled protocol and in a large number of animals will be needed to explore the real potential of these compounds as SLNM agents in humans.

ACKNOWLEDGEMENTS

REFERENCES TO CHAPTER 8

[8.1] CABANAS, R.M., An approach for the treatment of penile carcinoma, Cancer **39** (1977) 456–466.

[8.2] ALAZRAKI, N.P., et al., Lymphoscintigraphy, the sentinel node concept, and the intraoperative gamma probe in melanoma, breast cancer, and other potential cancers, Semin. Nucl. Med. **27** (1997) 55–67.

[8.3] VERONESI, U., et al., Sentinel-node biopsy to avoid axillary dissection in breast cancer with clinically negative lymph-nodes, Lancet **349** (1997) 1864–1867.

[8.4] KESHTGAR, M.R.S., ELL, P.J., Sentinel lymph node detection and imaging, Eur. J. Nucl. Med. **26** (1999) 57–67.

[8.5] MARIANI, G., et al., Radioguided sentinel lymph node biopsy in breast cancer surgery, J. Nucl. Med. **42** (2001) 1198–1215.

[8.6] BUSCOMBE, J., et al., Sentinel node in breast cancer procedural guidelines, Eur. J. Nucl. Med. Mol. Imaging **34** (2007) 2154–2159.

[8.7] GIAMMARILE, F., et al., The EANM and SNMMI practice guideline for lymphoscintigraphy and sentinel node localization in breast cancer, Eur. J. Nucl. Med. Mol. Imaging. **40** (2013) 1932–1947.

[8.8] ALAZRAKI, N., GLASS, E.C., CASTRONOVO, F., OLMOS, R.A., PODOLOFF, D., Society of Nuclear Medicine Procedure guideline for lymphoscintigraphy and the use of intraoperative gamma probe for sentinel lymph node localization in melanoma of intermediate thickness 1.0, J. Nucl. Med. **43** (2002) 1414–1418.

[8.9] WONG, S.L., et al., Sentinel lymph node biopsy for melanoma: American Society of Clinical Oncology and Society of Surgical Oncology joint clinical practice guideline, J. Clin. Oncol. **30** (2012) 2912–2918.

[8.10] ALKUREISHI, L.W., et al., Joint practice guidelines for radionuclide lymphoscintigraphy for sentinel node localization in oral/oropharyngeal squamous cell carcinoma, Eur. J. Nucl. Med. Mol. Imaging **36** (2009) 1915–1936.

[8.11] WILHELM, A.J., MIJNHOUT, G.S., FRANSSEN, E.J., Radiopharmaceuticals in sentinel lymph-node detection: an overview, Eur. J. Nucl. Med. **26** (1999) S36–S42.

[8.12] TSOPELAS, C., Particle size analysis of ^{99m}Tc-labeled and unlabeled antimony trisulfide and rhenium sulfide colloids intended for lymphoscintigraphic application, J. Nucl. Med. **42** (2001) 460–466.

[8.13] ALAZRAKI, N.P., et al., Sentinel node staging of early breast cancer using lymphoscintigraphy and the intraoperative gamma-detecting probe, Semin. Nucl. Med. **30** (2000) 56–64.

[8.14] VERA, D.R., WALLACE, A.M., HOH, C.K., MATTREY, R.F., A synthetic macromolecule for sentinel node detection: (^{99m})Tc-DTPA-mannosyl-dextran, J. Nucl. Med. **42** (2001) 951–959.

[8.15] SONDAK, V.K., et al., Combined analysis of phase III trials evaluating [^{99m}Tc] tilmanocept and vital blue dye for identification of sentinel lymph nodes in clinically node-negative cutaneous melanoma, Ann. Surg. Oncol. **20** (2013) 680–688.

[8.16] ALBERTO, R., SCHLIBI, R., EGLI, A., SCHUBIGER, P.A., A novel organometallic aqua complex of technetium for the labeling of biomolecules: synthesis of [^{99m}Tc(H$_2$O)$_3$(CO)$_3$]$^+$ from [^{99m}TcO$_4$]$^-$ in aqueous solution and its reaction with a bifunctional ligand, J. Am. Chem. Soc. **120** (1998) 7987–7988.

[8.17] ALBERTO, R., ORTNER, K., WHEATLEY, N., SCHIBLI, R., SCHUBIGER, A., Synthesis and properties of boranocarbonate: a convenient in situ CO source for aqueous preparation of fac-[^{99m}Tc(H$_2$O)$_3$(CO)$_3$]$^+$, J. Am. Chem. Soc. **123** (2001) 3135–3136.

[8.18] VAN STAVEREN, D.R., et al., Functionalized cysteine: powerful ligands for the labelling of bioactive molecules with triaquatricarbonyltechnetium-99m(1+) ([^{99m}Tc(OH$_2$)$_3$(CO)$_3$]$^+$), Helv. Chim. Acta **88** (2005) 447–460.

[8.19] KARAGIORGOU, O., et al., (S)-(2-(2'-pyridyl)ethyl)cysteamine and (S)(2-(2'-pyridyl)ethyl)-d,l-homocysteine as ligands for the "fac-[M(CO)$_3$]$^+$" (M = Re, ^{99m}Tc) core, Inorg. Chem. **44** (2005) 4118–4120.

[8.20] HE, H., et al., Re(CO)$_3$ complexes synthesized via an improved preparation of aqueous fac-[Re(CO)$_3$(H$_2$O)$_3$]$^+$ as an aid in assessing ^{99m}Tc imaging agents. Structural characterization and solution behavior of complexes with thioether-bearing amino acids as tridentate ligands, Inorg. Chem. **44** (2005) 5437–5446.

[8.21] XAVIER, C., PAK, J.-K., SANTOS, I., ALBERTO, R., Evaluation of two chelators for labeling a PNA monomer with the fac-[^{99m}Tc(CO)$_3$]$^+$ moiety, J. Organomet. Chem. **692** (2007) 1332–1339.

[8.22] ALVES, S., et al., Pyrazolyl derivatives as bifunctional chelators for labeling tumor-seeking peptides with the fac-[M(CO)$_3$]$^+$ moiety (M) = ^{99m}Tc, Re): synthesis, characterization, and biological behaviour, Bioconjug. Chem. **16** (2005) 438–449.

[8.23] CORREIA, J.D.G., PAULO, A., SANTOS, I., Re and Tc complexes with pyrazolyl-containing chelators: from coordination chemistry to target specific delivery of radioactivity, Curr. Radiopharm. **2** (2009) 277–294.

[8.24] SPIES, H., GLASER, M., PIETZSCH, H.-J., HAHN, F.E., LÜGGER, T., Synthesis and reactions of trigonal-bipyramidal rhenium and technetium complexes with tripodal, tetradentate NS_3 ligand, Inorg. Chim. Acta **240** (1995) 465–478.

[8.25] PIETZSCH, H.-J., GUPTA, A., SYHRE, R., LEIBNITZ, P., SPIES, H., Mixed-ligand technetium(III) complexes with tetradentate/monodentate NS_3/isocyanide coordination: a new nonpolar technetium chelate system for the design of neutral and lipophilic complexes stable in vivo, Bioconjug. Chem. **12** (2001) 538–544.

[8.26] SEIFERT, S., et al., Novel procedures for preparing [99m]Tc(III) complexes with tetradentate/monodentate coordination of varying lipophilicity and adaptation to [188]Re analogues, Bioconjug. Chem. **15** (2004) 856–863.

[8.27] KÜNSTLER, J.-U., et al., Impact of functionalized coligands on the pharmacokinetics of [99m]Tc(III) '4 + 1' mixed-ligand complexes conjugated to bombesin, J. Inorg. Biochem. **105** (2011) 1383–1390.

[8.28] PIRMETTIS, I., et al., ([99m])Tc(CO)$_3$ New mannosylated dextran bearing S-derivatized cysteine chelator for sentinel lymph node detection, Mol. Pharm. **9** (2012) 1681–1692.

[8.29] MORAIS, M., et al., Mannosylated dextran derivatives labeled with fac-[M(CO)$_3$]$^+$ (M = (99m)Tc, Re) for specific targeting of sentinel lymph node, Mol. Pharm. **8** (2011) 609–620.

[8.30] GIGLIO, J., et al., Design and development of ([99m])Tc-'4 + 1'-labeled dextran-mannose derivatives as potential radiopharmaceuticals for sentinel lymph node detection, Cancer Biother. Radiopharm. **28** (2013) 541–551.

[8.31] VERA, D.R., WALLACE, A.M., HOH, C.K., [^{99m}Tc]MAG$_3$-mannosyl-dextran: a receptor-binding radiopharmaceutical for sentinel node detection, Nucl. Med. Biol. **28** (2001) 493–498.

CONTRIBUTORS TO DRAFTING AND REVIEW

Arano, Y.	Chiba University, Japan
Arteaga de Murphy, C.	Salvador Zubirán National Institute of Medical Sciences and Nutrition, Mexico
Boschi, A.	University of Ferrara, Italy
Chen, B.J.	China Institute of Atomic Energy, China
Colombo, L.	A. Roffo Institute of Oncology, Argentina
Correia, J.D.G.	Universidade Técnica de Lisboa, Portugal
Dar, U-e-K.	Institute of Nuclear Medicine and Oncology, Pakistan
De León Rodriguez, L.M.	University of Guanajuato, Mexico
De Oliveira, E.A.	Nuclear and Energy Research Institute, National Nuclear Energy Commission, Brazil
De Oliveira Filho, R.S.	Federal University, Brazil
D'Orio, E.G.	A. Roffo Institute of Oncology, Argentina
Duatti, A.	University of Ferrara, Italy, and International Atomic Energy Agency
Erzsébet, S.	Institute of Isotopes, Hungarian Academy of Sciences, Hungary
Faintuch, B.L.	Nuclear and Energy Research Institute, National Nuclear Energy Commission, Brazil
Fernández, S.	Universidad de la República, Uruguay
Ferro-Flores, G.	National Nuclear Research Institute, Mexico
Giglio, J.	Universidad de la República, Uruguay
Gomez, S.I.	Tecnonuclear S.A., Argentina
Guerrini, R.	University of Ferrara, Italy
Hall, D.J.	UCSD Moores Cancer Center, University of California, San Diego, United States of America

Hernandez, M.	Tecnonuclear S.A., Argentina
Hoh, C.K.	UCSD Moores Cancer Center, University of California, San Diego, United States of America
Horváth, V.	Institute of Isotopes, Hungarian Academy of Sciences, Hungary
Hyder, S.W.	Institute of Nuclear Medicine & Oncology, Pakistan
Janevik-Ivanovska, E.	Goce Delcev University, Stip, The Former Yugoslav Republic of Macedonia
Javed, M.	Institute of Nuclear Medicine and Oncology, Pakistan
Jentschel, C.	Forschungszentrum Dresden-Rossendorf, Germany
Khan, I.U.	Institute of Nuclear Medicine and Oncology, Pakistan
Környei, J.	Institute of Isotopes, Hungarian Academy of Sciences, Hungary
Li, H.Y.	China Institute of Atomic Energy, China
Liang, J.X.	China Institute of Atomic Energy, China
Lu, J.	China Institute of Atomic Energy, China
Luo, H.Y.	China Institute of Atomic Energy, China
Luo, Z.F.	China Institute of Atomic Energy, China
Mallia, M.	Bhabha Atomic Research Centre, India
Mariani, G.	Regional Center of Nuclear Medicine, University of Pisa Medical School, Italy
Medina, L.A.	UNAM e Instituto Nacional de Cancerología, Mexico
Morais, M.	Universidade Técnica de Lisboa, Portugal
Morales-Avila, E.	National Nuclear Research Institute, Mexico
Mustaciosu, C.	Horia Hulubei National Institute for Physics and Nuclear Engineering, Romania
Niculae, D.	Horia Hulubei National Institute for Physics and Nuclear Engineering, Romania

Nunez, E.G.F.	Nuclear and Energy Research Institute, National Nuclear Energy Commission, Brazil
Ocampo-García, B.E.	National Nuclear Research Institute, Mexico
Orsini, F.	Regional Center of Nuclear Medicine, University of Pisa Medical School, Italy
Pandey, U.	Bhabha Atomic Research Centre, India
Paolino, A.	Universidad de la República, Uruguay
Papadopoulos, M.	Demokritos National Center for Scientific Research, Greece
Pasquali, M.	University of Ferrara, Italy
Pasqualini, R.	CIS bio international/IBA, Saclay, RP Innovative, France
Patrascu, I.	Horia Hulubei National Institute for Physics and Nuclear Engineering, Romania
Pedraza-Lopez, M.	Salvador Zubirán National Institute of Medical Sciences and Nutrition, Mexico
Pelecanou, M.	Demokritos National Center for Scientific Research, Greece
Pietzsch, H.-J.	Forschungszentrum Dresden-Rossendorf, Germany
Pirmettis, I.	Demokritos National Center for Scientific Research, Greece
Ramirez, F.M.	National Nuclear Research Institute, Mexico
Rey, A.	Universidad de la República, Uruguay
Salvadori, S.	University of Ferrara, Italy
Samuel, G.	Bhabha Atomic Research Centre, India
Santos, I.	Universidade Técnica de Lisboa, Portugal
Santo-Cuevas, C.L.	National Nuclear Research Institute, Mexico
Silva, N.G.	Nuclear and Energy Research Institute, National Nuclear Energy Commission, Brazil

Subramanian, S.	Bhabha Atomic Research Centre, India
Tokin, C.A.	UCSD Moores Cancer Center, University of California, San Diego, United States of America
Tóth, G.	Biological Center of the Hungarian Academy of Sciences, Hungary
Trapella, C.	University of Ferrara, Italy
Tsotakos, T.	Demokritos National Center for Scientific Research, Greece
Tuta, C.	Horia Hulubei National Institute for Physics and Nuclear Engineering, Romania
Uccelli, L.	University of Ferrara, Italy
Venkatesh, M.	Bhabha Atomic Research Centre, India
Vera, D.R.	UCSD Moores Cancer Center, University of California, San Diego, United States of America
Wallace, A.M.	UCSD Moores Cancer Center, University of California, San Diego, United States of America
Yang, C.H.	China Institute of Atomic Energy, China
Zheng, D.Q.	China Institute of Atomic Energy, China

Technical Meetings

Vienna, Austria: 2–7 September 2012

Research Coordination Meetings

Vienna, Austria: 12–16 November 2007
Athens, Greece: 18–22 May 2009
Vienna, Austria: 22–26 November 2010

IAEA
International Atomic Energy Agency

ORDERING LOCALLY

In the following countries, IAEA priced publications may be purchased from the sources listed below or from major local booksellers.

Orders for unpriced publications should be made directly to the IAEA. The contact details are given at the end of this list.

AUSTRALIA
DA Information Services
648 Whitehorse Road, Mitcham, VIC 3132, AUSTRALIA
Telephone: +61 3 9210 7777 • Fax: +61 3 9210 7788
Email: books@dadirect.com.au • Web site: http://www.dadirect.com.au

BELGIUM
Jean de Lannoy
Avenue du Roi 202, 1190 Brussels, BELGIUM
Telephone: +32 2 5384 308 • Fax: +32 2 5380 841
Email: jean.de.lannoy@euronet.be • Web site: http://www.jean-de-lannoy.be

CANADA
Renouf Publishing Co. Ltd.
5369 Canotek Road, Ottawa, ON K1J 9J3, CANADA
Telephone: +1 613 745 2665 • Fax: +1 643 745 7660
Email: order@renoufbooks.com • Web site: http://www.renoufbooks.com

Bernan Associates
4501 Forbes Blvd., Suite 200, Lanham, MD 20706-4391, USA
Telephone: +1 800 865 3457 • Fax: +1 800 865 3450
Email: orders@bernan.com • Web site: http://www.bernan.com

CZECH REPUBLIC
Suweco CZ, spol. S.r.o.
Klecakova 347, 180 21 Prague 9, CZECH REPUBLIC
Telephone: +420 242 459 202 • Fax: +420 242 459 203
Email: nakup@suweco.cz • Web site: http://www.suweco.cz

FINLAND
Akateeminen Kirjakauppa
PO Box 128 (Keskuskatu 1), 00101 Helsinki, FINLAND
Telephone: +358 9 121 41 • Fax: +358 9 121 4450
Email: akatilaus@akateeminen.com • Web site: http://www.akateeminen.com

FRANCE
Form-Edit
5 rue Janssen, PO Box 25, 75921 Paris CEDEX, FRANCE
Telephone: +33 1 42 01 49 49 • Fax: +33 1 42 01 90 90
Email: fabien.boucard@formedit.fr • Web site: http://www.formedit.fr

Lavoisier SAS
14 rue de Provigny, 94236 Cachan CEDEX, FRANCE
Telephone: +33 1 47 40 67 00 • Fax: +33 1 47 40 67 02
Email: livres@lavoisier.fr • Web site: http://www.lavoisier.fr

L'Appel du livre
99 rue de Charonne, 75011 Paris, FRANCE
Telephone: +33 1 43 07 50 80 • Fax: +33 1 43 07 50 80
Email: livres@appeldulivre.fr • Web site: http://www.appeldulivre.fr

GERMANY
Goethe Buchhandlung Teubig GmbH
Schweitzer Fachinformationen
Willstätterstrasse 15, 40549 Düsseldorf, GERMANY
Telephone: +49 (0) 211 49 8740 • Fax: +49 (0) 211 49 87428
Email: s.dehaan@schweitzer-online.de • Web site: http://www.goethebuch.de

HUNGARY
Librotrade Ltd., Book Import
PF 126, 1656 Budapest, HUNGARY
Telephone: +36 1 257 7777 • Fax: +36 1 257 7472
Email: books@librotrade.hu • Web site: http://www.librotrade.hu

INDIA

Allied Publishers
1st Floor, Dubash House, 15, J.N. Heredi Marg, Ballard Estate, Mumbai 400001, INDIA
Telephone: +91 22 2261 7926/27 • Fax: +91 22 2261 7928
Email: alliedpl@vsnl.com • Web site: http://www.alliedpublishers.com

Bookwell
3/79 Nirankari, Delhi 110009, INDIA
Telephone: +91 11 2760 1283/4536
Email: bkwell@nde.vsnl.net.in • Web site: http://www.bookwellindia.com

ITALY

Libreria Scientifica "AEIOU"
Via Vincenzo Maria Coronelli 6, 20146 Milan, ITALY
Telephone: +39 02 48 95 45 52 • Fax: +39 02 48 95 45 48
Email: info@libreriaaeiou.eu • Web site: http://www.libreriaaeiou.eu

JAPAN

Maruzen Co., Ltd.
1-9-18 Kaigan, Minato-ku, Tokyo 105-0022, JAPAN
Telephone: +81 3 6367 6047 • Fax: +81 3 6367 6160
Email: journal@maruzen.co.jp • Web site: http://maruzen.co.jp

NETHERLANDS

Martinus Nijhoff International
Koraalrood 50, Postbus 1853, 2700 CZ Zoetermeer, NETHERLANDS
Telephone: +31 793 684 400 • Fax: +31 793 615 698
Email: info@nijhoff.nl • Web site: http://www.nijhoff.nl

SLOVENIA

Cankarjeva Zalozba dd
Kopitarjeva 2, 1515 Ljubljana, SLOVENIA
Telephone: +386 1 432 31 44 • Fax: +386 1 230 14 35
Email: import.books@cankarjeva-z.si • Web site: http://www.mladinska.com/cankarjeva_zalozba

SPAIN

Diaz de Santos, S.A.
Librerias Bookshop • Departamento de pedidos
Calle Albasanz 2, esquina Hermanos Garcia Noblejas 21, 28037 Madrid, SPAIN
Telephone: +34 917 43 48 90 • Fax: +34 917 43 4023
Email: compras@diazdesantos.es • Web site: http://www.diazdesantos.es

UNITED KINGDOM

The Stationery Office Ltd. (TSO)
PO Box 29, Norwich, Norfolk, NR3 1PD, UNITED KINGDOM
Telephone: +44 870 600 5552
Email (orders): books.orders@tso.co.uk • (enquiries): book.enquiries@tso.co.uk • Web site: http://www.tso.co.uk

UNITED STATES OF AMERICA

Bernan Associates
4501 Forbes Blvd., Suite 200, Lanham, MD 20706-4391, USA
Telephone: +1 800 865 3457 • Fax: +1 800 865 3450
Email: orders@bernan.com • Web site: http://www.bernan.com

Renouf Publishing Co. Ltd.
812 Proctor Avenue, Ogdensburg, NY 13669, USA
Telephone: +1 888 551 7470 • Fax: +1 888 551 7471
Email: orders@renoufbooks.com • Web site: http://www.renoufbooks.com

United Nations
300 East 42nd Street, IN-919J, New York, NY 1001, USA
Telephone: +1 212 963 8302 • Fax: 1 212 963 3489
Email: publications@un.org • Web site: http://www.unp.un.org

Orders for both priced and unpriced publications may be addressed directly to:

IAEA Publishing Section, Marketing and Sales Unit, International Atomic Energy Agency
Vienna International Centre, PO Box 100, 1400 Vienna, Austria
Telephone: +43 1 2600 22529 or 22488 • Fax: +43 1 2600 29302
Email: sales.publications@iaea.org • Web site: http://www.iaea.org/books

This publication summarizes the current status of and future trends in the development of radiopharmaceuticals for sentinel lymph node detection (SLND), a widely recognized, essential diagnostic tool for the effective treatment of superficial cancers such as breast tumours and melanoma. The first part of the publication covers all current aspects of this diagnostic methodology, including the production of nanocolloidal particles, their biological mechanism of action and relevant clinical applications. In the second part, recent outstanding developments in the field fuelled by the introduction of molecular imaging agents for SLND and of multimodality optical and radioactive agents are discussed. A portion of the results on the novel generation of SLND radiopharmaceuticals presented here were obtained through an IAEA co-ordinated research project.